

MODIFIED VANADIUM BASED OXIDE CATALYSTS
FOR SELECTIVE OXIDATION OF *n*-BUTANE TO
MALEIC ANHYDRIDE

LOH PEI XUAN

MASTER OF SCIENCE

FACULTY OF ENGINEERING AND SCIENCE
UNIVERSITI TUNKU ABDUL RAHMAN
AUGUST 2012

**MODIFIED VANADIUM BASED OXIDE CATALYSTS FOR
SELECTIVE OXIDATION OF *n*-BUTANE TO MALEIC ANHYDRIDE**

By

LOH PEI XUAN

A thesis submitted to the Department of Chemical Engineering,
Faculty of Engineering and Science,
Universiti Tunku Abdul Rahman,
in partial fulfillment of the requirements for the degree of Master of Science
August 2012

**This thesis is dedicated with love
to my parents.**

ABSTRACT

Three series of modified vanadium phosphate catalysts were prepared via vanadyl hydrogen phosphate sesquihydrate precursors ($\text{VOHPO}_4 \cdot 1.5\text{H}_2\text{O}$) were investigated. The undoped precursors were synthesised by refluxing vanadyl phosphate dihydrate ($\text{VOPO}_4 \cdot 2\text{H}_2\text{O}$) in 1-butanol. The first series of precursors were doped with Cr at the mole ratio of $\text{Cr/V} = 0.01, 0.03, \text{ and } 0.05$. The second series of precursors were supported on silica at different loadings. But for the third series, silica supported 30 wt% VPO precursors were calcined at different temperatures. All the modified precursors were calcined under a flow of 0.75% *n*-butane/air at 733K to generate the active vanadyl pyrophosphate ($(\text{VO})_2\text{P}_2\text{O}_7$) catalyst. The techniques used to characterize the catalysts were XRD, SEM, BET, ICP-OES, redox titration, TPD of O_2 and TPR in H_2 . The catalytic performances of these catalysts for selective oxidation of *n*-butane to maleic anhydride were determined by using a fixed bed microreactor (673 K, GHSV = 2400 h^{-1}). Active phase of vanadyl pyrophosphate has been confirmed by XRD analyses for all the synthesised catalysts. Morphologies of all the synthesised catalysts have shown the characteristic rosette-shape of vanadyl pyrophosphate in SEM micrographs, except for low loading of silica-supported VPO_s catalysts. Cr dopant has found to promote the formation of V^{5+} , with increased specific surface areas from 19.29 to $22.77 \text{ m}^2 \text{ g}^{-1}$, and provide a better catalytic performance, i.e. 29–35 % *n*-butane conversion and 78–89% MA selectivity compared to that of undoped VPO_s, i.e. 21% conversion and 68% MA selectivity. The optimum ratio of Cr/V at 0.01 has shown the highest activity among the Cr-doped catalysts, i.e.

35% and relatively high selectivity, i.e. 73%. The silica-VPO interaction had greatly influenced the specific surface areas of the catalysts and the average pore size distributions. The amounts of desorbed and removed oxygen were increased with the VPO_s loadings on the silica support. Silica supported 30% VPO_s catalyst gave an improved selectivity i.e. 93%, and activity i.e. 33% as compared to unsupported VPO_s. Sintering effect of VPO_s phase was suggested to happen at high calcination temperature. Calcination temperature of 673 K has shown to be the optimum calcination temperature to give a better catalytic performance.

ACKNOWLEDGEMENT

The work described in this dissertation could not have been completed without the assistance of many people. I would like to express my heartfelt gratitude to people who made success of this project possible.

First, a very special thank you to my supervisor, Asst. Prof. Dr. Leong Loong Kong of Universiti Tunku Abdul Rahman (UTAR). With his enthusiasm, his inspiration, and his great efforts to explain things clearly and simply, he helped to make this project fun for me. Throughout my thesis-writing period, he provided encouragement, good teaching, and lots of good ideas.

This research would not have been possible without the funding of UTAR Research Fund and the facilities that have been provided. Thus, I would also like to extend special thanks to UTAR.

I would like to express my sincere appreciation to Prof. Dr. Taufiq-Yap Yun Hin of Universiti Putra Malaysia (UPM) for his supervision and valuable advice throughout the this research. In addition, I would like to thank Ms. Deena, Dr. Wong Yee Ching, Ms. Nurul Suziana binti Nawi @ Mohamed, Ms. Voon Lee Hwei, and Mr. Yuen Choon Seon of UPM for their patience and guidance throughout my research when I carried out analyses in UPM.

I also must give great credit to Ms. Seow Siew Siew of Hi-Tech Instruments Sdn. Bhd., who kindly helped me to run my samples by using the FESEM instrument, which was crucial for my research. Special thanks must also go to Mr. Andy Guee Eng Hwa and Mr. Hau Tien Boon of CNG Instruments Sdn. Bhd. for their advices and technical assistances in running BET Sorptomatic, TPDRO instrument, and catalytic reactor.

Also indebted to my fellow teammates: Mr. Chin Kah Seng, Ms. Kang Jo Yee, and Mr. Lim Kuan Hoe, lab officers: Mr. Lee Ming Lay for providing help, suggestions, and encouragement throughout my project.

Last but not least, I would like to thank my family for giving unconditional support, love and conviction that will always inspire me.

APPROVAL SHEET

This thesis entitled “**Modified Vanadium Phosphate Catalysts for Selective Oxidation of *n*-Butane to Maleic Anhydride**” was prepared by LOH PEI XUAN and submitted as partial fulfilment of the requirements for the degree of Master of Science at Universiti Tunku Abdul Rahman.

Approved by,

Supervisor



(Asst. Prof. Dr. Leong Loong Kong)

Supervisor

Department of Chemical Engineering
Faculty of Engineering and Science
Universiti Tunku Abdul Rahman

Date: 30/7/2012

**FACULTY OF ENGINEERING AND SCIENCE
UNIVERSITI TUNKU ABDUL RAHMAN**

Date: 30/7/2012

SUBMISSION OF THESIS

It is hereby certified that **LOH PEI XUAN (08UEB08129)** has completed this thesis entitled “MODIFIED VANADIUM BASED OXIDE CATALYSTS FOR SELECTIVE OXIDATION OF *n*-BUTANE TO MALEIC ANHYDRIDE” under supervision of **ASST. PROF. DR. LEONG LOONG KONG** (Supervisor) from Department of Chemical Engineering Faculty of Engineering and Science, Universiti Tunku Abdul Rahman.

I understand that University will upload softcopy of my thesis in pdf format into UTAR Institutional Repository, which may be made accessible to UTAR community and public

Yours truly,



(LOH PEI XUAN)

DECLARATION

I hereby declare that the project report is based on my original work except for quotations and citations which have been duly acknowledged. I also declare that it has not been previously or concurrently submitted for any other degree



Loh Pei Xuan

Date: 30/7/2012

TABLE OF CONTENTS

DEDICATION	Page ii
ABSTRACT	iii
ACKNOWLEDGEMENTS	v
APPROVAL SHEET	vii
PERMISSION SHEET	viii
DECLARATION	ix
TABLE OF CONTENTS	x
LIST OF TABLES	xiii
LIST OF FIGURES	xv
LIST OF ABBREVIATIONS	xviii

CHAPTER

1.0	INTRODUCTION	1
	1.1 Fundamental Aspects of Catalysis	1
	1.2 Development of Catalysis and Green Chemistry	4
	1.3 Importance of Heterogeneous Catalysis	5
	1.4 Selective Oxidation of Light Hydrocarbon	7
	1.5 Objectives of this Study	9
 2.0	 LITERATURE REVIEW	 11
	2.1 History of Commercial Process for Maleic Anhydride	11
	2.1.1 Economic Importance of Maleic Anhydride	12
	2.1.2 Industrial Technologies for Maleic Anhydride Production from <i>n</i> -Butane	14
	2.2 VPO Phases for Selective Oxidation of <i>n</i> -Butane	17
	2.2.1 Structure of VPO phases	18
	2.2.2 The Mechanism of Selective Oxidation	20
	2.2.3 Role of oxygen	24
	2.2.4 Active sites	26
	2.3 Recent approaches to the improvement of the catalytic performance	30
	2.3.1 Modification of precursor routes	30
	2.3.2 Introduction of novel processes in the precursor preparation	33
	2.3.3 The Control of P/V Atomic Ratio	35
	2.3.4 Addition of Dopants	37

2.3.5	The use of highly-heat-conductivity supports	39
2.3.6	The effect of Calcination Duration /Condition	43
2.3.7	The influence of the reaction atmosphere	45
3.0	MATERIALS AND METHODOLOGY	48
3.1	Preparation of Vanadyl Pyrophosphate Catalysts	48
3.1.1	Gases and Materials	48
3.1.2	Preparation of Bulk Catalysts	49
3.1.3	Preparation of Cr-doped Catalysts	53
3.1.4	Preparation of Silica Supported Catalysts	53
3.2	Characterisation of Vanadyl Pyrophosphate Catalysts	55
3.2.1	Gases and Materials	55
3.2.2	Instrumentation	56
3.2.2.1	X-ray Diffraction (XRD) Analyses	56
3.2.2.2	Scanning Electron Microscopy (SEM)	57
3.2.2.3	Brunauer-Emmett-Teller (BET) Surface Area Measurements	58
3.2.2.4	Chemical Analyses	60
3.2.2.5	Redox Titration Analyses	61
3.2.2.6	Temperature-programmed Desorption (TPD) of O ₂ Analyses	63
3.2.2.7	Temperature-programmed Reduction (TPR) in H ₂ Analyses	65
3.3	Catalytic Tests	66
4.0	SELECTIVE OXIDATION OF <i>n</i>-BUTANE OVER CHROMIUM-DOPED VPO_s CATALYSTS	68
4.1	Introduction	68
4.2	Effect of Different Mole Percentages of Cr Dopant on the Physico-chemical, Reactivity and Catalytic Properties of Cr-Doped Vanadyl Pyrophosphate Catalysts	69
4.2.1	X-ray Diffraction (XRD) Analyses	69
4.2.2	Scanning Electron Microscopy (SEM)	72
4.2.3	Brunauer-Emmett-Teller (BET) Surface Area Measurements and Chemical Analyses	74
4.2.4	Temperature-programmed Desorption (TPD) of O ₂ Analyses	76
4.2.5	Temperature-programmed Reduction (TPR) in H ₂ Analyses	78
4.2.6	Catalytic Oxidation of <i>n</i> -Butane to Maleic Anhydride	82
4.3	Conclusions	84
5.0	SELECTIVE OXIDATION OF <i>n</i>-BUTANE OVER SILICA SUPPORTED VPO_s CATALYSTS	85
5.1	Introduction	85
5.2	Effect of Different Loadings of VPO _s on Silica Support towards Physico-chemical, Reactivity and Catalytic Properties of Supported Vanadyl Pyrophosphate Catalysts	86

5.2.1	X-ray Diffraction (XRD) Analyses	87
5.2.2	Scanning Electron Microscopy (SEM)	90
5.2.3	Brunauer-Emmett-Teller (BET) Surface Area Measurements and Chemical Analyses	93
5.2.4	Temperature-Programmed Desorption (TPD) of O ₂ Analyses	95
5.2.5	Temperature-Programmed Reduction (TPR) in H ₂ Analyses	97
5.2.6	Catalytic Oxidation of <i>n</i> -Butane to Maleic Anhydride	102
5.3	Effect of Different Calcination Temperatures on Physico-chemical, Reactivity and Catalytic Properties of Supported Vanadyl Pyrophosphate Catalysts	103
5.3.1	X-ray Diffraction (XRD) Analyses	104
5.3.2	Scanning Electron Microscopy (SEM)	106
5.3.3	Brunauer-Emmett-Teller (BET) Surface Area Measurements and Chemical Analyses	107
5.3.4	Temperature-Programmed Desorption (TPD) of O ₂ Analyses	109
5.3.5	Temperature-Programmed Reduction (TPR) in H ₂ Analyses	111
5.3.6	Catalytic Oxidation of <i>n</i> -Butane to Maleic Anhydride	114
5.4	Conclusions	115
REFERENCES		117
APPENDICES		133
	Appendix A	133
	Appendix B	134
	Appendix C	135
	Appendix D	138
	Appendix E	140
	Appendix F	148
	Appendix G	152
	Appendix H	154
	Appendix I	156
BIODATA OF THE AUTHOR		157

LIST OF TABLES

Table	Page
2.1 Proposed elementary steps in the oxidation of <i>n</i> -butane to MA	23
3.1 Gases and materials for preparation of vanadyl pyrophosphate catalysts	48
3.2 Gases and materials for sample analyses	55
4.1 XRD data of bulk VPO _s and Cr-doped VPO _s catalysts	71
4.2 Specific surface areas, chemical compositions, average oxidation numbers and percentages of V ⁴⁺ and V ⁵⁺ oxidation states for bulk VPO _s and Cr-doped VPO _s catalysts	75
4.3 Amounts of oxygen atoms desorbed and values of desorption activation energy obtained by TPD analyses for bulk VPO _s and Cr-doped VPO _s catalysts	77
4.4 Amounts of oxygen atoms removed and values of reduction activation energy obtained by TPR analyses for bulk VPO _s and Cr-doped VPO _s catalysts	80
4.5 Catalytic performances of bulk VPO _s and Cr-doped VPO _s catalysts	84
5.1 XRD data of bulk VPO _s and silica supported VPO _s catalysts	90
5.2 Specific surface areas, chemical compositions, average oxidation numbers and percentages of V ⁴⁺ and V ⁵⁺ oxidation states for bulk VPO _s and silica supported VPO _s catalysts	93
5.3 Amounts of oxygen atoms desorbed and values of desorption activation energy obtained by TPD analyses for bulk VPO _s and silica supported VPO _s catalysts	96
5.4 Amounts of oxygen atoms removed and values of reduction activation energy obtained by TPR analyses for bulk VPO _s and silica supported VPO _s catalysts	100
5.5 Catalytic performances of bulk VPO _s and silica supported VPO _s catalysts	103
5.6 XRD data of bulk VPO _s and silica supported VPO _s catalysts	106

5.7	Specific surface areas, chemical compositions, average oxidation numbers and percentages of V^{4+} and V^{5+} oxidation states for bulk VPO_s and silica supported VPO_s catalysts	108
5.8	Amounts of oxygen atoms desorbed and values of desorption activation energy obtained by TPD analyses for bulk VPO_s and silica supported VPO_s catalysts	110
5.9	Amounts of oxygen atoms removed and values of reduction activation energy obtained by TPR analyses for bulk VPO_s and silica supported VPO_s catalysts	112
5.10	Catalytic performances of bulk VPO_s and silica supported VPO_s catalysts	115

LIST OF FIGURES

Figure	Page
1.1 Sequential elementary steps in catalytic reaction	2
1.2 Potential energy diagram of gas-solid heterogeneous catalytic reaction	2
2.1 Maleic Anhydride	12
2.2 World consumption of MA	13
2.3 Fixed-bed reactor	15
2.4 Fluidised-bed reactor	16
2.5 DuPont transported-bed reactor	17
2.6 Idealised structure of (0 0 1) plane of $\text{VOHPO}_4 \cdot 0.5\text{H}_2\text{O}$	18
2.7 Idealised structure of (1 0 0) plane of $(\text{VO})_2\text{P}_2\text{O}_7$	19
2.8 Structure of (a) $\alpha_{\text{I}}\text{-VOPO}_4$; (b) $\alpha_{\text{II}}\text{-VOPO}_4$; (c) $\beta\text{-VOPO}_4$	20
2.9 (a) Electrostatic alignment of <i>n</i> -butane at the surface (b) Acid and acid-base attack on <i>n</i> -butane by vanadium at the $(\text{VO})_2\text{P}_2\text{O}_7$ surface	21
2.10 Two alternative orientations for electrostatic alignment of MA at open active site	23
2.11 A simple non-selective reaction pathway for <i>n</i> -butane oxidation to CO_x	24
2.12 Activation of oxygen over metal oxides	25
2.13 Projection of crystal structure of $(\text{VO})_2\text{P}_2\text{O}_7$ along the (0 2 0) plane	27
2.14 Active crystal facets according to (a) Centi <i>et al.</i> (1988) and (b) Batis <i>et al.</i> (1991)	28
2.15 Selective and non-selective crystal faces of $(\text{VO})_2\text{P}_2\text{O}_7$	29
2.16 Three main methods for preparation of $\text{VOHPO}_4 \cdot 0.5\text{H}_2\text{O}$	31

2.17	Membrane reactor	48
3.1	First stage of reflux (Preparation of $\text{VOPO}_4 \cdot 2\text{H}_2\text{O}$ intermediate)	49
3.2	Second stage of reflux (Preparation of $\text{VOHPO}_4 \cdot 1.5\text{H}_2\text{O}$ precursor) and the activation of $(\text{VO})_2\text{P}_2\text{O}_7$	51
3.3	Wetness impregnation of $\text{VOHPO}_4 \cdot 1.5\text{H}_2\text{O}$ precursor onto silica support	54
3.4	Shimadzu XRD-6000 diffractometer	57
3.5	Hitachi SU8000 FESEM	58
3.6	Thermo Finnigan Sorptomatic 1990	59
3.7	Perkin Elmer Optima 2000 DV optical emission spectrometer	60
3.8	Colour changes when end point of titration of KMnO_4 reached	62
3.9	Colour changes when end point of titration of $(\text{NH}_4)_2\text{Fe}(\text{SO}_4)_2 \cdot 6\text{H}_2\text{O}$ reached	62
3.10	Thermo Electron TPDRO 1100	65
3.11	Fixed-bed microreactor with on-line Thermo Scientific TRACE GC Ultra TM	67
3.12	Schematic diagram of fixed-bed microreactor with on-line gas chromatograph for catalytic test	67
4.1	Powder XRD patterns of bulk VPO_s and Cr-doped VPO_s catalysts	70
4.2	SEM micrographs for (a) bulk VPO_s : (i) $\times 7000$ (ii) $\times 35,000$; (b) $\text{VPO}_s\text{-Cr1\%}$: (i) $\times 7000$ (ii) $\times 30,000$; (c) $\text{VPO}_s\text{-Cr3\%}$: (i) $\times 7000$ (ii) $\times 25,000$; (c) $\text{VPO}_s\text{-Cr3\%}$: (i) $\times 7000$ (ii) $\times 18,000$	73
4.3	TPD of O_2 profiles of bulk VPO_s and Cr-doped VPO_s catalysts	76
4.4	TPR in H_2 profiles of bulk VPO_s and Cr-doped VPO_s catalysts	79
5.1	Powder XRD patterns of bulk VPO_s and silica supported VPO_s Catalysts	88
5.2	SEM micrographs for (a) bulk VPO_s : $\times 35,000$; (b) bare silica support: (i) $\times 250$ (ii) $\times 200,000$	91
5.3	SEM micrographs for (a) 5% VPO_s/Si : (i) $\times 300$ (ii) $\times 7,000$	

	(iii) $\times 20,000$; (b) 10%VPO _s /Si: (i) $\times 300$ (ii) $\times 7,000$ (iii) $\times 20,000$; (c) 15%VPO _s /Si: (i) $\times 300$ (ii) $\times 7,000$ (iii) $\times 20,000$; (d) 20%VPO _s /Si: (i) $\times 300$ (ii) $\times 7,000$ (iii) $\times 20,000$; (e) 25%VPO _s /Si: (i) $\times 300$ (ii) $\times 7,000$ (iii) $\times 20,000$; (f) 30%VPO _s /Si: (i) $\times 300$ (ii) $\times 7,000$ (iii) $\times 20,000$	92
5.4	TPD of O ₂ profiles of silica and silica supported VPO _s catalysts	96
5.5	TPR in H ₂ profiles of silica and silica supported VPO _s catalysts	98
5.6	Molecular structure of silica supported (VO) ₂ P ₂ O ₇	101
5.7	Powder XRD patterns of bulk VPO _s and silica supported VPO _s catalysts	105
5.8	SEM micrographs for (a) T400VPO _s /Si: (i) $\times 300$ (ii) $\times 7,000$ (iii) $\times 20,000$; (b) T460VPO _s /Si: (i) $\times 300$ (ii) $\times 7,000$ (iii) $\times 20,000$; (c) T520VPO _s /Si: (i) $\times 300$ (ii) $\times 7,000$ (iii) $\times 20,000$	107
5.9	TPD of O ₂ profiles of silica and silica supported VPO _s catalysts	109
5.10	TPR in H ₂ profiles of silica and silica supported VPO _s catalysts	111

LIST OF ABBREVIATIONS

α_I	Alpha I
α_{II}	Alpha II
β	Beta
γ	Gamma
δ	Delta
ε	Epsilon
ω	Omega
Ba	Barium
BET	Brunauer-Emmett-Teller
Bi	Bismuth
Bi-Fe	Bismuth-Iron
=C-H	Double bond carbon single bond hydrogen
C-C bond	Carbon-carbon bond
C-H bond	Carbon-hydrogen bond
C=C	Carbon double bond carbon
C=O	Carbon double bond oxygen
Ca	Calcium
Ce	Cerium
Ce-Fe	Cerium-Iron
Co	Cobalt
CO _x	Carbon oxides
Cr	Chromium
Cr(NO ₃) ₃ ·9H ₂ O	Chromium nitrate
DNA	Deoxyribonucleic acid

FID	Flame ionization detector
FWHM	Full-Width at Half Maximum
Ga	Gallium
Ga(acac) ₃	Gallium(III) acetylacetonate
Ga ₂ O ₃	Gallium(III) oxide
GaPO ₄	Gallium phosphate
H ₂	Purified helium
H ₂ /air	Hydrogen in air
H ₂ O	Dihydrogen monoxide
H ₂ SO ₄	Sulphuric acid
HCl	Hydrochloric acid
HNO ₃	Nitric acid
HPO ₄ ²⁻	Hydrogen phosphate ion
ICP-OES	Inductively coupled plasma-optical emission spectroscopy
ICSD	Inorganic Crystal Structure Database
JCPDS	Joint Committee on Powder Diffraction Standards
KMnO ₄	Potassium permanganate
MA	Maleic Anhydride
Mg	Magnesium
Mo	Molybdenum
<i>n</i> -C ₄ H ₆ /air	<i>n</i> -Butane in air
(NH ₄) ₂ Fe(SO ₄) ₂ ·6H ₂ O	Ammonium iron(II) sulphate,
N ₂	Purified nitrogen
N ₂	Liquid nitrogen
N ₂ H ₄	Hydrazine

Nb	Niobium
$\text{NH}_4\text{H}_2\text{PO}_4$	Ammonia dihydrogen orthophosphate
NH_4VO_3	Ammonium metavanadate,
O^-	Oxygen ion
<i>o</i> - H_3PO_3	<i>ortho</i> -phosphoric acid,
O_2^-	Dioxide ion
O^{2-}	Oxide ion
O_2^{2-}	Peroxide ion
$(\text{Ph})_2\text{NH}$	Diphenylamine
P–O	Phosphorus-oxide
P/V	Phosphorus to vanadium
Pd	Palladium
PO_4	Phosphate
Ru	Rubidium
Sb	Antimony
SEM	Scanning electron microscopy
Si	Silica
TAP	Temporal analysis of products
TCD	Thermal Conductivity Detector
T_{max}	Peak maxima Temperature
TOF	Turnover frequency
TON	Turnover number
T_{onset}	Onset Temperature
TPD	Temperature Programmed Desorption
TPDRO	Temperature Programmed Desorption, Reduction and Oxidation

TPR	Temperature Programmed Reduction
US	United State
$(VO)_2P_2O_7$	Vanadyl Pyrophosphate
$(VOHPO_4 \cdot 0.5H_2O)$	Vanadyl hydrogen phosphate hemihydrate
V	Vanadium
V–O–P	Vanadium single bond oxygen single bond phosphorus
V–O–V	Vanadium single bond oxygen single bond vanadium
$V(PO_3)_3$	Vanadium phosphite
V=O	Vanadium double bond oxygen
V_2O_5	Vanadium(V) oxide
V^{3+}	Vanadium(III)
V^{4+}	Vanadium(IV)
$V^{4+}-O$	oxygen associated with Vanadium(IV) phase
V^{5+}	Vanadium(V)
$V^{5+}-O$	Oxygen associated with Vanadium(V) phase
V^{5+}/V^{4+} ratio	Vanadium(V) to vanadium(IV) ratio
$VO(H_2PO_4)$	Oxo-vanadium(IV) dihydrogen phosphate
$VO(PO_3)_2$	Vanadyl phosphite
VO_6	Vanadium hexaoxide
$VOHPO_4$	Vanadyl hydrogen phosphate
$VOHPO_4 \cdot 1.5H_2O$	Vanadyl hydrogen phosphate semihydrate
$VOHPO_4 \cdot xH_2O$	Vanadyl hydrogen phosphate hydrates
$VOPO_4$	Vanadyl phosphate
$VOPO_4 \cdot 2H_2O$	Vanadyl phosphate dihydrate

$\text{VOPO}_4 \cdot x\text{H}_2\text{O}$	Vanadyl phosphate hydrates
VPA route	Aqueous route
VPA-derived	Derived from aqueous route
VPD route	Dihydrate route
VPD-derived	Derived from dihydrate route
VPO	Vanadium Phosphorus Oxide
VPO route	Organic route
VPO-derived	Derived from organic route
VPO_4	Vanadium phosphate
VPO_s	Vanadium phosphorus oxide that produced via sesquihydrate route
XRD	X-ray diffraction
Zn	Zinc
Zr	Zirconium

CHAPTER 1

INTRODUCTION

1.1 Fundamental Aspects of Catalysis

The name “catalysis” was coined by Berzelius in 1836. Berzelius defined a catalyst as a substance which by its mere presence evokes chemical actions which would not have taken place in its absence. This definition simply describes the observation of the phenomenon, “catalysis”, without making any attempt to interpret or explain its nature. The word was formed from a combination of two Greek words, *κατα* (kata) means down and *λυδεν* (lysein) means to split or to break. According to Berzelius, by “awaking the affinities which are asleep”, a catalyst breaks down the normal forces which inhibit the reaction of molecules (Hartley, 1985).

Every catalytic reaction is a sequence of elementary steps, in which reactant molecules bind to the catalyst, where they react, after which the product detaches from the catalyst, liberating the latter for the next cycle (Figure 1.1). The catalyst offers an alternative path for the reaction, which is obviously more complex, but energetically much more favorable (Figure 1.2) (Chorkendorff and Niemantsverdriet, 2007).

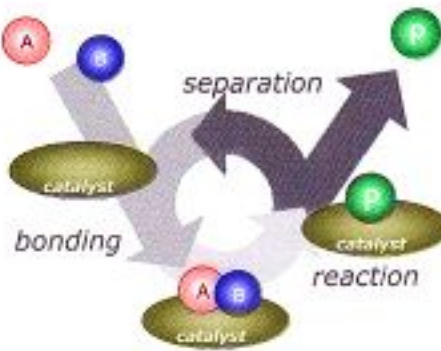


Figure 1.1: Sequential elementary steps in catalytic reaction (Chorkendorff and Niemantsverdriet, 2007)

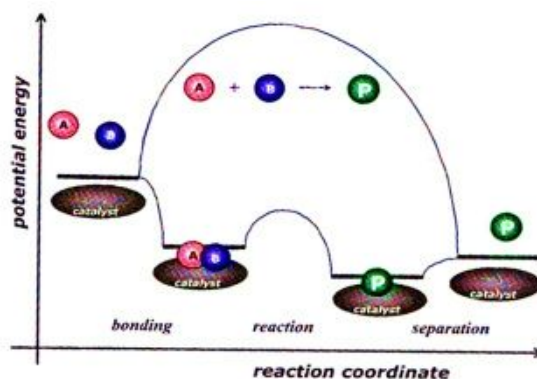


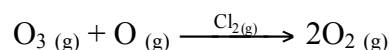
Figure 1.2: Potential energy diagram of gas-solid heterogeneous catalytic reaction (Chorkendorff and Niemantsverdriet, 2007)

Catalysts come in multitude of forms, varying from atoms and molecules to large structures such as zeolites or enzymes. In addition, catalysts may be employed in various surroundings: in liquids, gases, or at the surface of solids (Chorkendorff and Niemantsverdriet, 2007).

There are three major types of catalysis (Bartholomew and Farrauto, 2006):

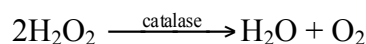
(a) Homogeneous Catalysis

In homogeneous catalysis, both the catalyst and the reactants are in the same phase. Normally, it possesses higher reaction rate as compared to heterogeneous system, since it does not subject to the diffusion limitation. For example, the decomposition of ozone via a reaction with chlorine atoms as catalyst:



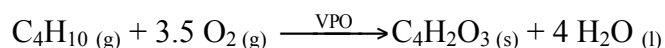
(b) Biocatalysis

Enzymes are nature's catalysts, which allow biological reactions to occur at the rates necessary to maintain life, such as the buildup of Deoxyribonucleic acid (DNA). For the moment it is sufficient to consider an enzyme as a large protein, the structure of which results in very shape-specific active sites. Thus, enzymes are highly specific and efficient catalysts. For example, the enzyme catalase catalyses the decomposition of hydrogen peroxide into water and oxygen:



(c) Heterogeneous Catalysis

Catalysis classified as heterogeneous if the catalyst and the reactants are present in the different phase. Normally, in heterogeneous catalysis, solids catalyse reactions of molecules in gas or solution. For example, oxidation of *n*-butane to Maleic Anhydride (MA) over the surface of vanadyl pyrophosphate catalyst:



1.2 Development of Catalysis and Green Chemistry

In the 1990s, the concept of “green chemistry” was initiated in both the US and Europe, and soon adopted by mass-media as the new approach of chemistry in opposition to the pollute-and-then-clean-up approach considered the common industrial practice. “Sustainable chemistry” is another concept that more focus on the use of not risky and polluting chemicals in production process, and also links eco-efficiency, economic growth and quality of life in term of a cost/benefit analysis (Anastas and Warner, 1998). One can say that Sustainability is the goal and Green Chemistry is the means to achieve it. A reasonable working definition of “green chemistry” has been formulated by Sheldon (2000): Green chemistry efficiently utilises (preferably renewable) raw materials, eliminates waste and avoids the use of toxic and/or hazardous reagents and solvents in the manufacture and application of chemical products.

Catalysis is a key technology for achieving social and economic objectives. The main goal of industrial catalysis is maximising selectivity of reaction in order to achieve atom economy. Besides, efforts has been focus on simplifying the complexity of process and reducing the formation of intermediates by making a single step over a solid catalyst to attain the principle of simple and safe process in “green chemistry”. Waste formation and solvent using are avoided in the

process, but the use of natural resources is encouraged to accomplish the principles of “green chemistry (Centi and Perathoner, 2003).

1.3 Importance of Heterogeneous Catalysis

Current areas of interest and activities in heterogeneous catalysis involve production and transformation of fuel materials, large-scale synthesis of inorganic and organic products, production of fine chemicals, and protection of the environment. The general trends are to conduct catalytic processes under milder conditions, *i.e.* moderate temperature and pressure, to minimize the waste products and to use cheaper feed stocks (Grzybowska-Swierkosz, 2000).

The petroleum-based process industry generates products with a value more than 4 trillion dollars. 75% productions need the aid of catalysts, 90% of newly productions involve catalysis and 95% of all based on the heterogeneous catalysis. How to supply the vast quantities of fuels, and chemicals when oil is no longer readily available is one of the most challenging and important problems now facing humanity. Besides, the growing needs of environmental protection make heterogeneous catalysis remain a great challenge for researchers in catalysis field especially the use of lower C₂-C₄ alkanes as raw materials due to its low cost and widely available (Gleaves *et al.*, 2010).

The interaction between heterogeneous catalyst and substrates, intermediates and products is extremely important. If it is too weak, the substrate will drift away from the catalyst and no reaction will take place. Conversely if too strong, the substrate will never leave catalyst and causing inhibition (Rothenberg, 2008). The following reaction steps are expected in the simplest case of catalytic gas reaction (Hagen, 2006):

- (i) Diffusion of the starting materials through the boundary layer to the catalyst surface.
- (ii) Diffusion of the starting materials into the pores, i.e. pore diffusion.
- (iii) Adsorption of the reactants on the inner surface of the pores.
- (iv) Chemical reaction on the catalyst surface.
- (v) Desorption of the products from the catalyst surface.
- (vi) Diffusion of the products out of the pores.
- (vii) Diffusion of the products away from the catalyst through the boundary layer and into gas phase.

The catalyst turnover number (TON) and the turnover frequency (TOF) are two important quantities used for comparing catalyst efficiency. In heterogeneous catalysis, TON and TOF are often defined as number of reactant molecules that are converted per active sites, or per gram catalyst in one second, minute, or hour (Rothenberg, 2008). Successful heterogeneous catalysts have to be developed into a material with the following properties (Chorkendorff and Niemantsverdriet, 2007):

- (i) High activity per unit of volume in the eventual reactor.
- (ii) High selectivity towards the desired product.
- (iii) Sufficiently long life time with respect to deactivation.
- (iv) Possibility to regenerate, particularly if deactivation is fast.
- (v) Reproducible preparation.
- (vi) Sufficient thermal stability.
- (vii) High mechanical strength with respect to crushing.
- (viii) High attrition resistance to mechanical wear.

1.4 Selective Oxidation of Light Hydrocarbon

The application of oxide-based catalysts in chemical reactions, are ranging from selective oxidation to total oxidation, hydrogenation, dehydrogenation and environmental applications. Selective oxidation reactions provide many attractive opportunities for developing new processes and alternate routes to chemical synthesis. This is because selective oxidation is extremely fast and can be highly selective. The opportunities to replace older slow processes with energy efficient processes that have lower capital cost, reduce unwanted by products and use different and cheaper feedstock are provided (Centi and Perathoner, 2001). The controlled partial oxidation of hydrocarbons, comprising alkanes, alkene and (alkyl)aromatics, is the single most important technology for the conversion of oil- and natural gas-based feedstocks to industrial chemicals (Sheldon and Kochi, 1981). Examples of catalytic oxidation of hydrocarbon and its desired products

are (Sheldon *et al.*, 2007).

- (i) Ethene to ethene oxide on Ag based catalyst.
- (ii) Propene to acrylonitrile on iron antimony oxide catalyst.
- (iii) *ortho*-Xylene to phthalic anhydride on vanadium pentoxide/titanium catalyst.
- (iv) Propane to acrolein on bismuth molybdenum composite oxide catalyst.
- (v) Isobutene to methyl methacrylate on molybdenum-bismuth containing catalyst.
- (vi) *n*-butane to MA on vanadium phosphorus oxide (VPO) catalyst.

The VPO catalyst system is the only system that has been found to be economically viable for the selective oxidation of *n*-butane to MA, which is the only industrially practiced selective oxidation involving an alkane (Wachs *et al.* 1997). Additionally, polyfunctional nature of VPO catalyst in the conversion of decalin, tetrahydro phthalic anhydride, naphthalene, 3-methyl tetrahydrophthalic anhydride and benzene has been reported as well (Centi *et al.*, 1990).

Conversions of *n*-butane are defined as the molar percentage of each reactant in the feed that is converted to product (Agaskar *et al.*, 1993):

$$\% \text{ Conversion} = \frac{\text{Moles of } n\text{-butane consumed}}{\text{Moles of } n\text{-butane in feed}} \times 100$$

The selectivity to each product is defined as the ratio of that yield of that product divided by *n*-butane conversion. Hence selectivity of *n*-butane to MA is represented as below (Agaskar *et al.*, 1993):

$$\text{Selectivity of MA} = \frac{\text{Moles of MA Produced}}{\text{Moles of butane consumed}} \times 100$$

1.5 Objectives of this Study

The objectives of this study are:

- (i) to synthesise and characterise undoped/unsupported VPO_s catalysts prepared via vanadyl hydrogen phosphate sesquihydrate precursor (VOHPO₄·1.5H₂O);
- (ii) to examine the effect of different mole percentages of chromium (Cr) dopant on the physico-chemical, reactivity and catalytic properties of Cr-doped VPO_s catalysts.
- (iii) to investigate the physical, chemical, reactivity and catalytic performances of various weight percentages.
- (iv) to study the effect of different calcinations temperatures on the physico-chemical, reactivity and catalytic properties of silica supported VPO_s catalysts.

The techniques used to characterise the catalysts are x-ray diffraction (XRD), scanning electron microscopy (SEM), Brunauer-Emmett-Teller (BET)

surface area measurements, inductively coupled plasma-optical emission spectrometry (ICP-OES), redox titration, temperature-programmed desorption (TPD) of O₂ and temperature-programmed reduction (TPR) in H₂. Catalytic tests were also carried out to determine the performance for selective oxidation of *n*-butane to MA.

CHAPTER 2

LITERATURE REVIEW

2.1 History of Commercial process for Maleic Anhydride

The first production of maleic anhydride (MA) for commercial sale was in 1933. Firstly, benzene was used as feedstock and oxidised over vanadia-molybdenum oxide catalysts. By 1966, the production of MA from *n*-butane could effectively catalysed by vanadium phosphorus oxide (VPO) compounds was reported by Bergman *et al.* However, until late of 1970s, vapor phase oxidation of benzene over vanadium-base catalyst was preferred because processes based on *n*-butane gave a lower yield (Hodnett and Delmon, 1985; Moser and Schrader, 1985; Sookraj and Engelbrencht, 1999). Nevertheless, the pollution control on limited amount of atmospheric benzene emissions, the high price of benzene, the wide spread availability of *n*-butane from the exploration of natural gas fields, the waste of two carbon atoms to transfer benzene to MA, the byproducts of benzene (phthalic anhydride and benzoquinone) and the classification of benzene as carcinogen all made *n*-butane preferred feedstock for MA production by the end of 1970s (Bej and Rao, 1991; Cavani and Trifiro, 2004).

MA was once tried to be produced with butene as the hydrocarbon source but the strong adsorption of butadiene on the surface of VPO catalyst is a critical

problem to maintain a sufficient level at surface to allow the oxidation of adsorbed intermediate up to MA (Varma and Saraf, 1979; Centi *et al.*, 1988). Besides, adsorbed intermediate also inhibits adsorption of other reactants onto surface of catalyst. Thus, MA yield from *n*-butane oxidation is higher than that of butene due to the reduced surface concentration. The different kinetic behavior exhibited by *n*-butane and butene is caused by their different surface effects and different reducing power (Centi *et al.*, 1988).

Began in 1974, Monsanto use *n*-butane as a feedstocks to produce MA from fixed-bed reactors, and by 1983 essentially all the MA production plants in United States (US) use *n*-butane as feedstock. By 2000, about 80% of world wide MA was produced from *n*-butane (Felthouse *et al.*, 2000).

2.1.1 Economic Importance of Maleic Anhydride

MA is the anhydride of cis-butenedioic acid (maleic acid), which carboxylic acid groups are next to each other in the cis form (Figure 2.1). MA has a cyclic structure with a ring containing four carbon atoms and one oxygen atom. It is synthesised industrially with high selectivity up to more than 80% at low conversion without any desorption of intermediate (Centi *et al.*, 2001).

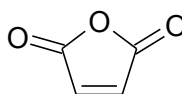


Figure 2.1: Maleic anhydride

The biggest MA exporters to the global market are the United States of America, Japan, Belgium and Italy. The countries of Western Europe, Canada, emerging economies of the Asia-Pacific region are major importers. Approximately 51% of all MA consumed in 2008 was for the production of unsaturated polyester resins. Production of 1,4-butanediol accounted for another 13%, fumaric acid for 4% and lubricating oil additives for 3%. The remainder was consumed in miscellaneous uses, including copolymers, malic acid, plasticizers, agricultural chemicals, alkenyl succinic anhydrides, alkyd resins and a number of specialty chemicals and organic intermediates (Funada and Greiner, 2009). The following pie chart shows world consumption of MA (Figure 2.2).

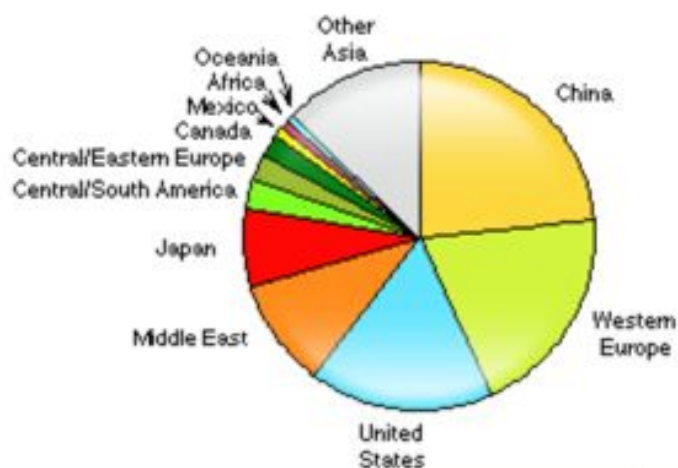


Figure 2.2 World consumption of MA (Funada and Griner, 2009)

World MA consumption has grown at around 3%/year over the long term. Growth is slower in Western Europe and the United State (US) but higher in central and eastern Europe, Latin America and Asia, in particular China. Growth in the US had been around 2.5%/year before the market was affected by the

economic crisis. The market was further impacted by the start-up of Huntsman's new 45,000 tonne/year plant at Geismar, Louisiana, in 2009. However, strong exports in 2010 have helped tighten the market considerably. In addition to Canada and Mexico, US producers have been exporting product to Europe. In Western Europe, the MA market is mature with growth predicted around 1.5–2.0% per year, while in central and Eastern Europe growth is much stronger. BASF closed its 115,000 tonne/year plant at Feluy, Belgium, in March 2010. While this closure initially had little impact, markets tightened considerably during 2010 due to supply constraints, exacerbated by a number of plant outages and higher consumption as consumers rebuilt inventories (Hodges, 2010).

2.1.2 Industrial Technologies for Maleic Anhydride Production from *n*-Butane

The production of MA is normally operated as a fixed-bed process (Figure 2.3) and at current industrial fixed-bed condition (400–450 °C, space velocity: 1100–2600 h⁻¹, 1–2 bar, 1–2.5% *n*-butane/air), which has a selectivity ~70% at 85% conversion. Since the partial oxidation of *n*-butane is highly exothermic reactions, it cannot be carried out in a simple fixed-bed of catalyst pellet but multi-tubular reactors. And a cooling media must be used to cool the reactor and prevent hotspots to prevent destroy of catalyst and detrimental to reactor performance. A molten salt or oil is used to keep the temperature of reaction zone within the desired range. The long residence times with conditions above the

explosive limit can be avoided by feeding *n*-butane and air separately (Centi *et al.*, 1988; Mota *et al.*, 2000).

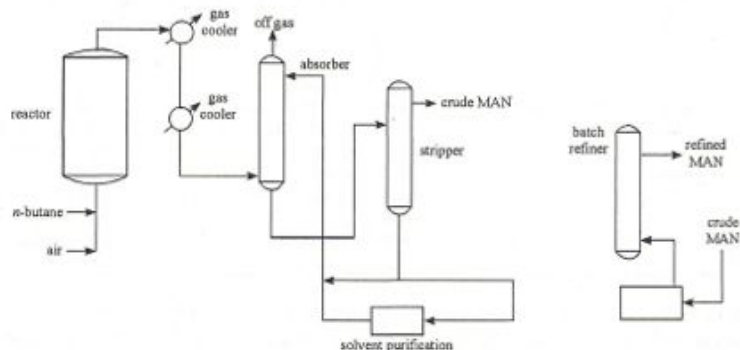


Figure 2.3: Fixed-bed reactor (Felthouse *et al.*, 2000)

In a fluidised-bed reactor (Figure 2.4), catalyst powder is used, which is kept in suspension by the gas flowing upwards at a sufficient high velocity. The frictional force exerted on the catalysts by upward flowing gas is the major problem concerned in this reactor. The *n*-butane fractions in the feed can be up to 4% because fluidised-bed reactor doesn't experience hot-spots. The advantages of this reactor include temperature uniformity, high rates of heat and mass transfer, and a high degree of catalyst utilisation. Since the gases can be fed directly into reactor rather than premixed, higher yields of MA and lower air throughput are allowed. There are two major disadvantages of this reactor, which include overoxidation of MA to carbon oxides by backmixing and the high catalyst attrition rate caused by constant motion (Johnsson *et al.*, 1987).

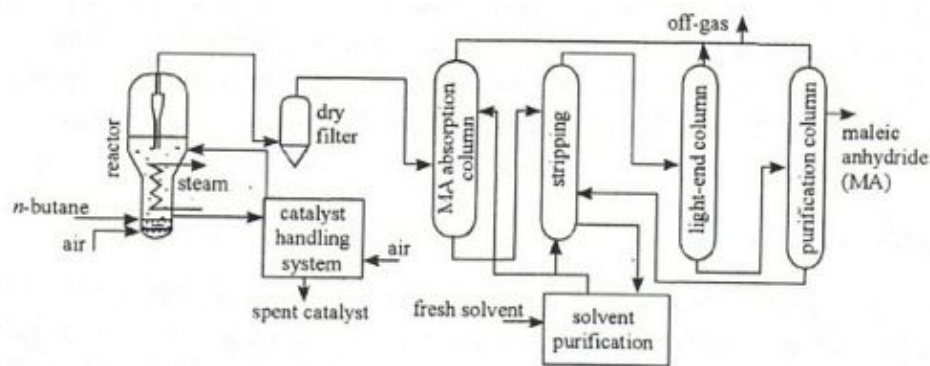


Figure 2.4: Fluidised-bed reactor (Felthouse *et al.*, 2000)

It is generally accepted that the selective *n*-butane oxidation over vanadium phosphorus oxide (VPO) catalyst proceeds by a redox cycle (Mars and van Krevelen, 1954). VPO catalyst uses lattice oxygen atoms to oxidise *n*-butane and be reduced. The catalyst is then reoxidised by gas phase oxygen to its initial oxidation state. Therefore, no gas phase oxygen is necessary for in desired reaction. With an oxygen free gas phase, the selectivity of MA can be increased about 7–10% (Lerou and Mills, 1993). Thus, a two reactor process utilising this unique property is designed, called Du Pont transported-bed reactor (Figure 2.5). In this process, the catalyst is oxidised at elevated temperatures and then transported to the riser section of the reactor where it is reacted anaerobically with *n*-butane. Since the oxidation and reduction cycles are separated from each other, both of the process can be optimised indepently to achieve a better catalytic performance (Contractor *et al.*, 1987; Mota *et al.*, 2000).

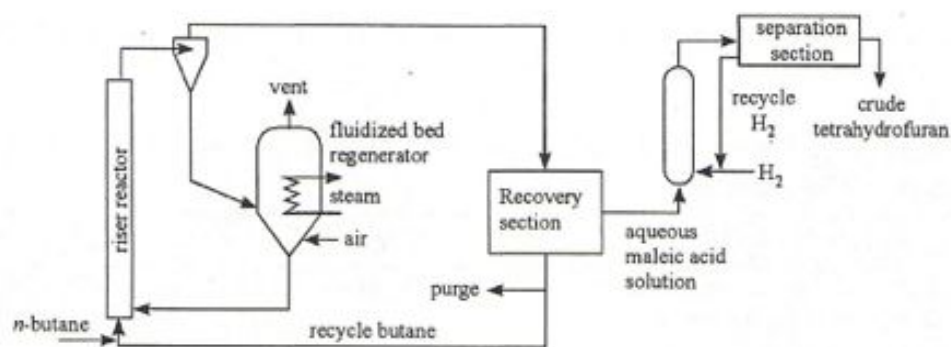


Figure 2.5: DuPont transported-bed reactor (Felthouse *et al.*, 2000)

2.2 VPO Phases for Selective Oxidation of *n*-Butane

Vanadium, phosphorus and oxygen can form a large number of distinct compounds that have been well characterised and easily transformed from one to another due to the redox characteristic of vanadium. The VPO phases include V^{5+} compounds (Bordes, 1987; Borders *et al.*, 1984; Ladwig, 1965; Gopal and Calvo, 1972) *e.g.* α_I , α_{II} , β , γ , δ , ϵ , ω -VOPO₄, and VOPO₄· x H₂O; V^{4+} compounds (Johnson *et al.*, 1984; Bordes, 1987; Torardi and Calabrese, 1984; Leonowicz *et al.*, 1985) *e.g.* VOHPO₄· x H₂O, (VO)₂P₂O₇, VO(PO₃)₂, VO(H₂PO₄); and V^{3+} (Bordes, 1987; Sananes *et al.*, 1995) compounds *e.g.* VPO₄, V(PO₃)₃. VPO phases with V^{3+} are rarely encountered in *n*-butane oxidation and will not be discussed further (Centi, 1993). Vanadyl pyrophosphate ((VO)₂P₂O₇) is regarded as the active phase in the VPO catalysts (Wenig and Schrader, 1986).

(VO)₂P₂O₇ phase usually is prepared from the thermal treatment of Vanadyl hydrogen phosphate hemihydrate (VOHPO₄·0.5H₂O) phase. This is the most recent and widely used commercial formulations. However, during the

transformation, it can be lead to other phases also, *e.g.* various VOPO_4 phases and $\text{VOPO}_4 \cdot 2\text{H}_2\text{O}$ phase. The conditions of activation determine which compounds are formed (Bordes, 1987).

2.2.1 Structure of VPO phases

The vanadyl hydrates and hydrogenophosphates are generally considered as catalysts precursors. The structure of $\text{VOHPO}_4 \cdot 0.5\text{H}_2\text{O}$ (Figure 2.6) is constituted of pairs of VO_6 octahedra sharing a common face. Couples of octahedral are connected together through PO_4 tetrahedra, forming the (0 0 1) planes. In one octahedra pair, the $\text{V}=\text{O}$ bonds are in *cis* position. Between the (0 0 1) planes, H_2O molecules are connected through hydrogen bonds.

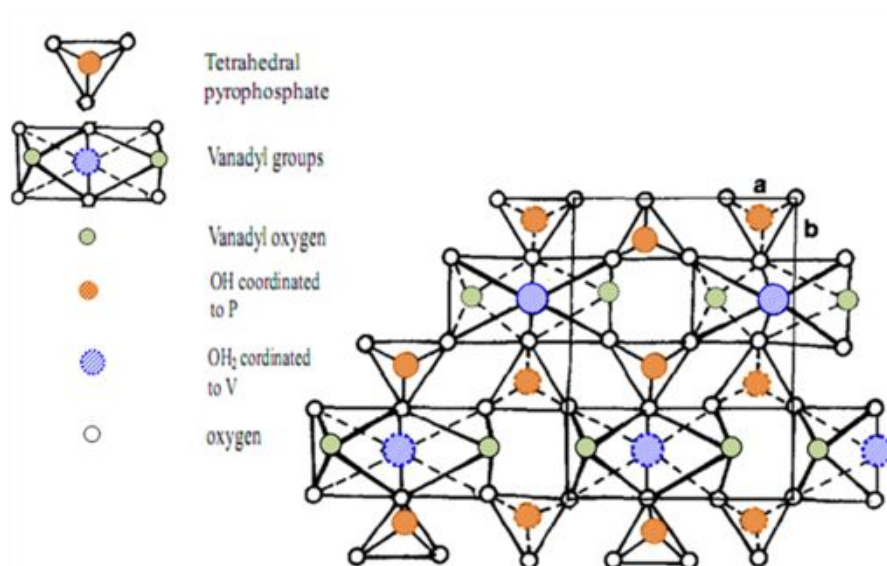


Figure 2.6: Idealised structure of (0 0 1) plane of $\text{VOHPO}_4 \cdot 0.5\text{H}_2\text{O}$ (Bordes, 1987)

$(VO)_2P_2O_7$ presents a structure in which two VO_6 octahedral pairs share edges and equatorially linked together by corner-sharing pyrophosphate tetrahedral (Figure 2.7). In opposition to $VOHPO_4 \cdot 0.5H_2O$, the $V=O$ bonds in the octahedral pairs are in *trans* position, the layers are connected together by pyrophosphate groups. The transformation $VOHPO_4 \cdot 0.5H_2O$ to $(VO)_2P_2O_7$ occurs according to a reaction which has been proposed by Borders *et al.* (1984) to be topotactic with the elimination of two water molecules.

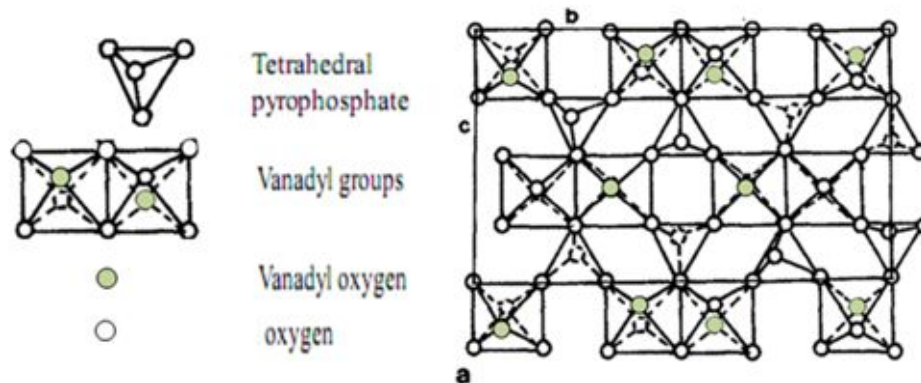


Figure 2.7: Idealised structure of (1 0 0) plane of $(VO)_2P_2O_7$ (Borders, 1987)

Furthermore, $(VO)_2P_2O_7$ is readily oxidised to various phases of $VOPO_4$ as well. The structure of α_I , α_{II} , β - $VOPO_4$ (Figure 2.8) have been discussed in the literature (Ladwig, 1965; Gopal and Calvo, 1972, Nakamura *et al.*, 1974). These phases are different from $(VO)_2P_2O_7$, they are built from single columns of VO_6 octahedra linked together through PO_4 tetrahedra. For α_I , α_{II} - $VOPO_4$, every PO_4 tetrahedra shares its four oxygen atoms with four different VO_6 octahedra columns, which are parallel to each other. Their structures differed in the relative position of $V=O$ as compared to the neighboring PO_4 groups. The β - $VOPO_4$ phase

has two of its four PO₄ oxygen atoms shared with two neighboring VO₆ octahedra in one column and other two oxygen shared with two different VO₆ columns. The structural γ and δ -VOPO₄ have not been solved (Bordes *et al.*, 1984).

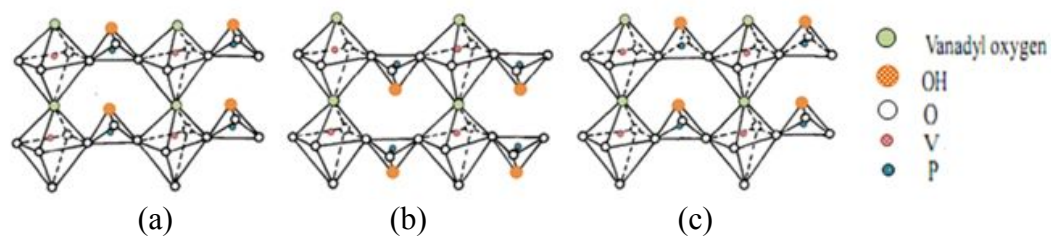


Figure 2.8: Structure of (a) α_I -VOPO₄; (b) α_{II} -VOPO₄; (c) β -VOPO₄ (Bordes, 1987)

2.2.2 The Mechanism of Selective Oxidation

n-Butane selective oxidation to MA over the VPO catalyst involves abstraction of eight hydrogen atoms, insertion of three oxygen atoms and transfer of fourteen electrons. The reaction is highly selective toward MA at low *n*-butane conversions with CO_x as the only by products (Centi *et al.*, 1988). The reaction is believed to follow a Mars-van Krevelen (redox) mechanism, in which the catalyst provides lattice oxygen to oxidize the absorbed reactants and is reduced; the consumed lattice oxygen is then replenished by the surface oxygen species converted from gaseous oxygen and the catalyst is regenerated (Mars and van Krevelen, 1954).

The first step in *n*-butane conversion to MA is obviously the activation of *n*-butane on the catalyst surface. Activation of *n*-butane can be broken down into

two types: C–H bond activation and C–C bond activation. Since the C–C bond activation would lead to cracking and non selective products, most work to date deals with the activation of C–H bond (Pepera *et al.*, 1985).

The action mode of the vanadyl pyrophosphate (1 0 0) surface in catalyzing the selective oxidation of *n*-butane to MA has investigated by Thompson *et al.* (2003) using quantum chemical calculations on small cluster models (Figure 2.9). Once *n*-butane anchored electrostatically at the surface of catalyst, any covalent interaction will be initiated by flow of electron density from methylene carbon to vanadium. This is known as nucleophilic attack of methylene carbon on vanadium, vanadium acts as a local acid site in this interaction. At the same time, methylene hydrogen exhibits the most electrophilicity and it is placed in the vicinity of vanadium, as close as their positive charges will allow. Now, vanadium acts as a local base site accompanying electron donation to methylene hydrogen. The donation electron density to methylene hydrogen is weakening methylene C–H bonds, with methylene C–H rupture activating *n*-butane at the surface. Vanadium has a much higher donor/acceptor power than the reaction sites on *n*-butane, thus vanadium may perform dual acid-base attack on *n*-butane. The mismatching of *n*-butane and active site in terms of relative electron donor/acceptor power suggests a weak interaction, in agreement with the observed low rate of conversion (Chattaraj, 2001; Cavani and Trifiro, 1994).

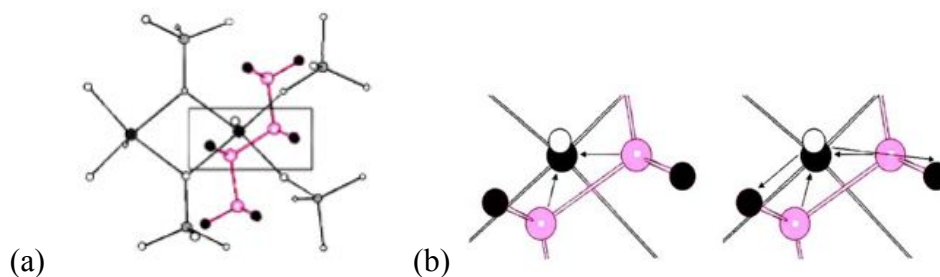


Figure 2.9: (a) Electrostatic alignment of *n*-butane at the surface (b) Acid and acid-base attack on *n*-butane by vanadium at the $(VO)_2P_2O_7$ surface (Thompson *et al.*, 2003)

MA, the selective oxidation product is always more electronegative than the clusters, hence, any covalent interaction will proceed via base attack from the surface of catalyst on acid sites in MA. Figure 2.10 has shown the two alternative orientations for electrostatic alignment of MA at the open active site. $=C-H$ hydrogens and $C=O$ oxygens are the sites of highest positive and negative charge, respectively. If the MA with the orientation as shown in Figure 2.10 (a), the local acid sites, $C=C$ is shielded from surface base sites. The electronegativity gradient prevent electron transfer from $C=O$ to vanadium. However, if MA with the orientation as shown in Figure 2.10 (b), electron donation from surface $P-O$ oxygens and vanadium to the $C=C$ carbons may initiate covalent chemisorptions. Fortunately, orientation as shown as in 2.10 (a) is what results from a chelating mechanism for *n*-butane oxidation as reported by Chen and Munson (2002). Hence, MA, once formed at the active site, will not be further transformed. If, however, it subsequently re-approaches the surface, MA may be re-absorbed in an orientation Figure 2.10 (b) which permits its degradation. Therefore, high level of conversion is usually undesirable due to the vulnerability of the selective oxidation product to further transformation.

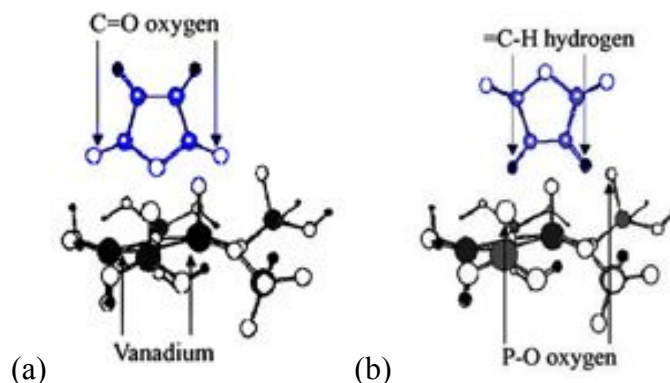


Figure 2.10: Two alternative orientations for electrostatic alignment of MA at open active site (Thompson *et al.*, 2003)

Infrequently, few chemicals other than MA and CO_x have been detected under commercial reaction conditions. Cavani and Trifiro (1994) has proposed a series of elementary steps and intermediates via steady-state and transient experiments as shown in Table 2.1. However, desorption of the intermediate is unlikely to occur during *n*-butane oxidation is attributed to the fast reaction rates of the elementary steps following *n*-butane activation (Centi *et al.*, 1984).

Table 2.1: Proposed elementary steps in the oxidation of *n*-butane to MA (Cavani and Trifiro, 1994)

Steps of reaction	Type of reaction
<i>n</i> -butane \rightarrow butenes	oxidative dehydrogenation
butenes \rightarrow butadiene	allylic oxidation
Butadiene \rightarrow 2,5-dihydrofuran	1,4-oxygen insertion
2,5-dihydrofuran \rightarrow furan	allylic oxidation
furan \rightarrow γ -butyrolactone	electrophilic insertion
γ -butyrolactone \rightarrow MA	electrophilic oxygen insertion

There are two mechanism path ways for the formation of CO_x , non-selective by products of *n*-butane oxidation (Figure 2.11), either by direct

combustion of *n*-butane or by the consecutive combustion of surface intermediates and/or MA (Centi *et al.*, 1989a; Bej and Rao, 1991 and 1992a).

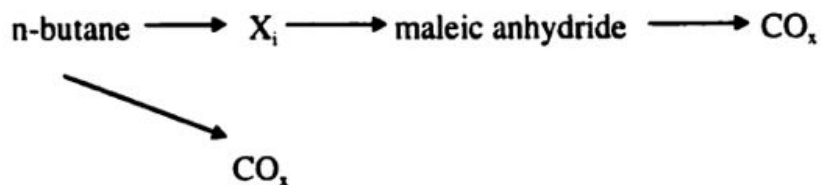


Figure 2.11: A simple non-selective reaction pathway for *n*-butane oxidation to CO_x (Centi *et al.*, 1989a)

2.2.3 Role of oxygen

The primary role of vanadyl pyrophosphate is to oxidise *n*-butane by removal of hydrogens from and the insertion of oxygens onto the four carbon chain. Thus, it is important to understand the types of oxygens involved in the complex nature of the redox mechanism, what the role of each is and how various factors affect them in order to completely understand the catalyst.

In very earlier, the activation of oxygen on metal oxides have been characterised and the mechanism has been proposed as shown in Figure 2.12 (Che and Tench, 1982). The gas phase oxygen first chemisorbs to form an activated species, [O_a], irreversibly. This species can become molecular surface species such as O₂²⁻ or O₂⁻, or dissociative adsorbed as monoatomic anions such as O²⁻ or O⁻. O⁻ and O₂⁻ species are known to be very reactive in the oxidative dehydrogenation and activation of lower alkane (Kung, 1986). Then the

chemisorbed oxygen may either react with the hydrocarbon or it may replenish the surface oxygen, surface lattice oxygen $[O_s]$. Surface lattice oxygen can continue to replenish the bulk oxygen $[O_l]$, or reacts with the hydrocarbon. The surface layer and bulk oxygen, together form the lattice oxygen of catalyst (Che and Tench, 1982).

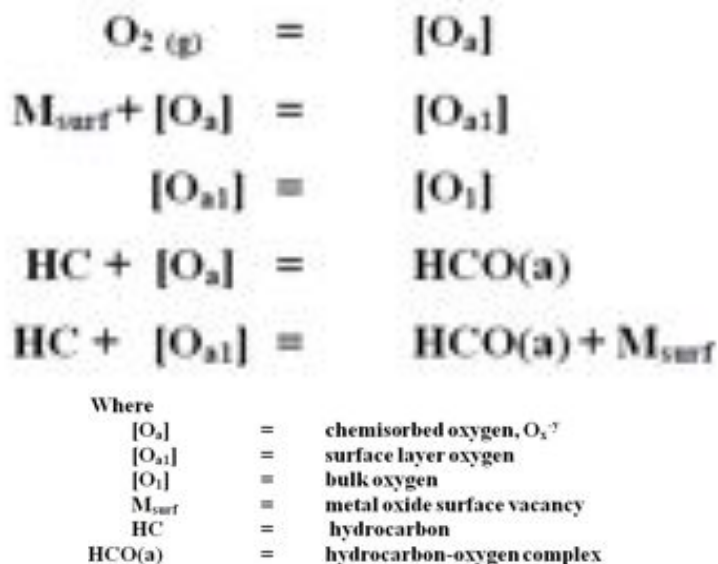


Figure 2.12: Activation of oxygen over metal oxides (Che and Tench, 1982)

On the other hand, Ebner and Gleaves (1988) have focused on determine the roles of lattice and surface oxygen in the selective oxidation of *n*-butane via temporal analysis of products (TAP) reactor. And they have proposed that the initial activation is performed by surface oxygen, while the intermediate oxidation steps are performed by lattice oxygen.

Herrmann *et al.* (1997) have make use of electrical conductivity measurements and proposed that O^- and O^{2-} are associated with V^{4+} and V^{5+} . He

also further proves that $V^{4+}-O^-$ pair as possible reactive oxygen species responsible for *n*-butane activation. This has been later supported by several papers, i.e. Abon *et al.* (2001), Taufiq-Yap (2006) and Taufiq-Yap *et al.* (2006a; 2011a; 2011b) also. On the other hand, Coulston *et al.* (1997) has claimed that $V^{5+}-O$ species is responsible for the rate of MA formation directly. And other literatures also support that $V^{5+}-O$ species is important in determine the selectivity of catalyst (Centi *et al.*, 1988; Granados *et al.*, 1993; Taufiq-Yap *et al.*, 2006b; Taufiq-Yap *et al.*, 2011a).

In the analysis of reactive sites on vanadyl pyrophosphate from Thompson *et al.* (2003), surface $V=O$ acting as both the active local base and local acid site to have attack on *n*-butane. Nevertheless, surface $P-O$ oxygen species exhibit only electron donor properties, which make it, show a significant basicity and nucleophilic properties. They may provide a source of selective oxygen species for $C-H$ rather than $C-C$ cleavage in post-activation steps. This may explain why surface enrichment in phosphate is necessary for selective vanadyl pyrophosphate. However, neither $V-O-V$ nor $V-O-P$ oxygens show reactivity.

2.2.4 Active sites

The presence of crystallographic plane of $(VO)_2P_2O_7$, which responsible for the MA formation has been observed through all characterization techniques. The representation of truncation for the model of the catalyst surface has

depended on the researchers and also the crystallographic database that has been used as reference, such as Joint Committee of Powder Diffraction (JCPDS) files or Inorganic Crystal Structure Database (ICSD) (Cavani and Trifiro, 1994).

By synthesising $\text{VOHPO} \cdot 0.5\text{H}_2\text{O}$ in alcoholic solvents under certain conditions, crystal with plate-like morphology having the (0 0 1) facet exposed are formed. The topotactic dehydration results in $(\text{VO})_2\text{P}_2\text{O}_7$ with the (0 2 0) facet of the resulting plate-like crystallite being the major crystal facet exposed, the VOHPO_4 layers are hydrogen bonded via HPO_4^{2-} groups initially in precursor phase become covalently bonded via pyrophosphate ($\text{P}_2\text{O}_7^{4-}$) groups (Johnson *et al.*, 1984). (0 2 0) facet of $(\text{VO})_2\text{P}_2\text{O}_7$ has presented in Figure 2.13. Thus, it has been widely accepted that the best performance of $(\text{VO})_2\text{P}_2\text{O}_7$ is directly related to the presence and extent of exposed (0 2 0) facets, which is related to the (0 0 1) facet of $\text{VOHPO} \cdot 0.5\text{H}_2\text{O}$.

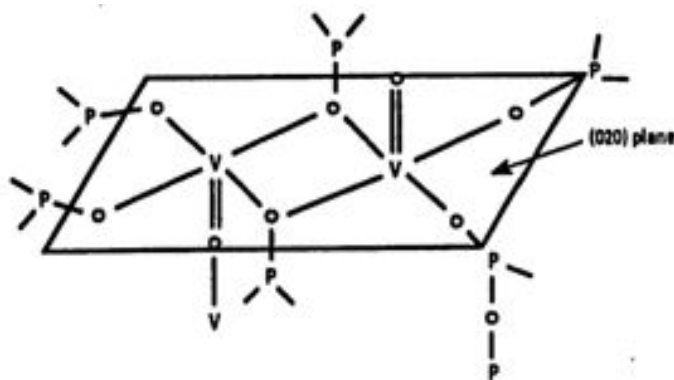


Figure 2.13: Projection of crystal structure of $(\text{VO})_2\text{P}_2\text{O}_7$ along the (0 2 0) plane (Busca *et al.*, 1986a; Centi *et al.*, 1989b)

Borders (1987) has suggested that the coherent interface between the slabs of (1 0 0) planes of VOPO_4 phases and the (1 0 0) planes of the $(\text{VO})_2\text{P}_2\text{O}_7$ along

the (0 0 1) and (2 0 1) planes is the active sites for *n*-butane to MA. However, Bergeret *et al.* (1987), reported that a mixture of well-crystallized $(VO)_2P_2O_7$ and an amorphous $VOPO_4$ phase is the active phase for selective oxidation of *n*-butane regardless the interfacial plane of different phases. Centi *et al.* (1988) also attributed the activity of the VPO catalysts in *n*-butane oxidation to vanadyl pyrophosphate, whereas the selectivity to MA was connected to the presence of very limited and controlled amount of V^{5+} sites, which has been proposed as being the (2 0 0) plane (Figure 2.14 (b)). The ratio of intensities of interlayer (2 0 0) to in-plane (0 2 4) reflections in the XRD patterns of $(VO)_2P_2O_7$ catalysts also show that $(VO)_2P_2O_7$ present a high exposure of the (2 0 0) plane. Later on, Batis *et al.* (1991) have reported that the V^{5+} phases are γ - $VOPO_4$ and β - $VOPO_4$ (Figure 2.14 (b)).

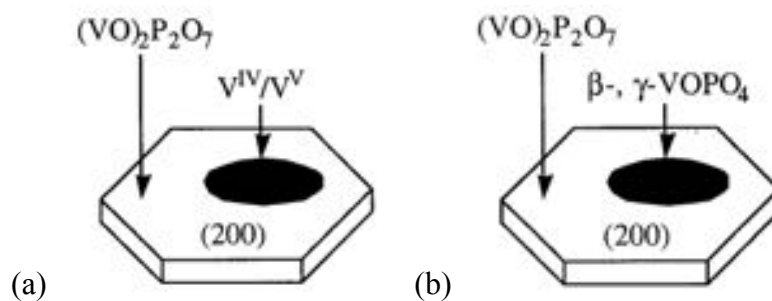


Figure 2.14: Active crystal facets according to (a) Centi *et al.* (1988) and (b) Batis *et al.* (1991)

Zhanglin *et al.* (1994) have also compared the equilibrated $(VO)_2P_2O_7$ with basically V^{4+} phase and non-equilibrated VPO catalysts with disordered $(VO)_2P_2O_7$, i.e. V^{4+} phase with some residual V^{5+} phases. And they find out that, the presence of V^{5+} phases on V^{4+} phase favours the *n*-butane transformation to

MA. Ait-Lachgar *et al.* (1998), estimated that the optimal V^{5+}/V^{4+} ratio would be around 0.25, i.e. one V^{5+} site for every four V^{4+} sites.

Misono (2002) has proved that the crystal plane which is active for selective oxidation is the (1 0 0) basal plane of $(VO)_2P_2O_7$ where V–O–V pair sites are located and that the side planes are non-selective, as illustrated in Figure 2.15. Additionally, Gulianti *et al.* (1995; 1996) has further suggested that well-ordered stacking of the (1 0 0) plane is the only VPO phase that responsible for highly selective MA formation.

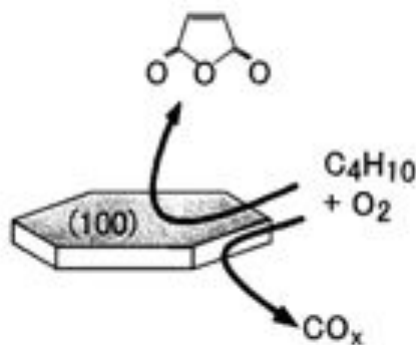


Figure 2.15: Selective and non-selective crystal faces of $(VO)_2P_2O_7$ (Misono, 2002)

The acidity of the catalysts surface has been considered to be important because the initial C–H cleavage on *n*-butane needs the cooperation between a Lewis acid site (V^{4+}) and an acidic Brønsted site (P–OH). This infrared study can be carried out by using the adsorption of ammonia, pyridine and acetonitrile on the Lewis and Brønsted site. A correlation was observed between the selectivity

to MA and the number of strong Lewis acid sites (Busca *et al.*, 1986b; Cornaglia and Lambardo, 1993).

2.3 Recent approaches to the improvement of the catalytic performance

Catalytic behavior of $(VO)_2P_2O_7$ varies according to their composition (*e.g.* P/V atomic ratio or oxidation state of V), synthesis and preparation procedure (*e.g.* hemihydrates, dehydrate or sesquihydrate route), calcinations procedure (*e.g.* in N_2 flow or *n*-butane/air), addition of dopant(s), and etc. Due to the dissatisfaction of selectivity to MA that can be provided by commercial catalyst currently (*i.e.* 53 to 65% molar yield to MA with 85% to 86% conversion of *n*-butane), intensive effort has been given to improve the catalytic performance of $(VO)_2P_2O_7$ according to the sensitivity of $(VO)_2P_2O_7$ to the synthetic route and reaction environment (Ballarini *et al.*, 2006).

2.3.1 Modification of precursor routes

In general, hemihydrates $(VOHPO_4 \cdot 0.5H_2O)$ route is the most studied and conventional preparation method for $(VO)_2P_2O_7$. There are many ways of preparing $VOHPO_4 \cdot 0.5H_2O$, and three typical designed aqueous routes (VPA), organic routes (VPO) and dihydrate routes (VPD) are shown in Figure 2.16

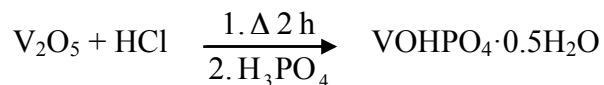
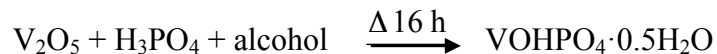
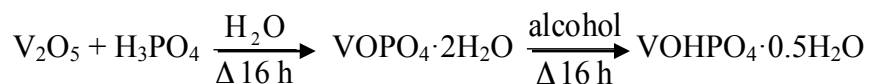
VPA route**VPO route****VPD route**

Figure 2.16: Three main methods for preparation of $\text{VOHPO}_4 \cdot 0.5\text{H}_2\text{O}$
(Hutchings, 2004)

In the aqueous route, V_2O_5 is reduced by mineral agent such as HCl and N_2H_4 in water and phosphoric acid. The morphologies of catalytic materials comprise mainly crystalline VOPO_4 (Hutchings, 2004). On the other hand a hydrothermal processing which involves the chemistry of hot water under pressure to carry out precipitation reactions has been reported. $\text{VOHPO}_4 \cdot 0.5\text{H}_2\text{O}$ is prepared by a mixture of vanadium pentoxide, *ortho*-phosphoric acid, water and oxalic acid, which was sealed in a stainless steel container then heated in an autoclave. The catalyst produced is less reactive as compared to other method (Taufiq-Yap *et al.*, 2006c).

The catalysts derived from the VPO route with isobutanol/benzyl alcohol as reducing agents, then activated under *n*-butane/air mixture is used in the commercial line (Cornaglia *et al.*, 1999). Additionally, various other organic compounds have been tried by researchers to have an improved catalytic material. Such as 2-butyl alcohol which also gives $\text{VOHPO}_4 \cdot 0.5\text{H}_2\text{O}$ (Johnson *et al.*, 1984).

The synthesis done in the presence of aliphatic alcohols leads to the development of vanadyl alkylphosphates where the basal (0 0 1) plane is similar to that of $\text{VOHPO}_4 \cdot 0.5\text{H}_2\text{O}$ (Kamiya *et al.*, 2003). When instead aldehydes or ketones are used, the product of $\text{VO}(\text{H}_2\text{PO}_4)_2$ is formed rather than $\text{VOHPO}_4 \cdot 0.5\text{H}_2\text{O}$ (Bartley *et al.*, 2000). An alternative route to the organic route is to reduce $\text{VOHPO}_4 \cdot 2\text{H}_2\text{O}$ by alcohols to $\text{VOHPO}_4 \cdot 0.5\text{H}_2\text{O}$ has been reported (Ellison *et al.*, 1994). Or $(\text{VO})_2\text{P}_2\text{O}_7$ also can be directly obtained from $\text{VOPO}_4 \cdot 2\text{H}_2\text{O}$ precursor after activation in 1.5% *n*-butane/air (Bartley *et al.*, 2001). Calcination of all these precursors lead to $(\text{VO})_2\text{P}_2\text{O}_7$, but none of the catalysts obtained performs as well as that of derived from conventional procedure, which gave ~75% of *n*-butane conversion and ~67% MA selectivity (Ballarini *et al.*, 2006).

The method to obtain sesquihydrate precursor, $\text{VOHPO}_4 \cdot 1.5\text{H}_2\text{O}$ by reducing $\text{VOPO}_4 \cdot 2\text{H}_2\text{O}$ in the less reductive but more environmental friendly 1-butanol is designed by Matsuura *et al.* (1995). According to Ishimura *et al.* (2000), a higher specific activity was achieved by the bulk catalyst derived from sesquihydrate route as compared to that of from hemihydrate route even though with a lower surface area. The layer structure of sesquihydrate with wide spacing capable of intercalating additives appears of benefits for preparing improved catalysts (Ishimura *et al.*, 2000; Leong *et al.*, 2011).

2.3.2 Introduction of novel processes in the precursor preparation

Some novel processes in the precursor preparation has been applied to increase the surface area of catalyst and so the catalytic performance. One of the methods is the mechanochemical treatment. Best results were achieved by Zazhigalov *et al.* (1997; 1998) with the use of the high intensity ball mill. Under a repeated fracture of solid, it takes only short time to increase the specific surface area of catalyst. This observation was agreed by Hutching and Higgins (1997) and Faith *et al.* (2000), and Taufiq-Yap *et al.* (2006a). The decreased of surface area have been proved would improve the catalytic properties of $(VO)_2P_2O_7$.

Microwave Irradiation has been shown to be a promising method to modify the texture and the morphology of catalysts due to its heating characteristic (Roussy *et al.*, 1994). The catalysts prepared with microwave irradiation are generally smaller compared with the one prepared in conventional heating along (0 2 0) and (2 0 4) planes, which enhance the selectivity of the catalyst (Taufiq-Yap *et al.*, 2007b).

Similar to microwave irradiation, ultrasound treatment is an alternative technique, which is capable of generating catalyst in a faster and cost effective manner. It enhances the chemical reaction and mass transfer via the process of acoustic cavitation. Pillai *et al.* (2003) found that ultrasound irradiation method

generates a catalyst in a relative shorter time of 6 h that has similar surface composition and comparable hydrocarbon oxidation activity with that prepared by conventional heating method. Taufiq-Yap *et al.* (2009) has also reported that an exposure of V_2O_5 to high intensity ultrasound irradiation under ambient air for a rather shorter time, i.e. ~30 min to 240 min, nanorod V_2O_5 can be produced to give a ~94% of *n*-butane conversion but a low MA selectivity.

A unique method to form delaminated sheets of layered materials has been proposed from the view point of constructing nanostructured materials, i.e. exfoliation of $VOPO_4 \cdot 2H_2O$ in various alcohols and subsequent reduction of exfoliated $VOPO_4$ sheets with alcohol to form $VOHPO_4 \cdot 0.5H_2O$. The catalyst produced has a smaller dimensions of the crystallites and the preferential exposure of the basal plane of $(VO)_2P_2O_7$ with ~78% selectivity to MA at 60% conversion at 663 K (Okuhara *et al.*, 2002; Yamamoto *et al.*, 2002; Hiyoshi *et al.*, 2004; Imai *et al.*, 2007).

Besides, ordered mesoporous metal oxides obtained in the presence of surfactant arrays and block copolymers are highly promising catalytic systems because of their high surface areas and enhanced rates of molecular transport of reactants and products. Carreon *et al.* (2004) have proposed two-step postsynthesis treatment, i.e. Soxhlet extraction and thermal activation in reducing atmosphere at 673 K to remove most of the template occluded on the mesopores of VPO phases. Resultant high surface area (~250 m^2g^{-1}) is produced with high selectivity but low conversions because the catalyst transformed under catalytic reaction conditions into various dense VPO phases.

2.3.3 The Control of P/V Atomic Ratio

It is well known that phosphorus plays an important role in the VPO catalysts although Geem and Nobel (1987) proposed that there is no correlation between the P/V atomic ratios with the catalytic activity (Centi *et al.*, 1988). The best industrial catalysts always have phosphorus to vanadium atomic ratios (P/V) slightly higher than unity (Centi, 1993; Bordes, 1993).

Some studies have emphasised the importance of the P/V atomic ratio in determining selectivity. High P/V atomic ratios are reported to enhance selectivity by stabilizing the +4 oxidation number of V. It appears that a large concentration of V^{+4} phase favours the MA selectivity (Nakamura *et al.*, 1974; Hodnett *et al.*, 1983). There are two reasons have been proposed to explain this: (i) the excess surface P may form pockets around the vanadium dimmers which creates an isolated sites for the production of MA (Ebner *et al.*, 1991; Thompson and Ebner, 1992), and (ii) the PO_4 groups may form “fence post” that prevent surface diffusion of partially oxidised carbon adspecies, or that block non-selective site which prevent overoxidation of alkane (Grasselli, 1983). Garbassi *et al.* (1986) studied a series of catalyst with P/V from 0.93 to 1.28 that produced via VPA route. They found the presence of V^{5+} phases i.e. β - VPO_5 was observed only for those with $P/V < 1$, whereas excess of P prevent the complete oxidation of V^{4+} to V^{5+} during calcinations in air. The finding of their work is in agreement with Hodnett *et al.* (1983).

Hutchings and Higgins (1996) have observed that on the surface of a well crystallized $(VO)_2P_2O_7$ with bulk $P/V = 1-1.2$, surface enrichment of P results in surface $P/V \sim 2$. Thus, $(VO)_2P_2O_7$ with $P/V \geq 2$ have been of interest among researchers. Catalysts with $P/V \geq 2$ can be derived from $VO(H_2PO_4)_2$ precursors. By using evaporation method, Morishige *et al.* (1990) obtained a catalyst with minor activity with 64.5% selectivity to MA. Sananes *et al.* (1995) and Hutchings *et al.* (1997) reported the VPD-derived catalyst that using 3-octanol as reducing agent leads to formation of $VO(H_2PO_4)_2$, gave 100% selectivity to MA at very low conversion, whereas Gulianti *et al.* (1996) found the VPA-derived catalyst to be completely inactive for *n*-butane oxidation. Wang *et al.* (2000), has used the same method as Sananes *et al.* (1995) to produce a catalyst with $P/V \sim 2$ and three times of recrystallization was applied to produce a catalyst with $P/V \sim 2.4$. The catalyst with $P/V \sim 2$ was poorly crystalline, whereas the catalyst with $P/V \sim 2.4$ was well crystalline but it deactivated with the time-on-stream with the formation of $V(PO_3)_3$. A amorphous as well as partly crystalline $VO(PO_3)_2$ catalyst with $P/V = 2$ was synthesized by Hannour *et al.* (1998) through $VO(H_2PO_4)_2$ precursor gave a lower *n*-butane and MA selectivity as compared to $(VO)_2P_2O_7$. This may due to the polyphosphate catalysts inhibit the rate of reoxidation, leading to a higher concentration of electrophilic oxygen species which results in increasing total oxidation.

2.3.4 Addition of Dopants

The use of dopants represents the most promising approach for improvement of the catalytic performance of VPO (Ballarini *et al.*, 2006). Hutchings (1991) points out two different structural roles played by dopant: (i) they allow the formation of the required VPO components while impairing the appearance of the “deleterious phase” and (ii) they participate in solid solutions which regulate the catalytic properties of the $(VO)_2P_2O_7$ formulations. The addition of dopants into $(VO)_2P_2O_7$ systems have been tried in various precursor routes with different technique.

Mg, Ca and Ba ions from chloride salts is doped into catalyst and provide a higher conversion of *n*-butane and selectivity as compared to unmodified catalyst that derived from VPA route. Conversion of *n*-butane was decreased in the order of Mg, Ca, Ba, however, the selectivity to MA increases with the basicity of dopants (Brutovsky *et al.*, 1997). Addition of multi-dopants via VPA route has been reported by Xu *et al.* (2002), they are Mo, Zr and Zn, which showed a high MA selectivity at fair *n*-butane conversion.

Xu and his co-workers have again tried to introduce Mo, Zr and Zn into catalyst via VPO route with mechanochemical treatment, i.e. ball milling, which show a notable increase in surface area and generate additional ca. 10 mol% MA yield (Ji *et al.*, 2002). Similarly, Bi-Fe bi-dopants were added into catalyst via

VPD routes by Goh *et al.* (2008) with mechanochemical treatment. But BiFe modified catalysts gave poor catalytic performance. Ce-Fe bi-dopants was pre-precipitation in a pH = 10 aqueous solution then only added into catalyst by Shen *et al.* (2002) via VPO route, which gave a higher amount of lattice oxygen and higher conversion and MA selectivity than that of undoped catalyst. Besides, Bej and Rao (1992b) has studied the simultaneously addition of Mo and Ce, and reported good yield of MA under severe operating condition as compared to undoped catalyst that derived from VPO route with mixture of allyl alcohol and isobutanol as reducing agent.

Abdelouahab *et al.* (1995) has used VPO route with single isobutanol reducing agent and reported that both Co and Fe from acetyl-acetate salt improve strongly selectivity to MA but conversion of *n*-butane is decreased for Co and increased for Fe. This has been explained by the different dispersion of VOPO₄ phases in the (VO)₂P₂O₇ matrix during the activation process. On the other hand, Taufiq-Yap (2006) has reported both Cr and Co from nitrate salt improve strongly the *n*-butane conversion without scarifying the MA selectivity MA via conventional VPO method. Co was added via conventional method by Cornaglia *et al.* (2003) too, but different modes of impregnation, i.e. at ambient temperature or at high temperature, and different salt i.e. acetate or acetyl acetate salts, was compared in their work. The best catalyst was obtained using Co acetyl acetate which impregnated at ambient temperature. Low Ga-doped of catalyst has been synthesised by Sartoni *et al.* (2004) via VPO route with different

Ga salts, $\text{Ga}(\text{acac})_3$ derived catalytic material gave a significant increase in surface area and enhanced activity as compared to that from Ga_2O_3 and GaPO_4 . Zazhigalov *et al.* (1996) studied alkaline and alkaline earth dopants to achieve a fine control of the acid-base properties of surface. However, their catalysts did not show a significant improvement in performance.

Hutchings and Higgins (1996) used a simple kinetic analysis to gauge the effect of a dozen elements upon the catalytic performance. Cr, Nb, Pd, Sb, Ru, Th, Zn and Zr were found to have a very little effect on specific activity, although with Cr, Zn and Zr a significant increase in surface area was observed. Fe, Cs and Ag were found to decrease significantly in specific activity. Only Co and Mo gave an increase in specific activity.

Co and Bi have been tried to be introduced in the catalysts through the sesquihydrate route too (Ishimura *et al.*, 2000; Leong *et al.*, 2011). As compared to the Co-doped catalyst produced by Hutchings and Higgins (1996) via the nonaqueous HCl hemihydrate route, the Co-doped catalyst produced via the sesquihydrate route has shown a better activity and selectivity to MA. Bi also gave a better catalytic performance.

2.3.5 The use of highly-heat-conductivity supports

One of the most significant improvements in *n*-butane oxidation has been reported by Ledoux *et al.* (2000), who studied the use of heat-conducting supports, i.e. β -SiC. The β -SiC-supported 30 wt% of active phase gave a significant gain in MA yield when used in a fixed-bed reactor, because of the better control of the catalyst surface temperature. The chemical inertness of the support did not modify the reactivity properties of the precursor and of the active phase.

Other than β -SiC, the conventional supports have been investigated include alumina, titania, silica, zirconia, ceria, niobium dioxide and etc (Wachs *et al.*, 1997; Taufiq-Yap *et al.*, 2007a; Martinez-Lara *et al.*, 1992; Overbeek *et al.*, 1996a; Overbeek *et al.*, 1996b; Feng *et al.* 2007). The use of highly-heat-conductivity supports have claimed to give catalyst a(n): (i) high attrition resistance for the use in fluidised-bed reactor due to better mechanical strength, (ii) controllable texture leading to decrease internal and external mass-transfer limitation, (iii) enhanced life-time due to better heat transfer character, (iv) easier adaptation of catalyst properties to the desired behavior, (v) larger surface area to volume ratio of active compound, and (iv) easily investigation without the complex contribution from bulk system (Harding *et al.*, 1994; Overbeek *et al.*, 1996a; Nie *et al.*, 2001; Li *et al.*, 2006a; Bueno *et al.*, 1988).

The earliest studies of supported VPO catalysts was reported by Nakamura *et al.* (1974), who investigated alumina-supported VPO catalyst for 1-butene oxidation. They found that the MA selectivity was increased with P/V atomic ratio to maximum with the oxidation number of +4. The support oxide interactions can strongly affect the formation of VPO phases, which tends to hinder the crystalline formation. Nevertheless, most supported VPO catalysts are reported to consist mainly V^{5+} phosphates (Overbeek *et al.*, 1996a). Titania-supported VPO was found to be active at moderate temperature (i.e. 523 K), but the selectivity is low due to the strong oxide interactions. However, silica-supported VPO catalysts showed a reasonable yield (Overbeek *et al.*, 1996a; Overbeek *et al.*, 1996b). A few studies about the silica-supported VPO catalysts which have been reported are summarized in the following part of this section.

Zazhigalov *et al.* (1986) prepared immobilized VPO/SiO₂ catalysts by adsorption onto the silanol groups of the silica surface of VOCl₃/POCl₃ in a CCl₄ environment. The catalysts were not well characterized, but the selectivity is increased with P/V atomic ratio to 23% (P/V = 1.8), beyond which the formation rate decreased.

Martinez-Lara *et al.* (1992) investigated both titania- and silica- supported VOPO₄ catalysts. Strong VPO/titania interaction produce highly dispersed amorphous VPO phase, which gave exclusively to CO₂ during the catalytic tests. On the other hand, no interaction was found between the VPO and silica supports,

which exhibited crystalline VOPO_4 but low conversion of *n*-butane. Overbeek *et al.* (1996a; 1996b) used deposition-precipitation V^{3+} ions, has also reported the use of silica instead of titania support enhanced the MA selectivity in *n*-butane oxidation, but decreased the activity.

Li *et al.* (2006a; 2006b), have studied SBA-15, MCM-41 and fumed SiO_2 supported VPO catalysts using desorption-precipitation method, all the samples present predominantly in the form of well-crystallised $(\text{VO})_2\text{P}_2\text{O}_7$ phase, and the VOPO_4 -like phase were absent. The severe structure disorder of the VPO component on fumed SiO_2 gave more lattice defects that leads to the higher catalytic activity. The activity can be ranked as $45\%\text{VPO}/\text{fumed SiO}_2 > 45\%\text{VPO}/\text{MCM-41} > 45\%\text{VPO}/\text{SBA15}$. Xiao *et al.* (2004) and Zhou *et al.* (2004) have also produced fumed SiO_2 supported VPO catalysts with the addition of polyethylene glycol via hemihydrate route. Their catalysts gave a higher conversion, i.e. 33–40%, and higher MA selectivity, i.e. 87–65 mol% as compared to that of Li *et al.* (2006b), i.e. 13% and 23 mol%, respectively.

Al-MCM-41 and large pore silica supported VPO catalysts were produced by Nie *et al.* (2001; 2003). Al-MCM-41 supported VPO catalysts exhibited a remarkable enhancement in MA selectivity with slight decrease in *n*-butane conversion, which might due to the unique interaction that has involved.

Bueno *et al.* (1998) have used hydrophilic silica i.e. VPO/SiO₂-OH and hydrophobic silica i.e. VPO/SiO₂-CH₃ to study the effect of nature of silica support on the catalytic properties. They found the hydrophobic silica interacts less strongly with VPO than hydrophilic silica does, and the transformation of the VPO phases on its surface is more similar to the unsupported catalyst. Crystalline (VO)₂P₂O₇ can be formed on a hydrophobic silica. However, the MA selectivity depends much more strongly on the P/V ratio than on the method of preparation. That is the highest selectivity achieved when the P/V atomic ratio is ~2.

2.3.6 The effect of Calcination Duration /Condition

Transformation of precursor to the active phase can be affected by the temperature, time and atmosphere of calcination process. A “non-equilibrated” catalyst known as “fresh” catalyst if the precursors calcined for a period less than 100 h, while a calcinations time more than 1000 h will yield the “equilibrated” catalysts, which are thermodynamically more stable under usual reaction conditions. The transformation of the precursor to (VO)₂P₂O₇ occurs according to two routes: (i) A direct epitaxial transformation along the (0 0 1) and (2 0 1) facets planes leading to the development of a pyrophosphate fringe at the edge of the precursor crystallite; (ii) An indirect transformation occurring in the interior of the precursor leading first to δ -VOPO₄ which then leads to (VO)₂P₂O₇ (Abon and Volta, 1997; Taufiq-Yap *et al.*, 2001).

Hodnett and Delmon (1985) have investigated the influence of calcinations temperature on the formation of phases in catalyst that produced via VPA route and calcined under a flow of air. The catalyst with excess P strongly stabilises the +4 oxidation of vanadium either at 773 K or 923 K. However, the catalyst with low P/V atomic ratio favours the formation of β -VPO₅ and resulted in lower surface area at high temperature. A catalyst promoted by Iridium and tetraorthosilicate via VPO route was calcined in air, N₂ and CO₂, respectively. The calcination in air at 723 K has lead to mainly VOPO₄ phase. However, calcination in CO₂ and air lead to the formation of crystalline (VO)₂P₂O₇ phase. Its crystallinity increases with temperature and with decreasing oxidizing strength of the calcinations atmosphere (Cheng and Wang, 1997).

Furthermore, hemihydrate precursor which derived from VPD has been calcined in two different hydrocarbon reaction environments, i.e. *n*-butane/air and propane/air, and denoted as VPDB and VPDP, respectively. Both revealed a good crystalline with characteristic peaks of (VO)₂P₂O₇ in XRD. However, VPDB gave a higher surface area, higher amount of V⁵⁺ phases, better characteristic rosette-shape morphology and higher amount of V⁴⁺-O²⁻ which eventually lead to a better conversion rate in selective oxidation of *n*-butane (Taufiq-Yap and Saw, 2008).

Three catalysts that derived from hemihydrate precursors via VPO route were prepared in different length of calcination time, i.e. 40, 100 and 132 h under

a flow of 0.75% *n*-butane/air. The surface areas and the amounts of oxygen removed in the TPR analyses were directly proportional to the length of calcination time. Conversely, the amounts of oxygen desorbed in the TPD analyses were decreased with the length of calcination time. This can be explained by the different transition state required for the thermal evolution of O₂ compared with that for H₂ reduction of the surface (Taufiq-Yap *et al.*, 2001).

Another series of catalysts that derived from sesquihydrate precursors were also calcined in a reaction flow of 0.75% *n*-butane/air for 10, 30 and 75 h, respectively. The results are in contrast with the catalysts prepared by VPO route. The surface areas and the amounts of removed oxygen were decreased with the length of calcinations time. And the amount of oxygen desorbed was increased as the period of calcination increased (Taufiq-Yap *et al.*, 2004).

2.3.7 The influence of the reaction atmosphere

The concentrations of *n*-butane used in industry are ordinarily about 1.5% and 4.0% for fixed-bed and fluidised-bed reactor, respectively. Most laboratory studies with VPO catalysts involve fixed-bed microreactors with very small sample sizes in order to maintain homogeneity of the reaction atmosphere in contact with the catalyst. Thus, it is necessary to avoid explosions at a fixed-bed reactor. From an industrial view point, the operation under a high *n*-butane

concentration makes it possible to achieve a higher space-time yield of MA (Kamiya *et al.*, 2001).

Two sets of experimental conditions were used by Mallada *et al.* (2000), namely oxidizing condition (2%*n*-butane/20%oxygen/78%He) and reducing condition (10%*n*-butane/15%oxygen/75%He). The results obtained indicate a more remarkable MA selectivity was exhibited in the oxidizing condition. This was explained by the pulse re-oxidation experiment that reduction of catalyst happened in the reducing condition leading to the appearance of V^{3+} phases, which causes a strong decrease in the MA selectivity.

Kamiya *et al.* (2001), have introduced three kinds of $(VO)_2P_2O_7$ catalysts with different shaped microcrystallite, i.e. rose-petal, plates and blocks, which denoted as catalyst A, B and C, respectively, under a wide range of *n*-butane concentration atmosphere (from 0.75% to 5.0%). Catalyst A gave a higher rate of *n*-butane oxidation and subsequently re-oxidation with O_2 among the catalysts. Additionally, the rate of MA formation increased over catalyst A as the *n*-butane concentration increased, while the rate of CO_x formation was independent of *n*-butane concentration.

By comparing both the hydrocarbon-lean condition (1.7%*n*-butane/17%oxygen/81.3%He) and hydrocarbon-rich condition (10%*n*-butane/17%oxygen/73%He), the conversion of *n*-butane under the latter one was

remarkable lower especially above 673 K. Under hydrocarbon-lean condition, the byproducts were only CO_x. However, in that of hydrocarbon-rich condition, acrylic and acetic acids, and tetrahydrophthalic and phthalic anhydride were found as well. In order to confirm the role of oxygen, hydrocarbon-rich tests with higher oxygen concentration (10%*n*-butane/25%oxygen/65%He) were carried out again by Ballarini *et al.* (2005). Consequently, a higher conversion and decreased of C₈ byproducts selectivity was obtained. Besides, MA selectivity was surprisingly found to be lowest at 623 K and increased gradually to 50% at 733 K. This gives the best yield of MA, which ever reported in literature for operation under *n*-butane rich conditions.

Based on the literatures, a suitable balance between (i) oxidizing sites, which are in charge for hydrocarbon transformation, and (ii) reducing sites, which activate molecular oxygen to replenish the anionic vacancies, was found to be the function of the ratio between the hydrocarbon (the reducing agent) and molecular oxygen (the oxidizing agent) in the gas phase (Ballarini *et al.*, 2005).

CHAPTER 3

MATERIALS AND METHODOLOGY

3.1 Preparation of Vanadyl Pyrophosphate Catalysts

Sesquihydrate route was employed in the current research due to the usage of more environmental friendly reducing agent as discussed in Chapter 2, i.e. 1-butanol. Chromium (Cr) was added as dopant with the expectation to enhance the catalytic performances. Besides, the application of silica as catalyst support would be employed too. The newly designed combination of modifications upon conservative method was hoped to give an improved catalytic performance.

3.1.1 Gases and Materials

The required gases and materials were listed in Table 3.1.

Table 3.1: Gases and materials for preparation of vanadyl pyrophosphate catalysts

		Brand	Purity/Size
Gases	<i>n</i> -Butane in air, <i>n</i> -C ₄ H ₆ /air	MOX	0.75%
Materials	vanadium(V) oxide, V ₂ O ₅	Merck	
	<i>ortho</i> -phosphoric acid, <i>o</i> -H ₃ PO ₃	Merck	85%
	chromium nitrate, Cr(NO ₃) ₃ ·9H ₂ O	Merck	
	silica, SiO ₂	Sigma-Aldrich	Davisil, grade 646, 35–60 mesh

3.1.2 Preparation of Bulk Catalysts

The undoped/unsupported vanadyl hydrogen phosphate sesquihydrate precursor, $\text{VOHPO}_4 \cdot 1.5\text{H}_2\text{O}$ was prepared via vanadyl phosphate dihydrate, $\text{VOPO}_4 \cdot 2\text{H}_2\text{O}$, as the intermediate product (denoted as VPO_s method) involving two stages of reflux. In the first stage (Figure 3.1), V_2O_5 (15.0 g) and $o\text{-H}_3\text{PO}_4$ (90 mL) were refluxed in distilled water (360 mL). The resulting yellow $\text{VOPO}_4 \cdot 2\text{H}_2\text{O}$ solid was recovered by centrifugation and oven-dried at 358 K for 72 h and finally identified by x-ray diffraction (XRD).

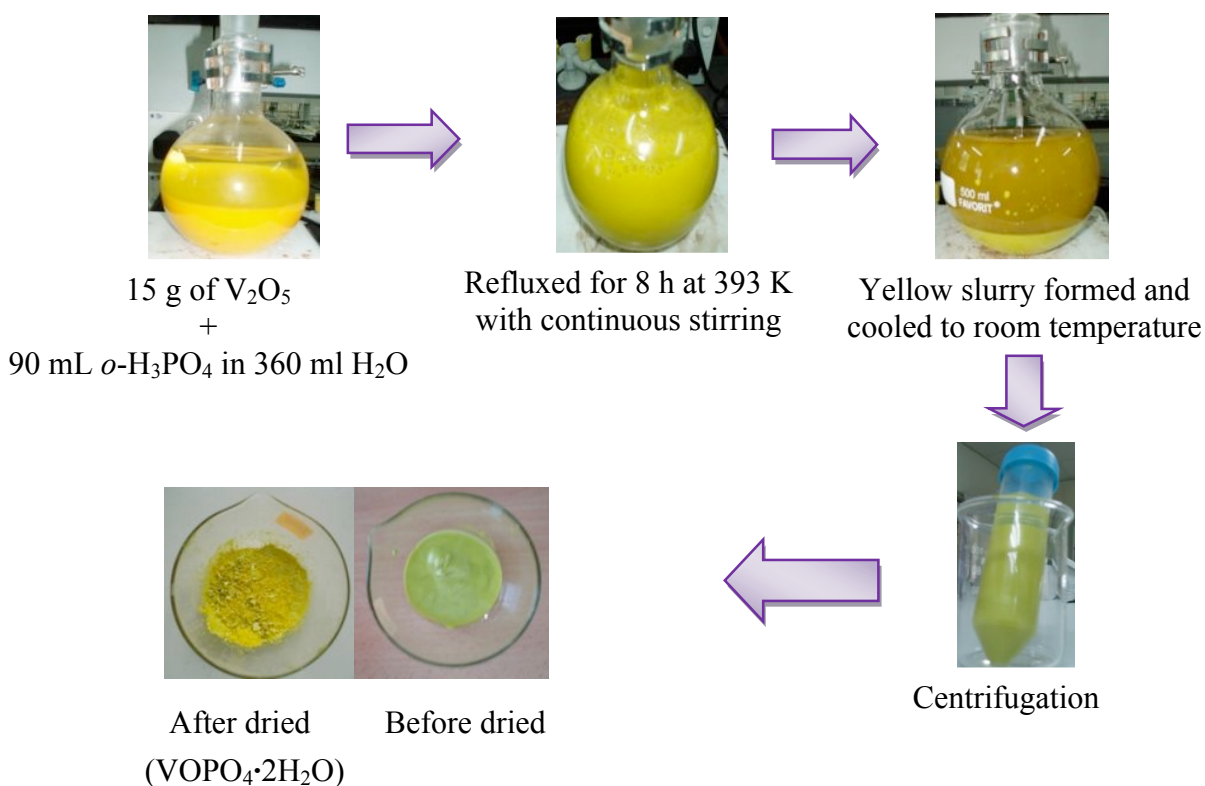


Figure 3.1: First stage of reflux (Preparation of $\text{VOPO}_4 \cdot 2\text{H}_2\text{O}$ intermediate)

In the second stage (Figure 3.2), the synthesised $\text{VOPO}_4 \cdot 2\text{H}_2\text{O}$ (10.0 g) was then refluxed in 1-butanol (150 mL) with continuous stirring at 393 K for 8 h and the resulting light blue solid, $\text{VOHPO}_4 \cdot 1.5\text{H}_2\text{O}$ precursor. This precursor was denoted as pre-undoped-VPO_s in first series, however, it was denoted as pre-unsupported-VPO_s in second and third series of samples in present research project.

The sesquihydrate precursor was calcined in a reaction flow of 0.75% *n*-butane in air mixture at 733 K for 18 h to generate the active catalyst, $(\text{VO})_2\text{P}_2\text{O}_7$ (Figure 3.2). This activated catalyst was denoted as undoped-VPO_s in first series, however, it was denoted as unsupported-VPO_s in second and third series.

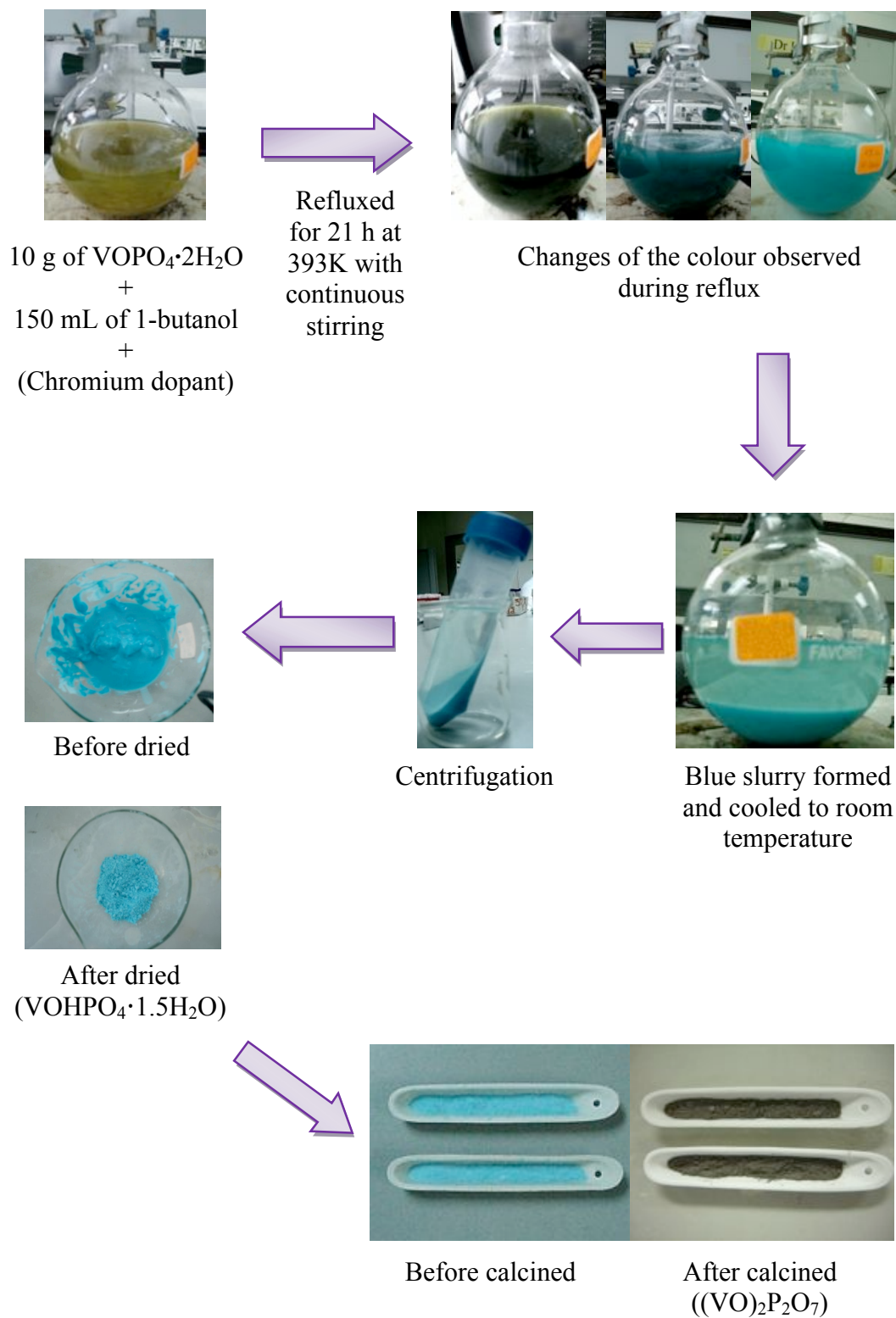


Figure 3.2: Second stage of reflux (Preparation of $\text{VOHPO}_4 \cdot 1.5\text{H}_2\text{O}$ precursor) and the activation of $(\text{VO})_2\text{P}_2\text{O}_7$

3.1.3 Preparation of Cr-doped Catalysts

The preparations of the Cr-doped precursors were similar to the preparation of undoped catalyst. Catalysts with different mole percentage, i.e. 1%, 3%, and 5% of Cr dopant would be prepared. In the second stage of reflux, the required mass of the $\text{Cr}(\text{NO}_3)_3 \cdot 9\text{H}_2\text{O}$ salt (mole ratio $\text{Cr/V} = 0.01, 0.03$ and 0.05) were dissolved in 1-butanol (Figure 3.2), prior to refluxing it with $\text{VOPO}_4 \cdot 2\text{H}_2\text{O}$. These Cr-doped precursors were denoted as pre- $\text{VPO}_s\text{-CrX\%}$ ($X = 1, 3, 5$). The activated Cr-doped catalysts after calcination at 733 K were denoted as $\text{VPO}_s\text{-CrX\%}$ ($X = 1, 3, 5$).

3.1.4 Preparation of Silica Catalysts

The preparations of the silica supported precursors were similar to the preparation of unsupported catalyst. Sesquihydrate precursors would be supported on silica with different weight percentage of precursors on silica, i.e. 5%, 10%, 15%, 20%, 25% and 30%. After the second stage of reflux, the required mass of the silica solid (weight percentage $\text{V/Si} = 0.05, 0.10, 0.15, 0.20, 0.25$ and 0.30) were mixed homogeneously with $\text{VOHPO}_4 \cdot 1.5\text{H}_2\text{O}$ precursors (Figure 3.3), called wetness impregnation that designed by Taufiq-Yap *et al.* (2007). These silica supported precursors were denoted as pre- $\text{X\%VPO}_s/\text{Si}$ ($X = 5, 10, 15, 20, 25, 30$). The activated silica supported VPO_s

catalysts was calcined for 6 h instead of 18 h as that for first series, because the comparative smaller amount of catalytic material on silica would be burnt in a prolonged calcination duration. After calcination, they were denoted as $X\%VPO_s/Si$ ($X = 5, 10, 15, 20, 25, 30$).



Figure 3.3: Wetness impregnation of $VOHPO_4 \cdot 1.5H_2O$ precursor onto silica support

In the last series of catalysts, similar to the previous series, the required mass of the silica solid (weight percent $V/Si = 0.30$) was mixed homogeneously with $VOHPO_4 \cdot 1.5H_2O$ precursor (pre-30% VPO_s/Si) through wetness impregnation. However, this silica supported precursor was calcined under various temperatures, i.e. 673, 733 and 793 K. The activated silica supported VPO_s catalysts after calcination were denoted as $TXVPO_s/Si$ ($X = 400, 460, 520$). Basically, 30% VPO_s/Si and T460 VPO_s/Si were the same catalyst.

3.2 Catalyst Characterisation

3.2.1 Gases and Materials

Table 3.2: Gases and materials for sample analyses

Methodology		Brand	Purity
BET surface area measurement			
Gases	purified nitrogen, N ₂	MOX	99.999%
	purified helium, N ₂	MOX	99.999%
Materials	liquid nitrogen, N ₂	MOX	
ICP-OES			
Materials	nitric acid, HNO ₃	Merck	69.0–70.0%
Redox titration			
Materials	sulphuric acid, H ₂ SO ₄	Merck	95–97%
	potassium permanganate, KMnO ₄	Fisher Scientific	
	ammonia dihydrogen orthophosphate, NH ₄ H ₂ PO ₄	Ajax chemicals	
	ammonium metavanadate, NH ₄ VO ₃	BDH Chemicals	
	ammonium iron(II) sulphate, (NH ₄) ₂ Fe(SO ₄) ₂ ·6H ₂ O	System	
	diphenylamine, (Ph) ₂ NH	Acros Organics	
TPD of O ₂			
Gases	purified oxygen, O ₂	MOX	>99.8%
	purified nitrogen, N ₂	MOX	99.999%
	purified helium, H ₂	MOX	99.999%
TPR in H ₂			
Gases	hydrogen in air, H ₂ /air	MOX	5.55%
	purified nitrogen, N ₂	MOX	99.999%

3.2.2 Instrumentation

3.2.2.1 X-ray Diffraction (XRD) Analyses

Catalyst is in a form of crystal structures that consist of planes in repetitive arrangements of atoms, which are capable of diffracting x-rays. The diffraction angles given by different planes are unique to each other. Broadening of the diffraction peaks can be used to estimate crystallite size. The crystallite size is given by Debye-Scherrer (Klug and Alexander, 1974):

$$t = \frac{0.89\lambda}{\beta_{hkl} \cos \theta_{hkl}}$$

where t is the crystallite size for $(h\ k\ l)$ phase; λ is the x-ray wavelength of radiation for $\text{CuK}\alpha$; β_{hkl} is the full-width at half maximum (FWHM) at $(h\ k\ l)$ peak; and θ_{hkl} is the diffraction angle for $(h\ k\ l)$ phase.

Shimadzu diffractometer model XRD-6000 Diffractometer (Figure 3.4) was used in the XRD characterisation. Catalysts were mounted on aluminium samples holder. Then, $\text{CuK}\alpha$ radiation generated by a glass diffraction x-ray tube (Toshiba, A-40-Cu) normal focus 2.0 kW type at 40 kV onto the catalyst, with wavelength range of 0.5–2 Å and scanned at the range of $2\theta = 2.0000\text{--}60.0000^\circ$ with a scanning rate of $1.2000^\circ\ \text{min}^{-1}$. Basal spacing was determined via powder technique. Subsequently, a diffractograms with diffraction patterns that produced by the $\text{CuK}\alpha$ radiation was obtained. Wavelength of x-ray is related to angle of

diffraction and spacing between atomic planes by Bragg's law (Bragg, 1913):

$$n\lambda = 2d \sin \theta$$

where n is the integer; λ is the x-ray wavelength of radiation; d is the spacing between atomic of the crystalline phase; and θ is the diffraction angle for phase. Eventually, the diffractograms obtained were match with the Joint Committee on Powder Diffraction Standards (JCPDS) PDF1 database version 2.6 to confirm the precursors and catalysts phases.



Figure 3.4: Shimadzu XRD-6000 diffractometer

3.2.2.2 Scanning Electron Microscopy (SEM)

The morphologies of catalysts were examined on Hitachi SU8000 FESEM. SU8000 (Figure 3.5) is featured with a top detector along with a semi-in-lens type of objective lens, which combined with the conventional upper detector technology to give an optimum contrast visualization of signal

generated from samples. A small amount of fresh catalyst was placed on the surface of a carbon tape, which had been fixed on an aluminium stub (diameter 10 mm). Then the catalysts were coated with gold with Sputter Coater. The captured images were saved in a computer, which linked to the scanning electron microscopy (SEM) machine and the morphologies of the catalysts were observed.



Figure 3.5: Hitachi SU8000 FESEM

3.2.2.3 Brunaur-Emmett-Teller (BET) Surface Area Measurements

The specific surface area of catalysts was measured by the Brunauer-Emmett-Teller (BET) method using Thermo Finnigan Sortomatic 1990 nitrogen adsorption-desorption analyser at 77 K (Figure 3.6). Prior to analysis, approximately 0.5 g of catalyst was degassed at 423 K for overnight for the pretreatment stage. The BET equation was used to determine the specific surface areas of the catalysts (Brunauer *et al.*, 1938):

$$\frac{p}{V(p_0 - p)} = \frac{1}{V_m C} + \frac{(C-1)p}{CV_m p_0}$$

where V is the volume, reduced to standard conditions, i.e. the standard temperature and pressure (STP) of gas adsorbed per unit mass of adsorbent at a given pressure, p and constant temperature; p_0 is the saturation pressure at the measurement temperature; V_m is the volume of gas required to form a complete monolayer adsorbed layer at STP per unit mass of adsorbent, when the surface is covered by a monolayer of adsorbate; and C is a constant related to free energy of adsorption which is represented by the equation below:

$$C = A_r \exp\left(\frac{(\Delta H_1 - \Delta H_2)}{RT}\right)$$

Where A_r is the pre-exponential factor; ΔH_1 is the heat of adsorption of the first layer; ΔH_2 is the heat of liquefaction; R is the gas constant; and T is the absolute temperature in Kelvin.



Figure 3.6: Thermo Finnigan Sorptomatic 1990

3.2.2.4 Chemical Analyses

The bulk chemical compositions were determined by inductively coupled plasma-optical emission spectrometry (ICP-OES) using a sequential scanning Perkin Elmer Optima 2000 DV optical emission spectrometer (Figure 3.7). A known amount of catalyst (0.025 g) was digested in 10 mL of 8 M HNO_3 with slight heating and continuous stirring. Except for silica supported catalyst, they were digested by means of microwave digester for 3 h at 473 K. The resulting solutions were diluted with deionised water to give nominal concentration of 100ppm.

Both the standard solutions of phosphorus and vanadium were prepared in concentrations 10, 20 and 30 ppm, respectively. The standard solutions of Cr were prepared in concentrations of 2.5, 5.0, 10, 20 and 30 ppm. Deionised water was used as a blank solution, i.e. the control. All the standard and blank solutions were added with 10 mL of 8 M HNO_3 in order to be consistent with the sample solutions, and then only be used in analyses.



Figure 3.7: Perkin Elmer Optima 2000 DV optical emission spectrometer

3.2.2.5 Redox Titration Analyses

Redox titration was used to determine the different valence states of vanadium according to the procedure developed by Niwa and Murakami (1982), which including V^{3+} , V^{4+} , and V^{5+} . This procedure was based on two stages. In the first stage, 0.1 g of catalyst was digested in the 2 M concentration H_2SO_4 . Then 20 mL of this solution was titrated by 0.01 N potassium permanganate, $KMnO_4$, end point achieved when greenish blue of solution change to pink color (Figure 3.8). V^{3+} and V^{5+} were oxidised to V^{5+} in this step. Volume of 0.01 N $KMnO_4$ used was recorded as V_1 . Then the same solution was continuous used to be titrated by 0.01 N ammonium iron(II) sulphate solution, $(NH_4)_2Fe(SO_4)_2 \cdot 6H_2O$ with diphenylamine as redox indicator. End point indicated by the changes of purple color to greenish blue (Figure 3.9). All the V^{5+} was converted into V^{4+} in this step. And the volume of 0.01 N $(NH_4)_2Fe(SO_4)_2 \cdot 6H_2O$ used was denoted as V_2 . In the second stage, a new 20 mL sample was titrated by 0.01 N $(NH_4)_2Fe(SO_4)_2 \cdot 6H_2O$ with diphenylamine as redox indicator. End point reached when purple color of solution changed to greenish blue (Figure 3.9). In this step, only V^{5+} that originally presented in the sample was reduced to V^{4+} . The volume of 0.01 N $(NH_4)_2Fe(SO_4)_2 \cdot 6H_2O$ required in second stage was denoted as V_2 (Niwa and Murakami, 1982).

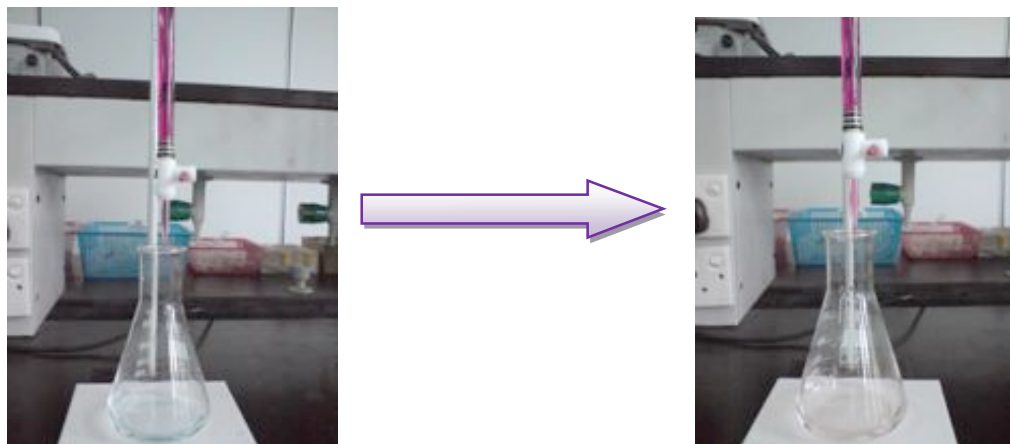


Figure 3.8: Colour changes when end point of titration of KMnO_4 reached

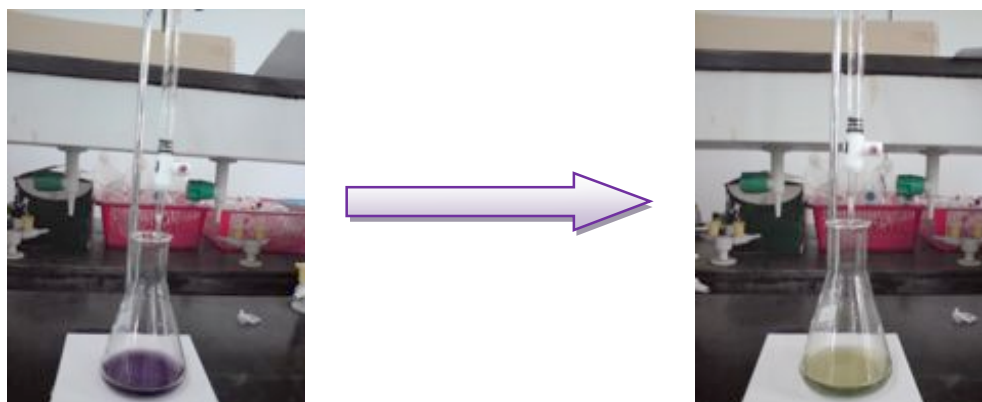


Figure 3.9: Colour changes when end point of titration of $(\text{NH}_4)_2\text{Fe}(\text{SO}_4)_2 \cdot 6\text{H}_2\text{O}$ reached

According to the equation that developed by Niwa and Murakami (1982) as below, it was possible to determine the relative amount of V^{3+} , V^{4+} , and V^{5+} .

$$\begin{aligned} (\text{V}^{4+} + 2\text{V}^{3+})(\text{V}_a) &= 20[\text{MnO}_4^-](\text{V}_1) \\ (\text{V}^{5+} + \text{V}^{4+} + \text{V}^{3+})(\text{V}_b) &= 20[\text{Fe}^{2+}](\text{V}_2) \\ (\text{V}^{5+})(\text{V}_c) &= [\text{Fe}^{2+}](\text{V}_3) \end{aligned}$$

Where V^{5+} , V^{4+} and V^{3+} are the concentration of vanadium at different oxidation state; $[\text{MnO}_4^-]$ is the concentration of potassium permanganate solution; $[\text{Fe}^{2+}]$ is the concentration of ammonium iron(II) sulphate solution;

V_1 is the volume of potassium permanganate solution used; V_2 and V_3 are the volume of ammonium iron(II) sulphate solution used; and V_a , V_b and V_c are the volume of the respective catalyst solution used.

The average oxidation state of vanadium (V_{AV}) can be calculated by using following equation (Niwa and Murakami, 1982):

$$V_{AV} = \frac{3V^{3+} + 4V^{4+} + 5V^{5+}}{V^{3+} + V^{4+} + V^{5+}}$$

3.2.2.6 Temperature-programmed Desorption (TPD) of O₂ Analyses

Temperature-programmed desorption (TPD) was originally developed by surface scientists to quantitatively investigate the kinetics of desorption of molecules from well-defined single crystal surface in high vacuum (Niemantsverdriet, 2007). TPD of O₂ was used to investigate the surface reactivity, the concentration and binding strengths of adatoms, the type of active site available, the reducibility degree of catalyst, which is related to the catalytic activity and selectivity. The measurement of the rate of desorption as a function of temperature at a linear temperature ramp, which allows the study of the total amount of surface lattice oxygen and Thermo Electron Temperature Programmed Desorption, Reduction and Oxidation (TPDRO) 1100 (Figure 3.10) is used.

0.02 g of fresh catalyst was weighed into the reactor then preliminary cleaning was carried out by purging purified nitrogen flow at $25 \text{ cm}^3 \text{ min}^{-1}$ for 5 mins to eliminate impurities. Subsequently, oxygen flow at $25 \text{ cm}^3 \text{ min}^{-1}$ was purging instead of nitrogen, and then temperature increased from room temperature to 673 K at 10 K min^{-1} and hold for 30 mins. Oxygen would react with the carbonaceous residues of calcination and then be eliminated as CO and CO_2 . Afterward, another purge of nitrogen at $25 \text{ cm}^3 \text{ min}^{-1}$ for 5 mins, was introduce to assure analysis profile involved only oxygen adsorbed on the investigated active phase by removing the residual oxygen purged in previous step. Next, analysis was initiated by a flow of helium at $25 \text{ cm}^3 \text{ min}^{-1}$ with linear increasing temperature from room temperature to 1173 K at 10 K min^{-1} . As the temperature rises, bond between oxygen molecules and the active sites would start vibrating at increasing frequency. Once the energy of activation was reached, the bond would break. Resultant desorbed oxygen molecules were removed from reactor by helium flow to thermal conductivity detector (TCD). Amount of desorbed oxygen molecules were determined by TCD with comparison to concentration of a reference flow. Finally, a plot of the amount of oxygen desorbed from catalyst as a function of time, which would be converted to the temperature was obtained.



Figure 3.10: Thermo Electron TPDRO 1100

3.2.2.7 Temperature-programmed Reduction (TPR) in H₂ Analyses

The objectives of TPR characterisation involved investigation of the different types of oxygen species present in the catalyst, the bulk reactivity, and the reduction temperature for different crystallite phase. Thermo Electron TPDRO 1100 (Figure 3.10) was used in TPR characterisation.

0.02g of fresh catalyst was weighed into the reactor and connected to the preparation port. First, the catalysts were cleaned by a flow of purified nitrogen gas at $20 \text{ cm}^3 \text{ min}^{-1}$ for 5 mins without increment of temperature. Next, temperature was increased from room temperature to 473 K at 10 K min^{-1} and then holding for 45 mins. Surface cleaning in the flow of purified nitrogen would remove the contaminants and moisture from catalyst. After pretreatment, reactor was switched to the analysis port. Hydrogen, which diluted in nitrogen in 5.55% at $25 \text{ cm}^3 \text{ min}^{-1}$ served as reducing gas, was passed through the bed of catalyst. The catalyst was submitted to a linear increase of temperature from room temperature to 1173 K at 5 K min^{-1} . Hydrogen would react with catalyst

and removed as water. This reduction had taken place as a function of the increasing of temperature, the percentage of reactive gas, the flow conditions in reactor, and the quantity of sample. Thermal conductivity difference between reactant and the carrier gas was optimised by the composition of reducing gas. Hydrogen consumed was measured by TCD, thus measure the change of thermal conductivity of the gas mixture before and after reaction.

Ultimately, a plot of the hydrogen consumption of a catalyst as a function of time, which would be converted to the temperature was obtained. Number of peaks would be observed in the profile due to the initiation of reduction at various thermal energy levels.

3.3 Catalytic Tests

The oxidation of *n*-butane was carried out in a fixed-bed microreactor (Figure 3.11) at 673 K with gas hourly space velocity (GHSV) = 2400 h⁻¹ with a standard mass of catalyst (0.25 g). The catalyst was held in place by plugs of quartz wool. A thermocouple was placed in the center of the fixed-bed stainless steel tube to control the reaction temperature at ± 1 K. *n*-Butane and air were fed to the reactor via calibrated mass flow controllers to provide a feedstock composition of 1.0% *n*-butane in air. 0.5 mL of product was fed via heated lines to an on-line gas chromatography, i.e. Thermo Scientific TRACE GC UltraTM (Figure 3.11), which equipped with an for analysis. The TCD

detector allows the detection of the fixed gases O₂, N₂, CO, CO₂ etc, this channel equipped with a Hysep-R packed column (1m, 1/8") and Molecular Sieve 5A column (3m, 1/8"). The flame ionization detector (FID) allows the detection of all hydrocarbon gases (C₁-C₄) and maleic anhydride, this channel equipped with a Rtx-1701 wide bore capillary column (30 m × 0.53 mm). Carbon mass balances of $\geq 95\%$ were typically observed.



Figure 3.11: Fixed-bed microreactor with on-line Thermo Scientific TRACE GC Ultra™

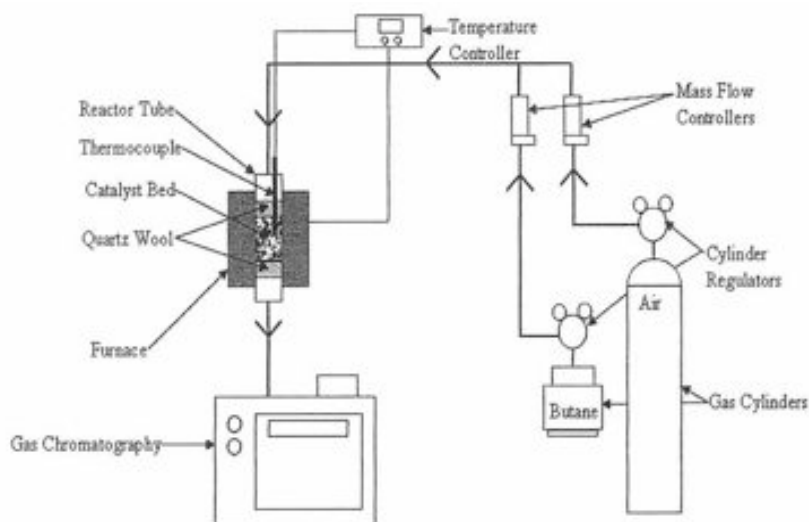


Figure 3.12: Schematic diagram of fixed-bed microreactor with on-line gas chromatograph for catalytic test

CHAPTER 4

SELECTIVE OXIDATION OF *n*-BUTANE OVER CHROMIUM-DOPED VPO_s CATALYSTS

4.1 Introduction

Industrial catalysts for oxidation reactions rarely use a single bulk phase. A number of promoter elements are added that can act purely as textural promoters, or enhance the activity and selectivity of the bulk catalyst (Jackson, 2009).

Vanadium phosphorus oxide (VPO) catalyst that derived from sesquihydrate route has been reported to give a higher specific activity even at a lower specific surface area as compared the conventional synthetic route (Ishimura *et al.*, 2000). On the other hand, chromium (Cr) has been reported to be able to improve the surface areas significantly (Hutchings and Higgins, 1996; Pierini *et al.*, 2005).

Therefore, the addition of Cr into the sesquihydrate-derived VPO_s catalyst is intended to have an improved catalytic activity with a higher surface area. A series of Cr-doped VPO_s catalysts was produced with different mole percentages of Cr added.

4.2 Effect of Different Mole Percentages of Cr Dopant on the Physico-chemical, Reactivity and Catalytic Properties of Cr-Doped Vanadyl Pyrophosphate Catalysts

The activated vanadyl pyrophosphate $((VO)_2P_2O_7)$ catalyst is denoted as Bulk VPO_s , where $_s$ represents the preparation method, i.e. via sesquihydrate route. The activated Cr doped $(VO)_2P_2O_7$ catalysts are denoted as $VPO_s\text{-Cr}X\%$, where X represents the amount of Cr incorporated, i.e. 1, 3 and 5 mol%. The effect of different mole percentages of Cr on the physicochemical properties, reactivity and catalytic properties of VPO_s catalysts were investigated.

4.2.1 X-ray Diffraction (XRD) Analyses

Three characteristic peaks of $(VO)_2P_2O_7$ at $2\theta = 22.98^\circ$, 28.45° , and 29.95° corresponded to $(0\ 2\ 0)$, $(2\ 0\ 4)$ and $(2\ 2\ 1)$ reflection planes (JCPDS File No. 34-1381) were shown in the diffractograms of synthesised VPO_s catalysts (Figure 4.1). However, an additional weak peak was emerged at $2\theta = 58.40^\circ$ for all Cr-doped VPO_s catalysts, corresponding to $\beta\text{-VOPO}_4$ phase (JCPDS File No. 27-0948). This is in agreement with the redox titration results showing that Cr doped VPO_s catalysts gave a slightly higher average oxidation number of vanadium as compared to bulk VPO_s catalyst. This has also been reported by Pierini *et al.* (2005) indicated that Cr dopant would favor the appearance of V^{5+} containing phases.

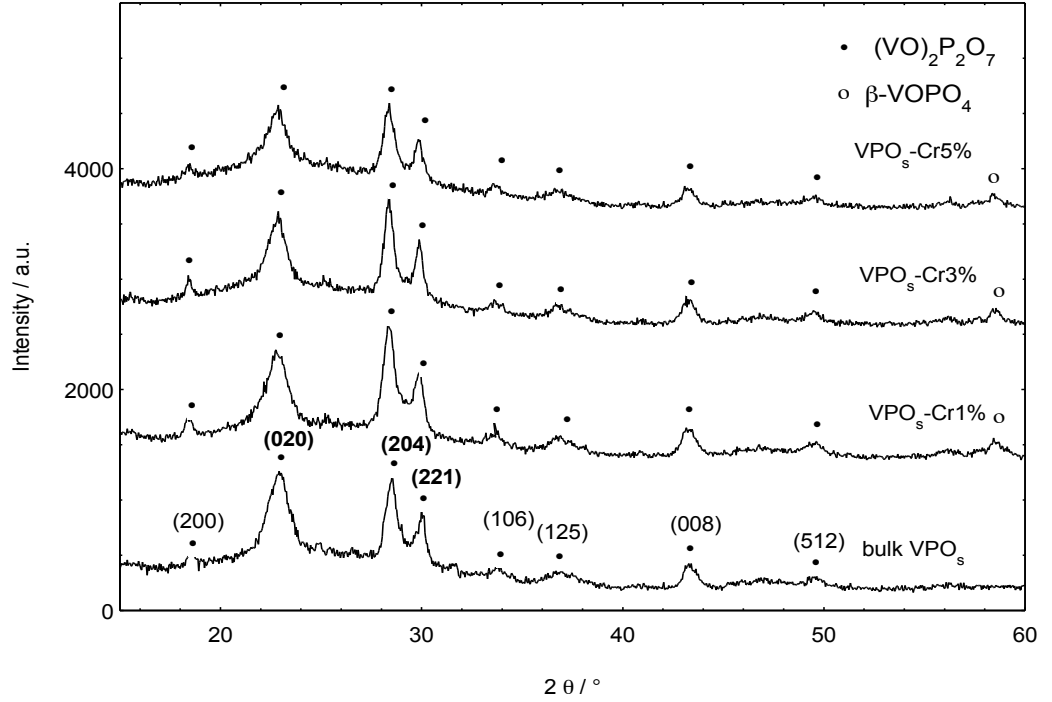


Figure 4.1: Powder XRD patterns of bulk VPO_s and Cr-doped VPO_s catalysts

The addition of Cr has led to the three characteristic peaks being narrower as compared to the bulk VPO_s counterpart (Figure 4.1). Therefore, the presence of Cr in the VPO_s catalyst system could produce catalysts with larger crystallite sizes for both (0 2 0) and (2 0 4) reflection planes. The crystallite size is calculated by Debye-Scherrer equation (Klug and Alexander, 1974):

$$t = \frac{0.89 \lambda}{\beta_{hkl} \cos \theta_{hkl}} \quad (\text{Equation 4.1})$$

where t is the crystallite size for $(h \ k \ l)$ phase, λ is the X-ray wavelength of radiation for Cu K α , β_{hkl} is the full-width at half maximum (FWHM) at $(h \ k \ l)$ peak and θ_{hkl} is the diffraction angle for $(h \ k \ l)$ phase.

The FWHM of the (0 2 0) and (2 0 4) reflection planes are used to determine the crystallite size of catalysts. The line width decreases with the increasing size of the crystallites (Cornaglia *et al.*, 1999). As tabulated in Table 4.1, the line width for both (0 2 0) and (2 0 4) reflections were inversely proportional to the mole percentage of Cr doping. This does reflect that the crystallite size of the catalysts was increasing as the mole percentage of Cr doping increased, i.e. 58.74, 59.24 and 61.59 Å for VPO_s-Cr1%, VPO_s-Cr3%, and VPO_s-Cr5%, respectively. This was due to the fact that the decrease in the FWHMs of the (0 2 0) reflection with a long time on stream indicates that the thickness of particles in the (1 0 0) direction increases (Taufiq-Yap *et al.*, 2004). The FWHMs of the (2 0 4) reflection is only an indicative of the mean “length” at the (2 0 4) face, while the thickness of (0 2 0) is a more representative of the actual thickness (Kesteman *et al.*, 1995; Taufiq-Yap *et al.*, 2007b). It has been proposed by some researchers that the oxidation of (VO)₂P₂O₇ catalyst starts at the side faces of the (1 0 0) plane. Thus, VPO_s with a high exposure of the (1 0 0) plane is less oxidisable (Matsuura and Yamazaki, 1990).

Table 4.1: XRD data of bulk VPO_s and Cr-doped VPO_s catalysts

Catalyst	Linewidth ^a (0 2 0) / °	Linewidth ^b (2 0 4) / °	Crystallite size ^c (0 2 0) / Å	Crystallite size ^c (2 0 4) / Å
Bulk VPO_s	1.3783	0.8222	58.0226	98.2005
VPO_s-Cr1%	1.3611	0.8085	58.7457	100.2637
VPO_s-Cr3%	1.3500	0.8030	59.2409	100.9596
VPO_s-Cr5%	1.3008	0.7300	61.5911	111.3116

^a FWHM of (020) reflection

^b FWHM of (204) reflection

^c Crystallite size by means of Scherrer's formula : $T (\text{Å}) = (0.89 \times \lambda) / (\text{FWHM} \times \cos\theta)$

4.2.2 Scanning Electron Microscopy (SEM)

The surface morphologies of bulk VPO_s and Cr-doped VPO_s catalysts have shown in Figure 4.2. The principal secondary structures of the catalysts were found to be the same consisting different sizes of plate-like crystals, which were agglomerated into the characteristics of rosette-shape clusters. This rosette-type agglomerates are made up of agglomerates of $(\text{VO})_2\text{P}_2\text{O}_7$ platelets that preferentially expose (1 0 0) crystal planes (Taufiq-Yap *et al.*, 2004; Taufiq-Yap *et al.*, 2006b; Kiely *et al.*, 1995). This kind of platelet arrangement could also be seen for $(\text{VO})_2\text{P}_2\text{O}_7$ catalysts obtained via typical conventional organic and dihydrate methods (Kiely *et al.*, 1995; Taufiq-Yap *et al.*, 2001).

Characteristic rosette-shape aggregates and the morphologies of the catalysts were discerned to be different for both bulk VPO_s and Cr-doped VPO_s catalysts. All Cr-doped VPO_s catalysts have more layered plate-like crystals as compared to bulk VPO_s , and exhibited clearer and more prominent rosette-shaped agglomerates.

The catalysts that were doped with 3% and 5% Cr (Figure 4.2(c) and (d)), appeared to have some small rectangular-shaped crystals, which could be assigned to the presence of $\beta\text{-VOPO}_4$ phase (Kiely *et al.*, 1996; Taufiq-Yap *et al.*, 2007a). This could further explain the decreasing trend of specific surface area (Table 4.2) when the amount of Cr doping increased from 1% to 5%.

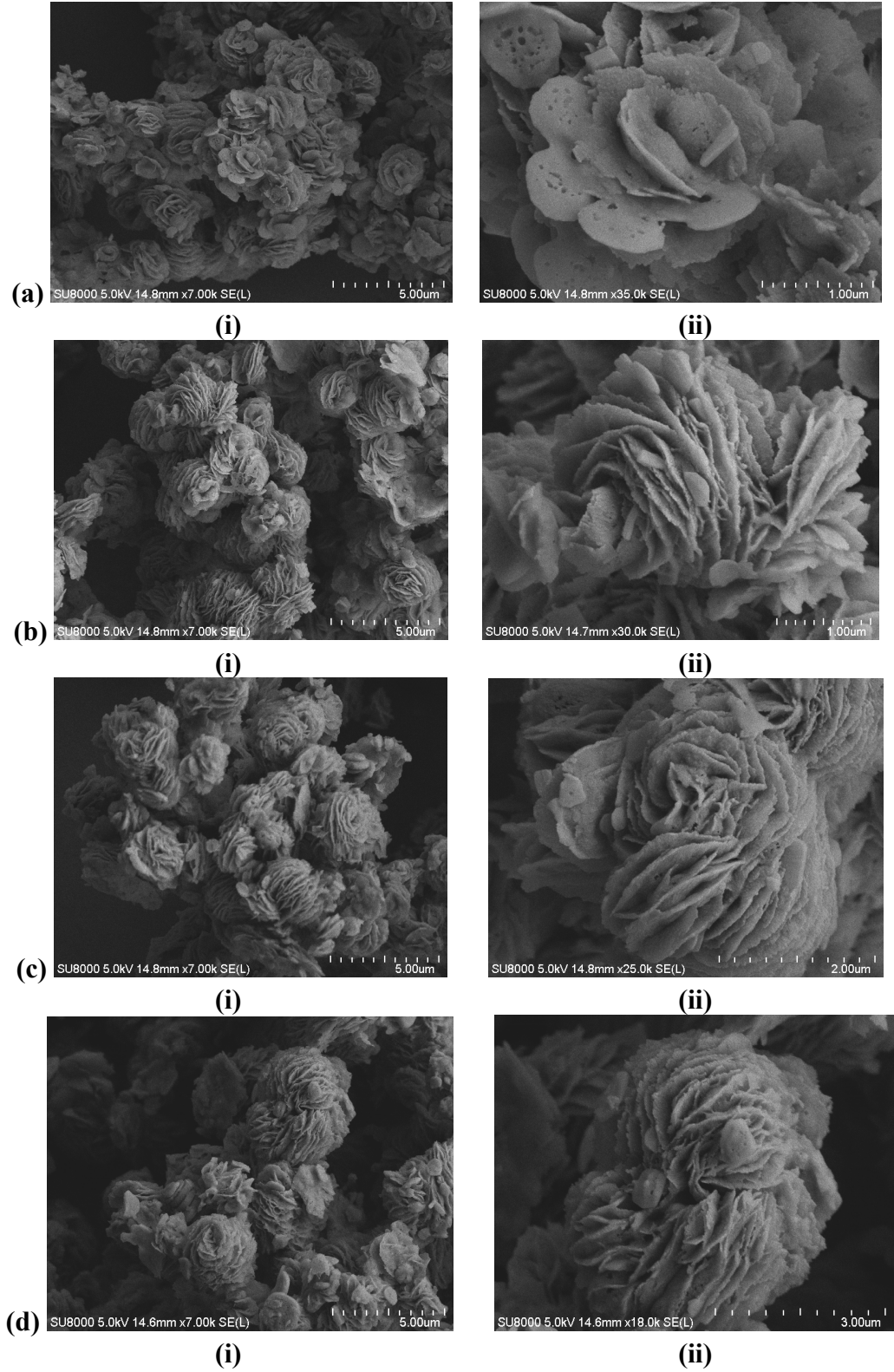


Figure 4.2: SEM micrographs for (a) bulk VPOs: (i) $\times 7000$ (ii) $\times 35,000$; (b) VPO_s-Cr1%: (i) $\times 7000$ (ii) $\times 30,000$; (c) VPO_s-Cr3%: (i) $\times 7000$ (ii) $\times 25,000$; (d) VPO_s-Cr3%: (i) $\times 7000$ (ii) $\times 18,000$

4.2.3 Brunauer-Emmett-Teller (BET) Surface Area Measurements and Chemical Analyses

Table 4.2 shows the BET specific surface area, the atomic ratio of P/V and the percentage of V^{4+} and V^{5+} oxidation states presence in the synthesised catalysts. The addition of 1 mol% of Cr dopant provide a slightly increase of specific surface area as compared to bulk VPO_s catalyst from 19.3 to 22.8 $m^2 g^{-1}$. This indicates that the small amount of Cr was intercalated in between the layers of VPO_s crystal plates which altered the basal (1 0 0) $(VO)_2P_2O_7$ face and gives a higher surface area (Taufiq-Yap *et al.*, 2006b). Conversely, specific surface areas of catalysts decreased gradually as the amount of Cr added increased to 3 mol% and 5 mol%, i.e. 20.06 and 17.88 $m^2 g^{-1}$, respectively.

According to the paper of Hutchings and Higgins (1996), that Cr had increase the surface area of VPO catalyst significantly from 14.0 to 21.0 $m^2 g^{-1}$ through nonaqueous HCl method. Pierini *et al.* (2005) also reported that the addition of Cr yields catalysts with ~50% higher surface area than the bulk VPO_s catalyst through hemihydrate route but an further increase amount of Cr load has no effect on surface areas. However, it can be clearly seen that, the specific surface areas of Cr-doped catalysts were decreased with the increasing of amount of Cr added by means of sesquihydrate route. This was consistent with the results obtained from XRD analyses, indicating that the surface areas were decreased as the crystallite size increased.

Table 4.2: Specific surface areas, chemical compositions, average oxidation numbers and percentages of V⁴⁺ and V⁵⁺ oxidation states for bulk VPO_s and Cr-doped catalysts

Catalysts	Specific surface area (m ² g ⁻¹)	ICP-OES		V ⁴⁺ (%)	V ⁵⁺ (%)	V _{AV}
		Cr/V	P/V			
Bulk VPO _s	19.3		1.05	91.81	8.19	4.0819
VPO _s -Cr1%	22.8	0.013	1.56	87.15	12.85	4.1285
VPO _s -Cr3%	20.1	0.034	1.54	82.16	17.84	4.1784
VPO _s -Cr5%	17.9	0.057	1.49	79.61	20.93	4.2039

Chemical analyses using ICP-OES has shown an apparent increase of P/V atomic ratio from 1.05 for bulk VPO_s to approximate 1.50 for all Cr-doped VPO_s catalysts. According to Mc Cormick *et al.* (1997) and Pierini *et al.* (2005), this phenomenon could be rationalised that CrPO₄ was formed and intercalated in the pyrophosphate matrix, helping to retain the excess phosphorus.

Chemical analyses confirmed the presence of Cr in the doped catalysts with the Cr/V atomic ratio of 0.013, 0.034 and 0.057 for VPO_s-Cr1%, VPO_s-Cr3%, and VPO_s-Cr5%, respectively. The doping of Cr has promoted the formation of V⁵⁺ as the percentage of V⁵⁺ increased from 8.19 % for bulk VPO_s to 12.85%, 17.84% and 20.93% for VPO_s-Cr1%, VPO_s-Cr3% and VPO_s-Cr5%, respectively. The average oxidation numbers of Cr-doped VPO_s catalysts were directly proportional to the mole percentage of Cr doping. This was due to the presence of a V⁵⁺ phase, as observed in the diffractograms (Figure 4.1)

4.2.4 Temperature-programmed Desorption (TPD) of O₂ Analyses

TPD of O₂ profiles shown in Figure 4.3 were obtained by pretreating the fresh catalysts by heating them to 673 K in an oxygen flow (1 bar, 25 cm³min⁻¹) and held at 673 K for 30 min in the same stream before cooling to ambient temperature. Then, the flow was switched to helium (1 bar, 25 cm³min⁻¹) and the temperature was raised to 1173 K. The peak maxima temperatures, the amount of desorbed oxygen and the derived desorption activation energies are summarized in Table 4.3.

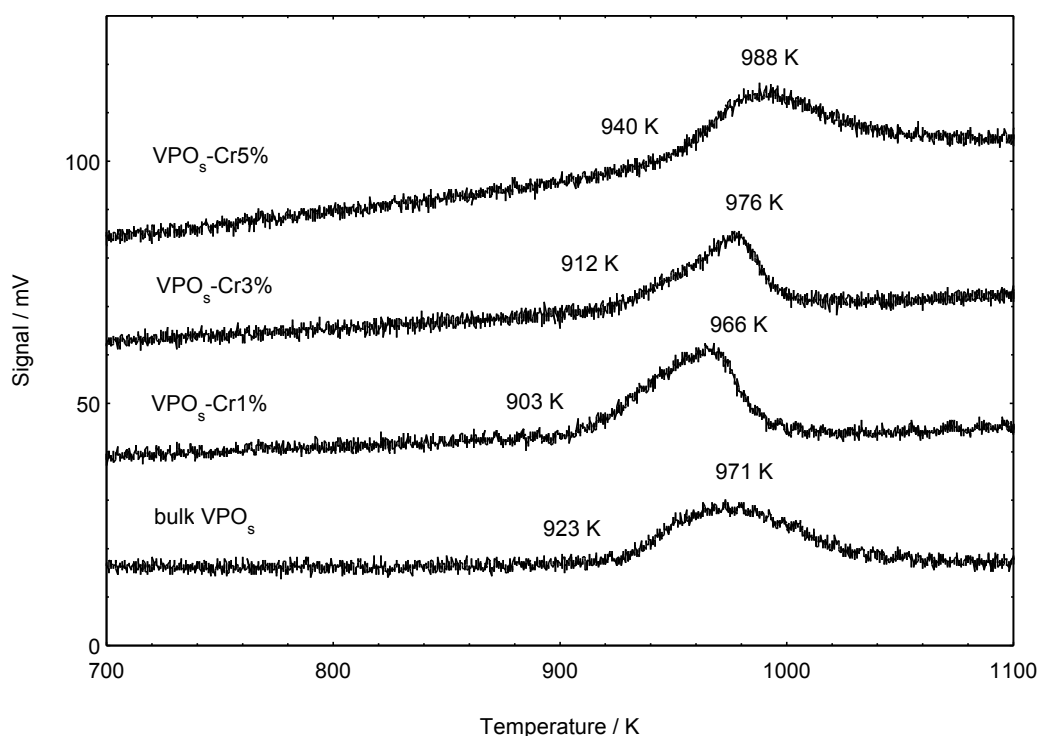


Figure 4.3: TPD of O₂ profiles of bulk VPO_s and Cr-doped VPO_s catalysts

Table 4.3: Amounts of oxygen atoms desorbed and values of desorption activation energy obtained by TPD analyses for bulk VPO_s and Cr-doped VPO_s catalysts

Catalyst	T _{onset} (K)	T _{max} (K)	Desorption activation energy, E _d (kJ mol ⁻¹)	Amount of oxygen desorbed (× 10 ⁻⁴ mol g ⁻¹)	Amount of oxygen desorbed (× 10 ¹⁹ atom g ⁻¹)
Bulk VPO_s	923	971	162.3846	1.1246	6.7726
VPO_s-Cr1%	903	966	161.5484	1.5205	9.1563
VPO_s-Cr3%	912	976	163.2208	1.3947	8.3989
VPO_s-Cr5%	940	988	165.2276	0.9039	5.4431

Bulk VPO_s gave a broad peak with a peak maximum at 971 K. However, introduction of 1 mol% Cr had shifted the peak maximum to lower temperature i.e. 966K, with an increase amount of oxygen desorbed from 6.77 x 10⁹ to 9.15 x 10⁹ atom g⁻¹ for bulk VPO_s and VPO_s-Cr1%, respectively. However, further addition of Cr dopant into the VPO_s system had gradually reduced the amount of oxygen desorbed from catalysts, i.e. 8.39 x 10⁹ atom g⁻¹ with peak maximum at 976 K and 5.44 x 10⁹ atom g⁻¹ with peak maximum at 988 K for VPO_s-Cr3%, and VPO_s-Cr5%, respectively. This could be attributed to the decrease of specific surface areas as discussed in Section 4.2.3. The lower the specific surface area would have lesser vacancies for the oxygen.

The values of the activation energies for desorption were calculated using Redhead (1962) equation:

$$\frac{E_d}{RT_m^2} = \left(\frac{A}{\beta} \right) \exp \left(\frac{-E_d}{RT_m} \right) \quad (\text{Equation 4.2})$$

where E_d is the desorption activation energies (kJ mol⁻¹), A is the desorption A factor (10¹³ s⁻¹, assumed), R is the gas constant (J K⁻¹ mol⁻¹), β is the heating rate

(K s⁻¹) and T_m (K) is the temperature of the peak maximum. The desorption activation energies for bulk VPO_s, VPO_s-Cr1%, VPO_s and VPO_s-Cr1% were 162.38, 161.54, 163.22 and 165.22, respectively. It can be clearly seen that the desorption activation energies were inversely proportional to the amount of oxygen desorbed from catalysts. Conversely, it was directly proportional to the mole percentage of Cr added into VPO_s system. This indicates a small amount of Cr doping (Cr/V = 0.01) helps to increase the mobility of surface oxygen. However, when up to certain mole percentage, it could induce a higher binding energy between lattice oxygen and vanadium and decrease the mobility of oxygen and thus harder to be thermally desorbed in TPD of O₂ analyses. This was in contrary with the Bi-doped VPO_s catalysts that produced through the same synthetic method, which also show an increase of desorbed surface oxygen at 1 mol %. However, when the amount of Bi doping increased, the amount of desorbed surface oxygen was increased accordingly (Leong *et al.*, 2011).

4.2.5 Temperature-programmed Reduction (TPR) in H₂ Analyses

Figure 4.4 shows the TPR profiles of VPO_s catalysts in H₂/N₂ stream (5.55% H₂ in N₂, 1 bar, 25 cm³ min⁻¹) using a fresh catalyst and raising the temperature from ambient to 1123 K at 5 K min⁻¹ in that stream. Table 4.4 lists the peak maxima temperatures, the amount of removed oxygen in each peak and the derived reduction activation energies. The values of the activation energies are obtained from the modified version of Redhead equation (1962):

$$\frac{E_r}{RT_m^2} = \left(\frac{A_r}{\beta} \right) [H_2]_m \exp \left(\frac{-E_r}{RT_m} \right) \quad (\text{Equation 4.3})$$

where E_r is the reduction activation energies (kJ mol^{-1}), A_r is the reduction pre-exponential term ($\text{cm}^3 \text{mol}^{-1} \text{s}^{-1}$) which is given the value of a standard collision number of $10^{13} \text{cm}^3 \text{mol}^{-1} \text{s}^{-1}$, R is the gas constant ($\text{J K}^{-1} \text{mol}^{-1}$), β is the heating rate (K s^{-1}), T_m (K) is the temperature of the peak maximum and $[H_2]_m$ is the gas phase concentration of hydrogen (mol cm^{-3}) at the maximum peak.

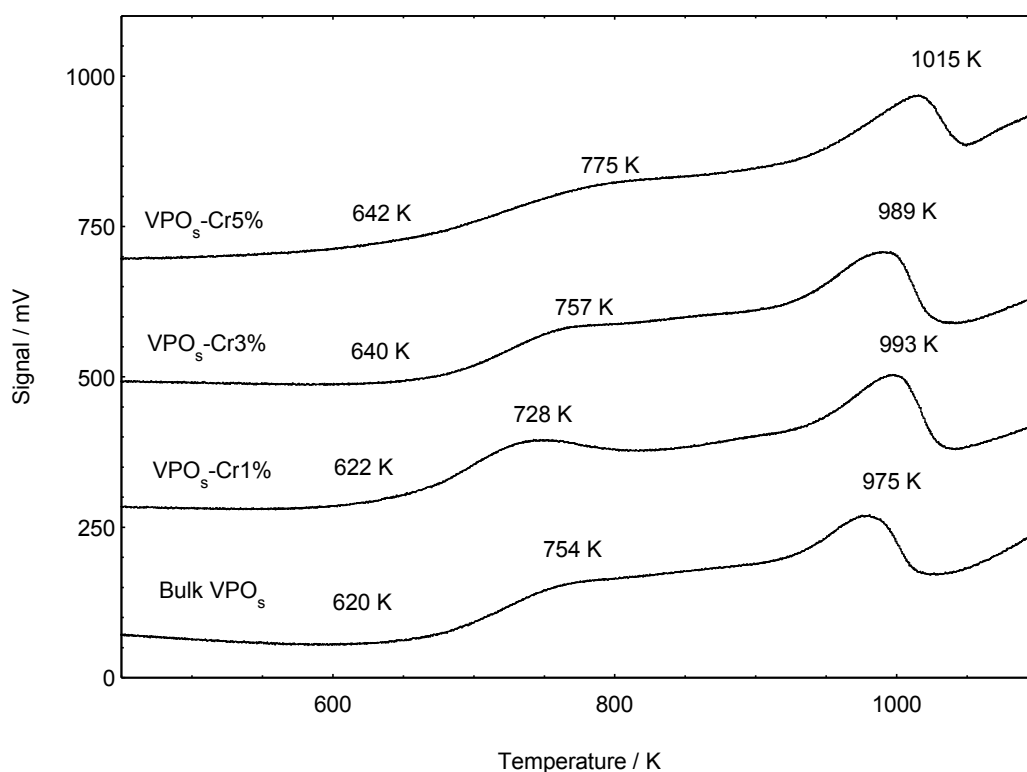


Figure 4.4: TPR in H_2 profiles of bulk VPO_s and Cr-doped VPO_s catalysts

Table 4.4: Amounts of oxygen atoms removed and values of reduction activation energy obtained by TPR analyses for bulk VPO_s and Cr-doped VPO_s catalysts

Catalyst	T _{onset} (K)	T _{max} (K)	Reduction activation energy, E _r (kJ mol ⁻¹)	Amount of oxygen reduced (× 10 ⁻³ mol g ⁻¹)	Amount of oxygen reduced (× 10 ²⁰ atom g ⁻¹)
Bulk VPO_s	620	754	126.0947	0.9326	5.6161
		975	163.0535	1.8404	11.0829
Total oxygen atoms removed				2.7730	16.6990
VPO_s-Cr1%	622	728	121.7466	1.8832	11.3408
		993	166.0638	2.6007	15.6615
Total oxygen atoms removed				4.4839	27.0023
VPO_s-Cr3%	640	757	126.5964	1.7589	10.5920
		989	165.3948	2.2233	13.3886
Total oxygen atoms removed				3.9822	23.9806
VPO_s-Cr5%	642	775	129.6067	1.2304	7.4096
		1015	169.7429	2.1751	13.0985
Total oxygen atoms removed				3.4055	20.5081

Two reduction peaks were observed for all catalysts at ~750 K and ~1000 K (Figure 4.4). The 1st and 2nd reduction peaks were assigned to the removal of oxygen species from V⁵⁺ and V⁴⁺ phases, respectively as reported by Pierini *et al.* (2005). An interesting observation from the TPR in H₂/N₂ profiles is noted where the 1st peak which attributed to the reduction of V⁵⁺ phase for VPO_s-Cr1% was shifted to lower temperature, i.e. from 754 K to 728 K as compared to bulk VPO_s catalyst. The reduction peak maximum was gradually increased with the mole percentage of Cr dopant added into the VPO_s system, i.e. 757 and 775 K for VPO_s-Cr3%, and VPO_s-Cr5%, respectively. On the other hand, the second peak which attributed to the reduction of V⁴⁺ phase for Cr-doped VPO_s appeared at higher temperatures (> 990 K) as compared to bulk VPO_s catalyst. Hence, it could

be concluded that the introduction of higher amount of Cr dopant could induce the increase of lattice energy as well (Taufiq-Yap *et al.*, 2006b).

Both V^{5+} and V^{4+} species were reported by previous researchers (Herrmann *et al.* 1997; Abon and Volta, 1997; Volta, 2000; Abon *et al.*, 2001), that they were associated with O^{2-} and O^- , respectively. $V^{4+}-O^-$ species was further proven by Volta (2000), Hermann *et al.* (1997) and Taufiq-Yap *et al.* (2006a; 2011a; 2011b) that it is responsible for the activity of partial oxidation of *n*-butane. On the other hand, $V^{5+}-O^{2-}$ species was claimed by Coulston *et al.* (1997) through time-resolved X-ray adsorption spectroscopy, that it is responsible for the rate of MA formation directly. This claim was also supported by other groups of researchers that it is important to determine the selectivity of partial oxidation of *n*-butane (Taufiq-Yap *et al.*, 2006a; Taufiq-Yap *et al.*, 2011a; Centi *et al.*, 1988; Granados *et al.*, 1993).

The 1st reduction peak (Figure 4.4), which responsible for the removal of $V^{5+}-O^{2-}$, was appeared to be more prominent for VPO_5 -Cr1%, this was attributed to the higher surface exposure that promote the reduction of vanadium (Pierini *et al.*, 2005). The amount of $V^{5+}-O^{2-}$ removed from VPO_5 -Cr1% was increased to 11.34×10^{20} atom g^{-1} from 5.61×10^{20} atom g^{-1} for that of bulk VPO_5 . As the amount of Cr added increased to 3 mol% and 5 mol%, the amount of $V^{5+}-O^{2-}$ reduced was decreased to 10.59×10^{20} and 7.41×10^{20} atom g^{-1} , for VPO_5 -Cr3%, and VPO_5 -Cr5%, respectively. Cr-doped $(VO)_2P_2O_7$ catalyst that produced

through hemihydrate route by Pierini *et al* (2005) also gave a lower amount of oxygen reduced from V^{5+} phase when the amount of Cr increase from 0.5 to 3 wt%. On the other hand, the highest amount of $V^{4+}-O^-$ was removed from the VPO_s -Cr1% also, i.e. 15.66×10^{20} atom g^{-1} as compared to that of bulk VPO_s , i.e. 11.08×10^{20} atom g^{-1} . With a further increment amount of Cr added, the amount of $V^{4+}-O^-$ reduced to 13.39×10^{20} and 13.10×10^{20} atom g^{-1} , for VPO_s -Cr3%, and VPO_s -Cr5%, respectively. As an overall, all the Cr-doped VPO_s catalyst gave higher total amount of lattice oxygen reduced form the catalysts as compared to that of bulk VPO_s . Therefore, this result could be suggested that Cr dopant would enhance the catalytic performance in terms of conversion of *n*-butane and selectivity to MA as well, especially VPO_s -Cr1%, which possessed the most labile of oxygen and highest amount of reactive oxygen.

4.2.6 Catalytic Oxidation of *n*-Butane to Maleic Anhydride

In order to investigate the catalytic performance of the synthesised VPO_s catalysts, all the catalysts were tested in the selective oxidation of *n*-butane to maleic anhydride (MA) at 673 K (GHSV = 2400 h^{-1}), a typical reaction temperature for VPO catalysts (Leong *et al.*, 2011).

By introducing of Cr into VPO_s catalyst, the catalytic activity and selectivity of MA were found to be improved (Table 4.5 and Figure 4.5–4.6). VPO_s -Cr1% provided the highest conversion (Figure 4.5) with 35% for partial *n*-butane oxidation to MA (673 K with GHSV = 2400 h^{-1}) as compared to only 21

% conversion of bulk VPO_5 . This could be attributed to the higher specific surface area of $\text{VPO}_5\text{-Cr1\%}$ that provides a higher accessibility of reactant onto the surface of catalyst. However, it was lower as compared to Cr-doped VPO_5 catalysts that produced through hemihydrate route (Taufiq-Yap, 2006; Taufiq-Yap *et al.*, 2011b). The *n*-butane conversion for $\text{VPO}_5\text{-Cr3\%}$, and $\text{VPO}_5\text{-Cr5\%}$, as expected in TPR analyses, gradually decrease to 33% and 29%, respectively.

The selectivity of MA was increased as the amount of Cr doping increased, from 73% for bulk VPO_5 to 78%, 85% and 88% for Cr-doped VPO_5 catalysts. The enhanced MA selectivity could be induced by minute amount of V^{5+} phase that formed after the introduction of Cr.

However, the selectivity for VPO catalysts that produced through hemihydrate route was not markedly affected by amount of Cr dopant. By means of hemihydrate route, ~60% MA selectivity was reported by Taufiq-Yap (2006) for micro-sized $(\text{VO})_2\text{P}_2\text{O}_7$ catalysts, while ~50% MA selectivity was reported by Taufiq-Yap *et al.*, 2011b for nano-sized $(\text{VO})_2\text{P}_2\text{O}_7$ catalyst.

On the other hand, as compared to Bi-doped VPO_5 which synthesised through the same synthetic route (Leong *et al.*, 2011), Bi dopant has increased the activity of $(\text{VO})_2\text{P}_2\text{O}_7$, however it doesn't further improve the catalytic activity with a higher amount Bi added into catalyst but only promote the selectivity of MA from 67% to 86%.

With respect to the results above, it could be concluded that Cr dopant could improve both the *n*-butane conversion and MA selectivity of (VO)₂P₂O₇ through sesquihydrate route. However, if more than 1% of Cr doping, it starts to reduce the activity of (VO)₂P₂O₇. This could be due to the blockage of active sites found in the pores of catalysts by excess Cr dopant.

Table 4.5: Catalytic performances of bulk VPO_s and Cr-doped VPO_s catalysts

Catalyst	<i>n</i> -butane conversion (%)	Product selectivity (5)		
		MA	CO ₂	CO
Bulk VPO _s	21	73	15	11
VPO _s -Cr1%	35	78	6	16
VPO _s -Cr3%	33	85	8	7
VPO _s -Cr5%	29	88	5	7

4.3 Conclusions

All the synthesised Cr-doped VPO_s catalysts showed 3 main characteristic peaks of (VO)₂P₂O₇ at $2\theta = 22.8^\circ$, 28.4° , and 29.8° , which were corresponding to (0 2 0), (2 0 4), and (2 2 1) planes, respectively. The average oxidation state of the vanadium of bulk VPO_s, VPO_s-Cr1%, VPO_s-Cr3% and VPO_s-Cr5% were found to be 4.08, 4.13, 4.18, and 4.20, respectively. The distinct increment of P/V ratio from 1.05 to 1.5 was attributed to the formation of CrPO₄. TPD and TPR analyses showed that the amounts of oxygen desorbed and reduced from the catalysts were inversely proportional to the amount of Cr dopant. It could also be noted that low level of Cr doping (Cr/V = 0.01) could increase the specific surface area of the

VPO_s catalyst slightly, i.e. 22.77 m²/g, together with significant improved of catalytic activity and selectivity to MA, i.e. 35% and 78%, respectively.

CHAPTER 5

SELECTIVE OXIDATION OF *n*-BUTANE OVER SILICA SUPPORTED VPO_s CATALYSTS

5.1 Introduction

The work presented in Chapter 5 was motivated, in part, by previous studies of selective oxidation of *n*-butane to maleic anhydride (MA) over supported vanadium phosphorus oxide (VPO) showing a promising catalytic performance (Ledoux *et al.*, 2000) and provide a better mechanical strength to catalyst (Harding *et al.*, 1994; Nie *et al.*, 2001; Bueno *et al.*, 1998). It is general accepted that a strong interaction between catalytic material and inert support could hinder the formation of active (VO)₂P₂O₇ phase, and the resulted catalysts would exhibit low *n*-butane conversion and/or poor MA selectivity (Zhou *et al.*, 2004; Overbeek *et al.*, 1996b). Additionally, reducible metal oxides, which are versatile solid state compounds that exhibiting a rich chemistry related to changes in the oxidation state of the metal, has been reported to interact strongly with the VPO phases. This could improve the catalytic activity but give a poor MA selectivity. Reducible metal oxides include TiO₂ and ZrO₂. In contrast to reducible metal oxides, the non-reducible nature of SiO₂ support gave an improved MA selectivity but lower catalytic activity (Overbeek *et al.*, 1996a; Overbeek *et al.*, 1996b).

On the other hand, the sesquihydrate route has been reported by Ishimura *et al.* (2000) to give a higher specific activity as compare to that from conventional synthetic method. Thus, in the second series of this research project, silica supported VPO_s catalyst that derived from sesquihydrate route is investigated with the goal to improve MA selectivity that caused by weak silica interaction and to maintain a good catalytic activity. Different loadings of VPO_s component were supported onto silica, and the effects on catalytic performance were examined.

In addition, the effect of various calcination temperatures on the silica supported VPO_s catalyst was reported in the section 5.3. The temperatures used include 673 K, 733 K and 793 K.

5.2 Effect of Different Loading of VPO_s on Silica Support towards Physico-chemical, Reactivity and Catalytic Properties of Supported Vanadyl Pyrophosphate Catalysts

The activated unsupported $(\text{VO})_2\text{P}_2\text{O}_7$ catalyst was denoted as Bulk VPO_s , where $_s$ represents the preparation method, i.e. via sesquihydrate route. The activated silica supported $(\text{VO})_2\text{P}_2\text{O}_7$ catalysts were denoted as $\text{X}\%\text{VPO}_s/\text{Si}$, where X represents the amount of VPO_s supported on silica, i.e. 5, 10, 15, 20, 25 and 30 wt%. The effect of different loadings of VPO_s on silica support on the physicochemical, reactivity and catalytic properties of supported VPO_s catalysts were investigated.

5.2.1 X-ray Diffraction (XRD) Analyses

Three main characteristic peaks for vanadyl pyrophosphate (VPO) were found in the bulk VPO_s catalyst (Figure 5.1) at $2\theta = 22.98^\circ$, 28.45° and 29.95° , which corresponded to (0 2 0), (2 0 4), and (2 2 1) planes, respectively (JCPDS File No. 34-1381). A broad peak located at $2\theta = 22.56^\circ$ (JCPDS 42-1401) in the silica supported VPO_s samples was assigned to silicone dioxide phase, which was observed to be suppressed as the VPO_s loadings increased due to the partial blocking of mesopores by VPO_s components and resulting a reduction of long-range order of silica (Nie *et al.*, 2003; Li *et al.*, 2006a; Li *et al.*, 2006b). All the diffractograms obtained were in close agreement with that obtained by fumed silica, MCM-41 and SBA-15 supported VPO catalysts through hemihydrates route with the addition of PEG, and there was no peak that can be attributable to V^{5+} phase-containing components (Li *et al.*, 2006b). This could be due to the crystalline V^{5+} phase was too small to be detected or they existed as amorphous phase.

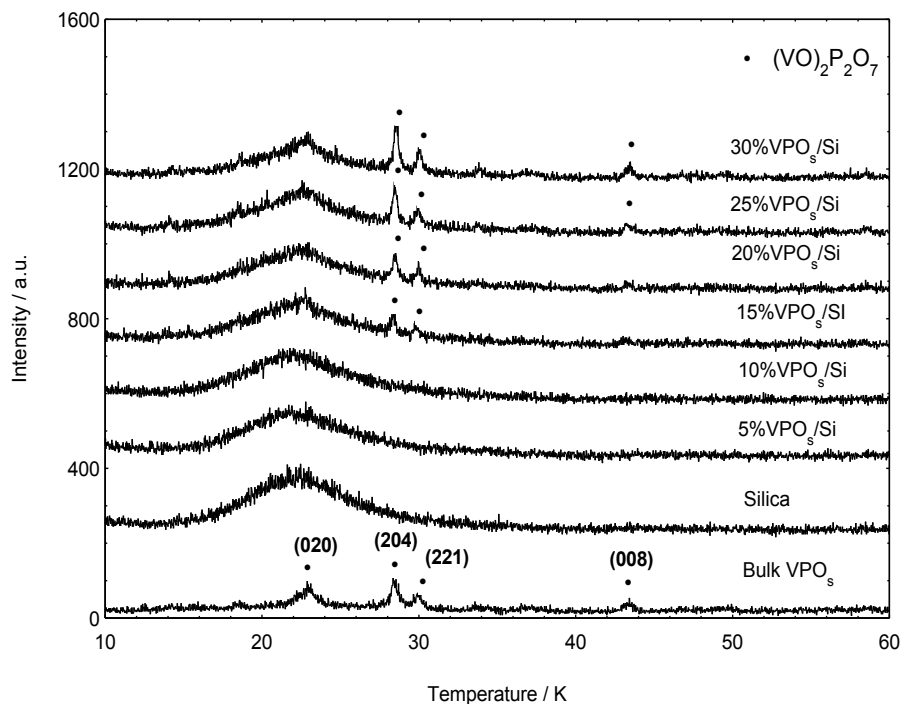


Figure 5.1: Powder XRD patterns of bulk VPO_s and silica supported VPO_s catalysts

At VPO_s loading below 15 wt%, there was no characteristic peaks belonging to (VO)₂P₂O₇ observed in the diffractograms. Similar to the work obtained by Nie *et al.* (2003) and Li *et al.* (2006a), diffraction peaks only found at VPO loading above 15 wt% on large pore silica and SBA-15, respectively. As shown in the SEM micrographs in Figure 5.3 (a): (iii). and also by the researchers (Nie *et al.*, 2003; Overbeek *et al.*, 1996a; Zhou *et al.*, 2004; Overbeek *et al.*, 1996b; Bueno *et al.*, 1998; Li *et al.*, 2006a; Li *et al.*, 2006b; Harding *et al.*, 1994), for 5%VPO_s/Si, the strong interaction of VPO_s-SiO₂ had caused a severe structural disorder and silica interference, which would hinder the crystalline formation of (VO)₂P₂O₇ phase and consequently promote the formation of amorphous VPO phase.

The formation of crystalline vanadyl pyrophosphate phase could be observed for silica supported VPO_s catalysts with 15 wt% of VPO_s loading and above. Additional peaks at $2\theta = 28.45^\circ$ and 29.95° became more intense when the VPO_s loading increased from 15-30 wt%. This was suggested by Nie *et al.* (2003), that weaker VPO_s-SiO₂ interaction happened onto the upper layers of vanadyl pyrophosphate platelets. Thus, the VPO_s components could easily be precipitated next to silica surface, which favors forming the bulk-like components at high VPO_s loading, i.e. > 10 wt%. Based on the above findings, the structure of loaded VPO components was affected significantly by the nature of the support material (Li *et al.*, 2006a).

In fact, the half width of the (0 2 0) and (2 0 4) planes is used to determine the crystallite size of (VO)₂P₂O₇ catalysts (Cornaglia *et al.*, 1999). However, the reflection angles for silica was observed to overlap the (0 2 0) reflection of (VO)₂P₂O₇, thus (2 0 4) and (2 2 1) reflection angles were used to determine the crystallite size of the VPO_s phase on the silica since they are the main reflection planes for (VO)₂P₂O₇ as well. The crystallite sizes of synthesised catalysts were calculated by Debye-Scherrer equation as shown in Equation 4.1 (Klug and Alexander, 1974). The line widths obtained decreased from the 15%VPO_s/Si to 30%VPO_s/Si gradually (Table 5.1), which showed an increase in the crystallite size. The crystallite size values obtained for 15%VPO_s/Si, 20%VPO_s/Si, 25%VPO_s/Si and 30%VPO_s/Si are 117.37, 112.74, 129.27 and 136.57 Å,

respectively for the (2 0 4) reflection plane, and 114.45, 136.23, 135.47 and 146.94 Å for the (2 2 1) reflection plane, respectively.

Table 5.1: XRD data of bulk VPO_s and silica supported VPO_s catalysts

Catalyst	Linewidth ^a (204) / °	Linewidth ^b (221) / °	Crystallite size ^c (204) / Å	Crystallite size ^c (221) / Å
Bulk VPO_s	0.8222	0.7696	98.2005	105.8720
Silica	-	-	-	-
5%VPO_s/Si	-	-	-	-
10%VPO_s/Si	-	-	-	-
15%VPO_s/Si	0.6900	0.7100	117.3700	114.4548
20%VPO_s/Si	0.6600	0.5967	122.7420	136.2326
25%VPO_s/Si	0.6267	0.6000	129.2711	135.4681
30%VPO_s/Si	0.5933	0.5533	136.5696	146.9419

^a FWHM of (204) reflection

^b FWHM of (221) reflection

^c Crystallite size by means of Scherrer's formula : $T (\text{Å}) = (0.89 \times \lambda) / (\text{FWHM} \times \cos\theta)$

5.2.2 Scanning Electron Microscopy (SEM)

The porous surface morphology of bare silica was shown in Figure 5.2 (b): (ii). It can be observed that at lower magnifications of silica supported VPO_s catalysts (Figure 5.3), the active components were fairly well dispersed on the surface of silica, which presents different sizes and structures of supported VPO_s phase. At higher magnifications, the micrograph for 5%VPO_s/Si was shown to be flattened-pieces (Figure 5.3 (a): (iii)). As can be seen clearly in the micrograph at 10 wt% of VPO_s loading, the structure of crystalline plates of (VO)₂P₂O₇ start to form and agglomerate into the characteristic rosette-shape cluster (Figure 5.3 (b): (iii)). Moreover, this rosette-shape cluster became more obvious and larger as at 15 wt% and higher VPO_s loadings (Figure 5.3 (c): (iii)-(f): (iii)). The layers of

rosette-shape cluster was well known to increase the exposure of the basal (100) $(\text{VO})_2\text{P}_2\text{O}_7$ (Kiely *et al.*, 1995; Taufiq-Yap *et al.*, 2006b).

Based on results from XRD and SEM analyses, the increase amount of VPO_s components was believed to promote agglomeration and thus the VPO_s platelets grow into rosette-shape forms which become more prominent and form more splits, unlike the morphology of the bulk VPO_s (Figure 5.2 (a)), which is shown to be flattened and covered up.

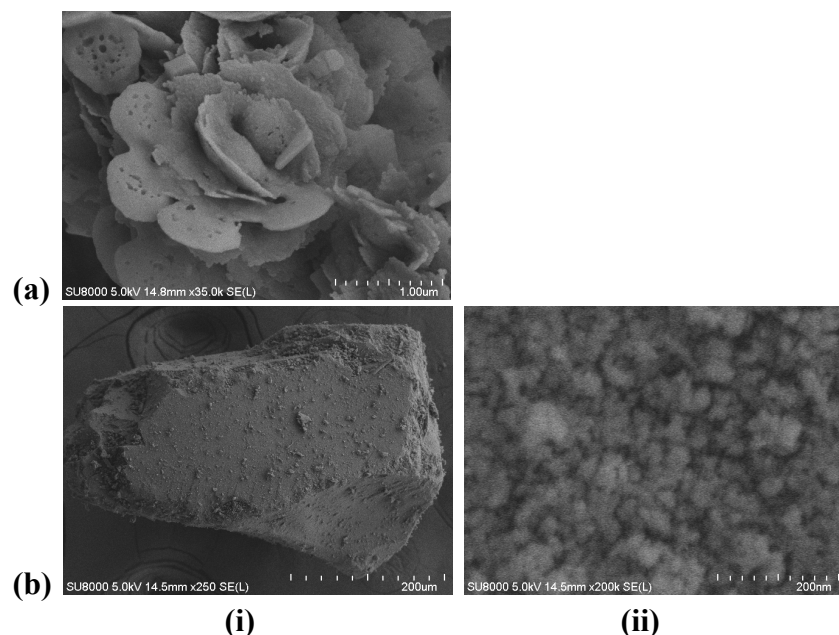


Figure 5.2: SEM micrographs for (a) bulk VPO_s : $\times 35,000$; (b) bare silica support: (i) $\times 250$ (ii) $\times 200,000$

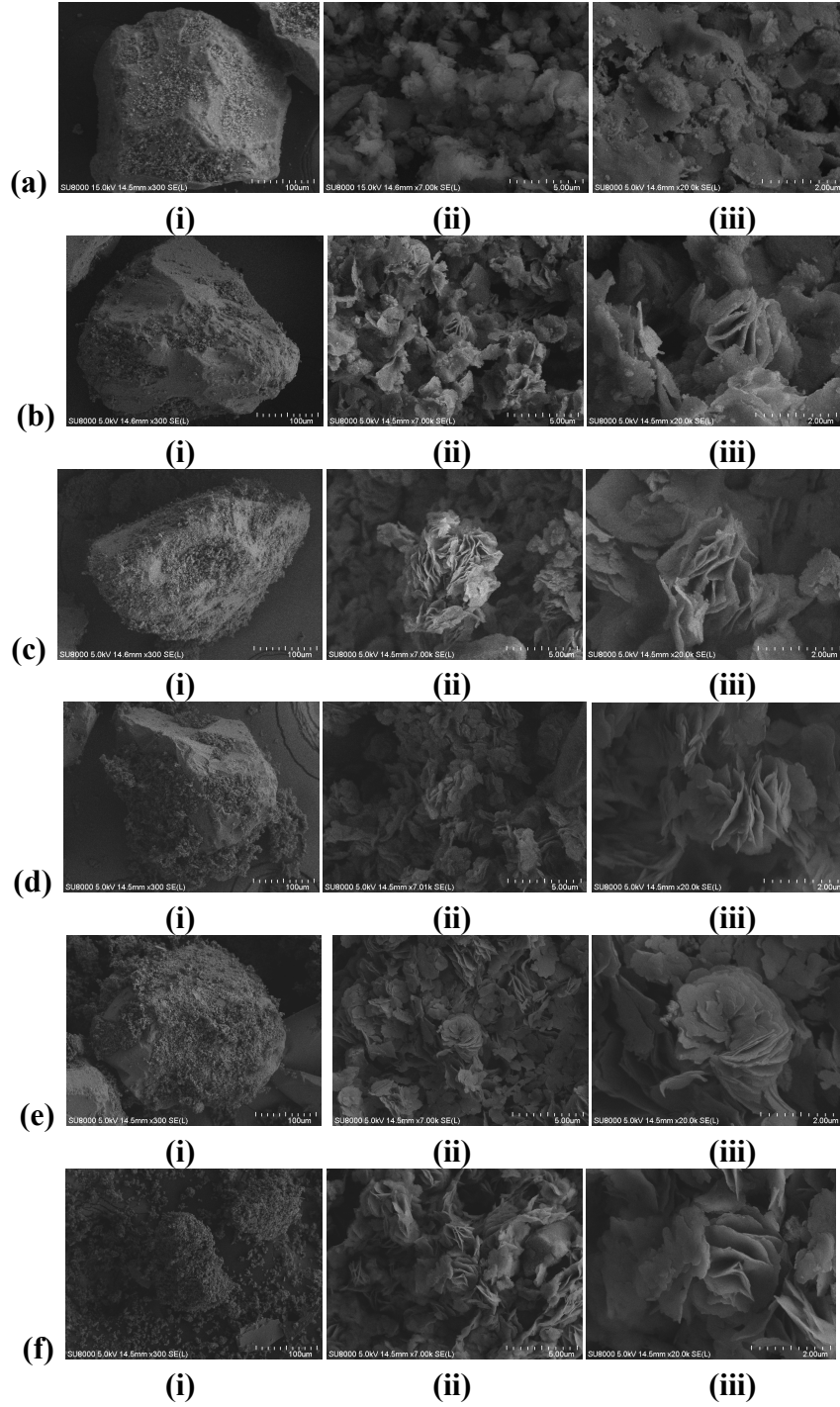


Figure 5.3: SEM micrographs for (a) 5%VPO_s/Si: (i) $\times 300$ (ii) $\times 7,000$ (iii) $\times 20,000$; (b) 10%VPO_s/Si: (i) $\times 300$ (ii) $\times 7,000$ (iii) $\times 20,000$; (c) 15%VPO_s/Si: (i) $\times 300$ (ii) $\times 7,000$ (iii) $\times 20,000$; (d) 20%VPO_s/Si: (i) $\times 300$ (ii) $\times 7,000$ (iii) $\times 20,000$; (e) 25%VPO_s/Si: (i) $\times 300$ (ii) $\times 7,000$ (iii) $\times 20,000$; (f) 30%VPO_s/Si: (i) $\times 300$ (ii) $\times 7,000$ (iii) $\times 20,000$

5.2.3 Brunauer-Emmett-Teller (BET) Surface Area Measurements and Chemical Analyses

Surface areas of the 5%VPO_s/Si catalyst had reduced to 263.78 m² g⁻¹ as compared to that of bare silica support, i.e. 278.61 m² g⁻¹ (Table 5.2). This was due to the near micro-size porous were readily plugged and uniformly covered with VPO_s components as shown, thereby causing the narrow pores to be no longer accessible for nitrogen molecules, which leads to an apparent decreased of specific surface area (Overbeek *et al.*, 1996a).

Table 5.2: Specific surface areas, chemical compositions, average oxidation numbers and percentages of V⁴⁺ and V⁵⁺ oxidation states presents in bulk VPO_s and silica supported catalysts

Catalysts	Specific surface area (m ² g ⁻¹)	P/V	V ⁴⁺	V ⁵⁺	V _{AV}
Bulk VPO _s	19.3	1.05	91.81	8.19	4.0819
Silica	278.6	-	-	-	-
Si-5%VPO _s	263.8	1.10	74.71	25.29	4.2529
Si-10%VPO _s	230.7	1.20	78.50	21.50	4.2150
Si-15%VPO _s	210.0	1.22	82.30	17.70	4.1770
Si-20%VPO _s	171.4	1.23	84.40	15.60	4.1560
Si-25%VPO _s	199.9	1.34	93.68	6.32	4.0632
Si-30%VPO _s	202.3	1.37	99.47	0.53	4.0053

The specific surface areas were gradually decreased as the VPO_s loadings increased from 5 to 20 wt% (Table 5.2), in accordance with the previous findings for the silica supported vanadyl pyrophosphate (Nie *et al.*, 2003; Overbeek *et al.*, 1996a; Nie *et al.*, 2001). This phenomenon indicated that VPO_s components were starting dispersed onto the silica successfully.

However, there was an increase of specific surface area as the VPO_s loadings further increased from 20 wt% to 30 wt%. As refer to the results from XRD analyses (Table 5.1), an increase of crystallite size was found at higher loading catalysts, i.e. 15-30 wt%. The agreement between the results of the BET surface area measurements and the XRD analyses suggested that the crystalline VPO_s phase start growing as the VPO_s phase layers up, which contributes to the surface areas measurements. Besides, the formation of prominent rosette-shape at high level of VPO_s loadings, i.e. > 10 wt%, also explains the increase of surface areas (Xiao *et al.*, 2004).

The P/V atomic ratios were increased from 1.05 to ~1.37, as the VPO_s loadings were increased (Table 5.2). Nie *et al.* (2001) also noted the degree of P enrichment becomes more pronounced at higher VPO loading in MCM-41 supported samples. The state of silica supported VPO_s phase was believed varied with the increasing VPO_s loadings (Nie *et al.*, 2001). This was due to the effect of SiO₂-VPO_s interaction onto the supported VPO_s phase, whereby tendency of P to remain in the catalysts increased as the amounts of VPO_s loading increased. On the other hand, the average oxidation numbers of the V was increased significantly at 5 wt% of VPO_s loading, i.e. from 4.08 to 4.25. However, the V_{AV} values gradually decreased to 4.01 as the VPO_s loadings increased to 30 wt%. The SiO₂-VPO_s interaction at low VPO_s loading sample (5%VPO_s/Si) not only hindered the formation of crystalline (VO)₂P₂O₇ phase, but also promoted the formation of amorphous V⁵⁺ phase (Nie *et al.*, 2001; Harding *et al.*, 1994).

Moreover, it is well known P/V atomic ratio plays an important role in determining the selectivity, where high P/V ratios were reported to promote selectivity, and also prevents the over oxidation of the V from its V^{4+} oxidation state (Nakamura *et al.*, 1974; Hodnett *et al.*, 1983). Hence, the decrease of average oxidation numbers of V to $\sim 4+$ was attributed to the enrichment of P element.

5.2.4 Temperature-programmed Desorption (TPD) of O_2 Analyses

TPD of O_2 profiles shown in Figure 5.4 were obtained through the process same as that described in Section 4.2.4. The TPD profiles of all the silica supported VPO_s catalysts (Figure 5.4) show a peak maximum at ~ 800 K. The intensities of the reduction peaks increased gradually with increasing of VPO_s loadings. Table 5.3 gives a summary of data obtained for the TPD of O_2 analysis. During the TPD analyses (He, 1 bar, $25 \text{ cm}^3 \text{ min}^{-1}$), the amount of lattice oxygen being desorbed thermally from the silica supported VPO_s catalysts were entirely contributed from the VPO_s phase since there was no desorbed oxygen determined for bare silica. The amounts of desorbed oxygen were increased from 0.1634×10^{19} to $0.9325 \times 10^{19} \text{ atom g}^{-1}$ when the amounts of VPO_s loading increased from 5 wt% to 30 wt% (Table 5.3). This was due to the increase of lattice oxygen atoms available as the amounts of VPO_s loading increased. Additionally, as the VPO_s loadings increased, VPO_s phase would layer up on the silica support. Hence,

the mobility of the lattice oxygen could be reduced, which caused more oxygen to be desorbed thermally.

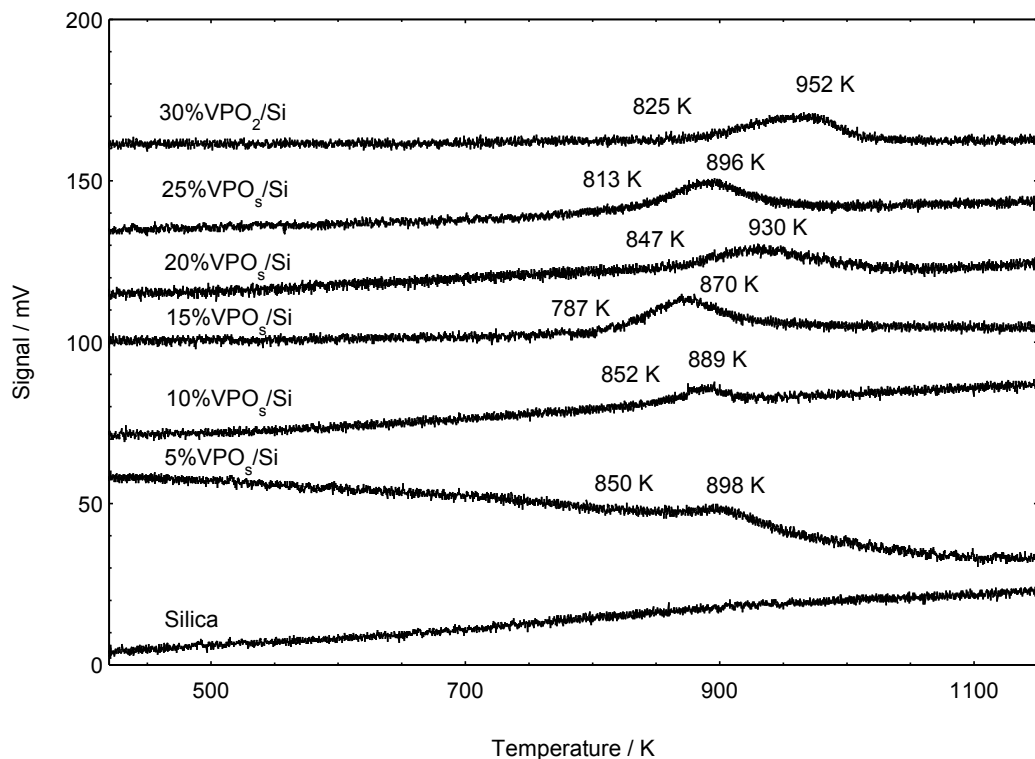


Figure 5.4 TPD of O₂ profiles of silica and silica supported VPO_s catalysts

Table 5.3: Amounts of oxygen atoms desorbed and values of desorption activation energy obtained by TPD analyses for bulk VPO_s and silica supported VPO_s catalysts

Catalyst	T _{onset} (K)	T _{max} (K)	Desorption activation energy, E _d (kJ mol ⁻¹)	Amount of oxygen desorbed (× 10 ⁻⁴ mol g ⁻¹)	Amount of oxygen desorbed (× 10 ¹⁹ atom g ⁻¹)
Bulk VPO_s	923	971	162.3846	1.0026	6.0377
Silica	-	-	-	-	-
5%VPO_s/Si	863	898	150.1765	0.02713	0.1634
10%VPO_s/Si	852	889	148.6714	0.1093	0.6584
15%VPO_s/Si	787	870	145.4939	0.1265	0.7615
20%VPO_s/Si	847	930	155.5280	0.1338	0.8058
25%VPO_s/Si	813	896	149.8420	0.1464	0.8816
30%VPO_s/Si	848	966	161.5484	0.1549	0.9325

5.2.5 Temperature-programmed Reduction (TPR) in H₂ Analyses

The partial oxidation of *n*-butane on VPO catalyst was well accepted to proceed via a redox mechanism as reported by Centi and his coworkers (Centi *et al.*, 1988). The nature of the oxidising species which directly affect the reduction property of a catalyst could give a great impact to its selectivity and activity. Therefore, it is important to determine the types of oxygen species available in the catalysts. For the partial oxidation of *n*-butane, the reaction only involves the reduction of V⁴⁺ and V⁵⁺. The further reduction of V³⁺ is not of concern since it was reported that V³⁺ sites were not observed in the first hours of *n*-butane activation at the moment where MA begins to be detected (Volta, 2000).

TPR in H₂ profiles shown in Figure 5.5 were obtained through the process same as that described in Section 4.2.4. Table 5.4 lists the peak maxima temperatures, the amount of removed oxygen in each peak and the derived reduction activation energies.

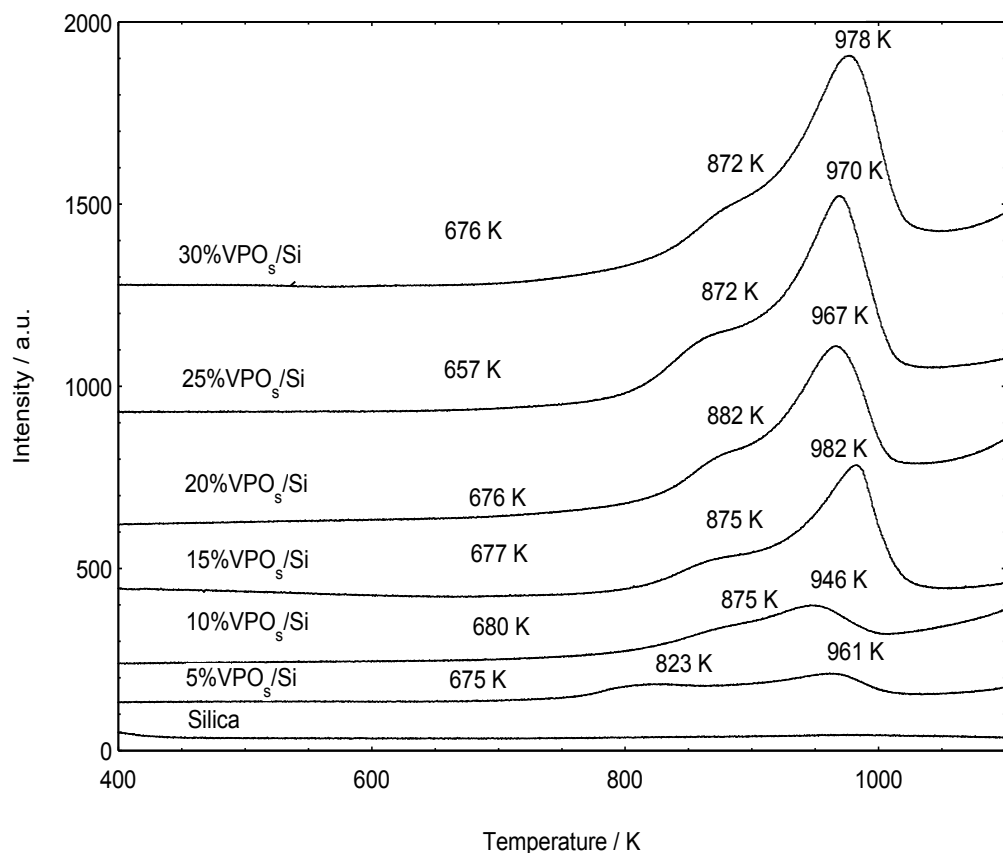


Figure 5.5: TPR in H₂ profiles of silica and silica supported VPO_s catalysts

The bare silica cannot be reduced at the temperatures used as no reduction peak could be observed. Thus, the reducibility of the catalysts obtained must be totally attributed to the supported VPO_s phase (Overbeek, 1996a). The silica supported VPO_s catalysts showed two reduction peaks during the analyses at ~850 K and ~950 K. As explained in Section 4.2.5, both peaks were assigned to the removal of oxygen species associated with V⁵⁺ and V⁴⁺ phases, respectively as stated by Pierini *et al.* (2005). Both V⁵⁺ and V⁴⁺ species were reported in literatures (Herrmann *et al.* 1997; Abon and Volta, 1997; Volta, 2000; Abon *et al.*,

2001) to be associated with O^{2-} and O^- , respectively. Furthermore, $V^{4+}-O^-$ and $V^{5+}-O^{2-}$ are responsible for activity and MA selectivity, respectively (Volta, 2000; Hermann *et al.*, 1997; Taufiq-Yap *et al.*, 2006a; Taufiq-Yap *et al.*, 2011a; Taufiq-Yap *et al.*, 2011b; Coulston *et al.*, 1997; Centi *et al.*, 1988; Granados *et al.*, 1993).

The consumption of H_2 starts at ~ 670 K with the calculated reduction activation energy (Equation 4.2) of ~ 135 kJ mol^{-1} for $V^{5+}-O^{2-}$ species and ~ 160 kJ mol^{-1} for $V^{4+}-O^-$ species. The major reduction process of O^- species was completed as the temperature rose to 1100 K. As listed in Table 5.4, the amounts of removal of both $V^{5+}-O^{2-}$ and $V^{4+}-O^-$ were increased with the amounts of VPO_5 loading due to the increase of reducible active phase on the silica support.

Table 5.4: Amounts of oxygen atoms removed and values of reduction activation energy obtained by TPR analyses for bulk VPO_s and silica supported VPO_s catalysts

Catalyst	T _{onset} (K)	T _{max} (K)	Reduction activation energy, E _r (kJ mol ⁻¹)	Oxygen Atom Removed (× 10 ⁻⁴ mol/g)	Oxygen Atom removed (atom/g × 10 ¹⁹)
Bulk VPO_s	620	754	126.0947	9.3256	56.1588
		975	163.0535	18.4044	110.8313
Total oxygen atoms removed				27.7300	166.9901
Silica	-	-	-	-	-
5%VPO_s/Si	675	823	137.6339	0.2032	1.2237
		961	160.7123	0.3565	2.1468
Total oxygen atoms removed				0.5597	3.3705
10%VPO_s/Si	680	875	146.3301	0.5162	3.1086
		946	158.2038	0.7133	4.2955
Total oxygen atoms removed				1.2294	7.4041
15%VPO_s/Si	677	875	146.3301	0.5835	3.5138
		982	164.2241	1.4987	9.0252
Total oxygen atoms removed				2.0822	12.5390
20%VPO_s/Si	676	882	147.5007	0.6744	4.0612
		967	161.7157	2.0236	12.1861
Total oxygen atoms removed				2.6980	16.2473
25%VPO_s/Si	657	872	145.8284	0.8127	4.8941
		970	162.2174	2.3555	14.1848
Total oxygen atoms removed				3.1682	19.0789
30%VPO_s/Si	659	872	145.8284	1.0615	6.3924
		978	163.5553	2.9716	17.8950
Total oxygen atoms removed				4.0331	24.2873

Therefore, an increase for both activity and selectivity to MA was expected in the catalytic reaction. Even though the amount of oxygen atoms removed from the silica supported VPO_s catalysts was lower than that of the bulk VPO_s catalyst (Table 5.4), but a higher reactivity was still expected. This was because Wachs *et al.* (1996) and Ramis *et al.* (1990) had studied the molecular structures of the surface metal oxide species and proved that these surface species possessed only one terminal $\text{V}=\text{O}$ bond. On the other hand, Tanenaka *et al.* (1997) found that the vanadia species supported on silica consist exclusively of isolated tetrahedral VO_x groups possessing three bridging $\text{V}-\text{O}-\text{support}$ bonds. The silica supported vanadia had longer $\text{V}-\text{O}-\text{support}$ and shorter $\text{V}=\text{O}$ bond length as compared to other metal oxide supports, such as titania and alumina. Besides that, microcrystalline phase of vanadia was also observed. Li *et al.* (2006b) had also explained the increase of *n*-butane conversion from a view point of steric effect and proposed a molecular structure of silica supported $(\text{VO})_2\text{P}_2\text{O}_7$ (Figure 5.6). Hence, the immobilised VPO_s phase on silica support could increase the number of active sites exposed to the reacting molecules and facilitate partial oxidation of *n*-butane.

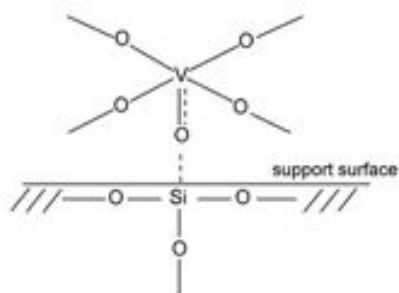


Figure 5.6: Molecular structure of silica supported $(\text{VO})_2\text{P}_2\text{O}_7$ (Li *et al.*, 2006b)

5.2.6 Catalytic Oxidation of *n*-Butane to Maleic Anhydride

Catalytic performances of all the samples in second series were investigated in the environment same as that described in Section 4.2.6. Table 5.5 lists the percentage of *n*-butane conversion and selectivity of each product for bulk VPO_s and silica supported VPO_s catalysts.

It could be clearly seen that the catalytic activity was gradually increased from 6 % to 33 % with the VPO_s loadings from 5 wt% to 30 wt% in Table 5.5. The increase of *n*-butane conversion at higher VPO_s loading could be correlated to the increased number of active sites available (Overbeek *et al.*, 1996a; Li *et al.*, 2006a; Xiao *et al.*, 2004). Chen and Munson (2002) had proposed a single site mechanism of *n*-butane oxidation on VPO catalysts through isotopic labelling studies and the terminal oxygen in (VO)_x unit of (VO)₂P₂O₇ was suggested to be involved in the redox cycle. Thus, the increase of activity with respect to VPO_s dispersion on the silica support strongly supports that the terminal oxygen has a direct relationship with the *n*-butane conversion (Li *et al.*, 2006b). According to Overbeek *et al.* (1996a), Nie *et al.* (2001) and Li *et al.* (2006b), the low activity for 5%VPO_s/Si and 10%VPO_s/Si could be attributed to a higher percentage of oxygen species available in catalysts which exhibits higher stability especially those at the interface of silica-VPO_s, which were shared among the neighboring Si and V. This leads to a lower reducibility of VPO_s components.

The MA selectivity of silica supported VPO_s catalysts were increased from 5% VPO_s/Si at 52% to 30% VPO_s/Si at 93% gradually (Table 5.5). The reason for the lower selectivity at lower VPO_s loading (5% VPO_s/Si) might be due to more reactive oxygen species that are responsible for the formation of CO_x (Li *et al.*, 2006a).

Table 5.5: Catalytic performances of bulk VPO_s and silica supported VPO_s catalysts

Catalyst	<i>n</i> -butane conversion (%)	Product selectivity (%)		
		MA	CO_2	CO
Bulk VPO_s	21	73	15	11
5%VPO_s/Si	6	52	19	29
10%VPO_s/Si	8	67	9	23
15%VPO_s/Si	20	80	5	15
20%VPO_s/Si	23	85	8	6
25%VPO_s/Si	26	88	10	2
30%VPO_s/Si	33	93	3	5

5.3 Effect of Different Calcination Temperatures on Physico-chemical, Reactivity and Catalytic Properties of Supported Vanadyl Pyrophosphate Catalysts

The activated unsupported $(\text{VO})_2\text{P}_2\text{O}_7$ catalyst was denoted as Bulk VPO_s , where $_s$ represents the preparation method, i.e. via sesquihydrate route. The precursor for 30% VPO_s/Si in the second series of samples which calcined at 733 K was calcined at another two different temperatures, i.e. 673 K and 793 K, respectively. The activated silica supported $(\text{VO})_2\text{P}_2\text{O}_7$ catalysts in third series of samples, were denoted as TXVPO_s/Si , where X represents the temperature during activation process, i.e. 400, 460 and 520. The effect of different calcination

temperatures on silica support on the physic-chemical, reactivity and catalytic properties of supported VPO_s catalysts were investigated.

5.3.1 X-ray Diffraction (XRD) Analyses

From the diffractograms of silica supported VPO_s catalysts (Figure 5.7), silica supported sesquihydrate precursors were successfully transformed into their final active phase after the activation under a flow of 0.75 % *n*-butane/air. The main characteristic peaks for vanadyl pyrophosphate, $(\text{VO})_2\text{P}_2\text{O}_7$ was found in the bulk VPO_s catalyst at $2\theta = 22.98^\circ$, 28.45° and 29.95° , which corresponded to (0 2 0), (2 0 4), and (2 2 1) planes, respectively (JCPDS File No. 34-1381). The broad peak which appeared at $2\theta = 22.56$ in the XRD patterns of the silica supported VPO_s catalysts was represented by the silicone dioxide phase (JCPDS 42-1401), which was being suppressed after the dispersion of the VPO_s components due to the partial blocking of mesopores by VPO_s components and thus resulting in a reduction of long-range order of silica (Nie *et al.*, 2003; Li *et al.*, 2006a; Li *et al.*, 2006b). Meanwhile, three additional characteristic peaks for $(\text{VO})_2\text{P}_2\text{O}_7$ appeared at $2\theta = 28.45^\circ$, 29.95° and 43.25° for all the three silica supported VPO_s catalysts. Besides that, the absence of peak at $2\theta = 22.98^\circ$, which corresponded to (0 2 0) reflection plane, in the diffractograms for silica supported VPO_s was overlapped by the broad peak of silica at $2\theta = 22.56$.

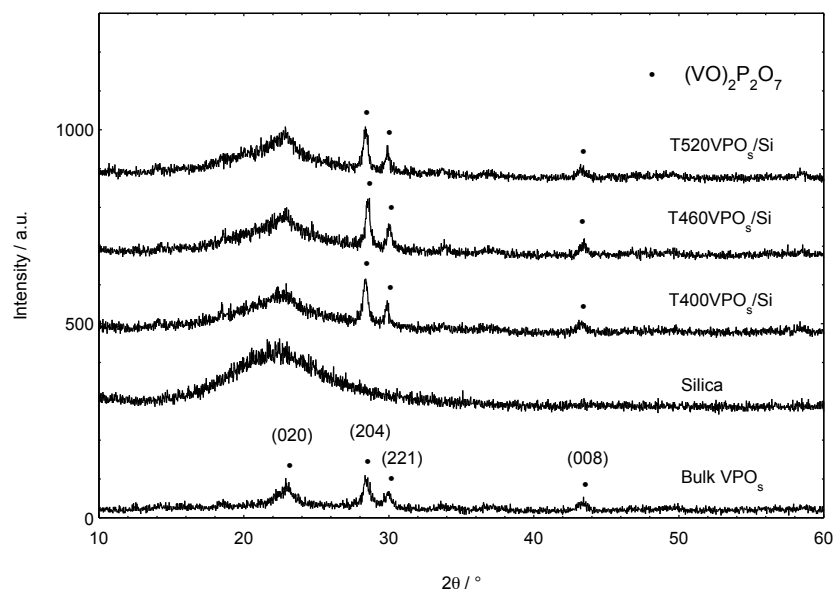


Figure 5.7: Powder XRD patterns of bulk VPO_s and silica supported VPO_s catalysts

The crystallite sizes of synthesised catalysts were calculated by Debye-Scherrer equation as shown in Equation 4.1 (Klug and Alexander, 1974). Based on the XRD data (Table 5.6), the line width was inversely proportionate with the calcination period. This phenomenon indicated that the crystallite size of the VPO_s phase was increasing, since the decrease in FWHMs of the reflection planes with a longer time on stream indicated that the crystalline size increased. This phenomenon was also observed by Taufiq-Yap *et al.* (2004) in the unsupported VPO catalysts which were synthesised through the sesquihydrate route whereby smaller surface areas and larger crystallite sizes were obtained for longer duration of calcinations of the catalysts. Thus, it could be rationalised that a sintering effect had occurred when the catalysts were subjected to either higher calcination temperatures or longer calcination duration.

Table 5.6: XRD data of bulk VPO_s and silica supported VPO_s catalysts

Catalyst	Linewidth ^a (204) / °	Linewidth ^b (221) / °	Crystallite size ^c (204) / Å	Crystallite size ^c (221) / Å
Bulk VPO_s	0.8222	0.7696	98.2005	105.8720
Silica	-	-	-	-
T400VPO_s/Si	0.7400	0.7300	109.4199	111.3399
T460VPO_s/Si	0.5933	0.5533	136.5696	146.9419
T520VPO_s/Si	0.6266	0.5800	129.6948	140.4475

^a FWHM of (020) reflection

^b FWHM of (204) reflection

^c Crystallite size by means of Scherrer's formula : $T (\text{Å}) = (0.89 \times \lambda) / (\text{FWHM} \times \cos\theta)$

5.3.2 Scanning Electron Microscopy (SEM)

Figure 5.2 (b): (ii) had clearly shown that there was porous surface on the bare silica support. After being impregnated with the VPO_s components, it could be observed that the pores of the silica support were plugged with the VPO_s components (Figure 5.8). At higher magnification, the characteristic rosette-shape of vanadyl pyrophosphate phase was observed in the structure of the supported VPO_s components (Kiely *et al.*, 1995). The supported VPO_s components exhibit similar principal structure as compared to that of the bulk VPO_s catalysts. The layers of rosette-shape cluster is well known to increase the exposure of the basal (1 0 0) (VO)₂P₂O₇ (Kiely *et al.*, 1995; Taufiq-Yap *et al.*, 2006b). When carefully studied Figure 5.8 (b): (iii) and (c): (iii), they showed the rosette-plates were flattened together for T520VPO_s/Si and less splits were observed. Besides that, some blocky type crystallites was found, according to Kiely *et al.* (1996), which were believed to be the VOPO₄ phase. However, as compared to the γ -alumina supported VPO catalysts which were calcined for ≥ 30 hours (Taufiq-Yap *et al.*,

2007a), it was too little to be detected under XRD analyses. This phenomenon suggested that sintering of VPO_s phase had occurred due to the relatively high calcination temperature used.

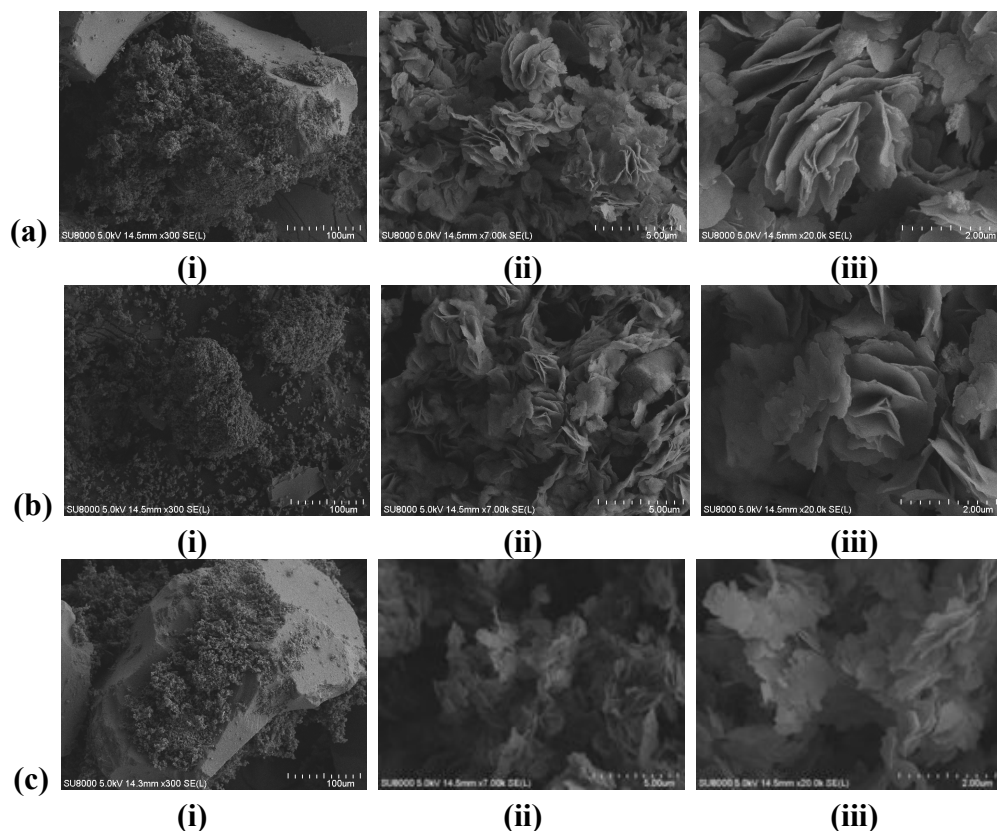


Figure 5.8: SEM micrographs for (a) T400VPO_s/Si: (i) $\times 300$ (ii) $\times 7,000$ (iii) $\times 20,000$; (b) T460VPO_s/Si: (i) $\times 300$ (ii) $\times 7,000$ (iii) $\times 20,000$; (c) T520VPO_s/Si: (i) $\times 300$ (ii) $\times 7,000$ (iii) $\times 20,000$

5.3.3 Brunauer-Emmett-Teller (BET) Surface Area Measurements and Chemical Analyses

According to BET surface area values tabulated as Table 5.7, the specific surface areas of the silica supported catalysts were significantly lower as compared to the bare silica support, i.e. $278 \text{ m}^2 \text{ g}^{-1}$. This was due to the narrow pores were readily plugged and uniformly covered with VPO_s components,

therefore causing the narrow pores to be no longer accessible for nitrogen molecules, which leads to an apparent decrease in specific surface area (Overbeek *et al.*, 1996a; Overbeek *et al.*, 1996b). Furthermore, the specific surface area was reduced from 211.49 m²/g to 160.30 m²/g when the calcination temperature was increased from 673 K to 793 K. In agreement with the XRD values, it could be rationalised that sintering effect had occurred when silica supported VPO_s catalysts subjected to higher calcination temperature.

Table 5.7: Specific surface areas, chemical compositions, average oxidation numbers and percentages of V⁴⁺ and V⁵⁺ oxidation states presents in bulk VPO_s and silica supported catalysts

Catalysts	Specific surface area (m ² g ⁻¹)	P/V	V ⁴⁺	V ⁵⁺	V _{AV}
Bulk VPO_s	19.29	1.05	91.81	8.19	4.0819
Silica	278.61	-	-	-	-
T400VPO_s/Si	211.49	1.40	97.98	2.02	4.0202
T460VPO_s/Si	202.30	1.37	99.47	0.53	4.0053
T520VPO_s/Si	160.30	1.39	89.62	10.38	4.1038

The P/V atomic ratios for all the catalysts obtained were increased from 1.05 for the bulk VPO_s to ~1.40 for the silica supported VPO_s (Table 5.7). P enrichment of VPO samples also had been reported by Nie *et al.* (2001) using MCM-41 as being caused by the varied state of VPO_s phase when supported onto the silica. The average oxidation number of V was found to be about 4.05 for all the silica supported VPO_s catalysts. According to Nakamura *et al.* (1974) and Hodnett *et al.* (1983), a high P/V atomic ratio could maintain the average oxidation number of V close to +4.

5.3.4 Temperature-programmed Desorption (TPD) of O₂ Analyses

Figure 5.9 showed the TPD of O₂ (He, 1 bar, 25 cm³ min⁻¹) profiles for bulk VPO_s and silica supported VPO_s that analysed at the temperature from ambient temperature to 1223 K at the rate of 5 K min⁻¹ in that stream. All the catalysts gave a maximum peak at ~940 K. T_{onset} for TPD is the temperature whereby the surface oxygen starts to be desorbed (Fadoni *et al.* 1999). T_{onset} was lowered to 937 K for T400VPO_s/Si as compared to that of the bulk VPO_s catalyst, i.e. 971 K (Table 5.8). However, it gradually increased with the calcination temperatures to 849 K. In Figure 5.9, it could be observed that the maxima peaks were shifted to higher temperature from T400VPO_s/Si to SiT520VPO_s.

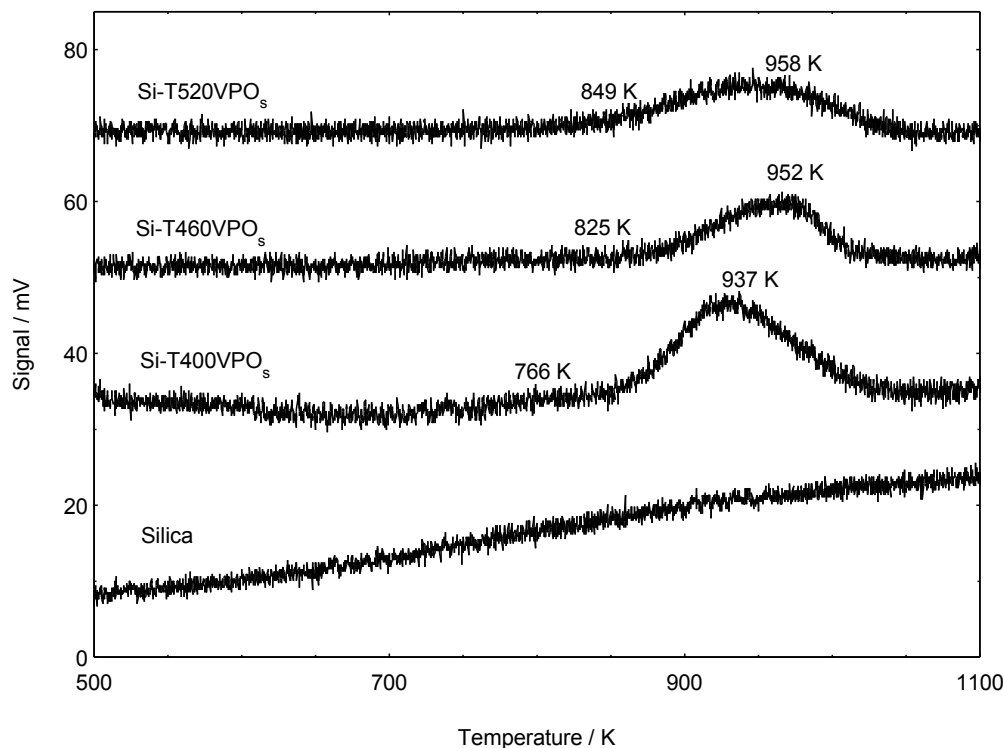


Figure 5.9: TPD of O₂ profiles of silica and silica supported VPO_s catalysts

Table 5.8: Amounts of oxygen atoms desorbed and values of desorption activation energy obtained by TPD analyses of O₂ for bulk VPO_s and silica supported VPO_s catalysts

Catalyst	T _{onset} (K)	T _{max} (K)	Desorption activation energy, E _d (kJ mol ⁻¹)	Amount of oxygen desorbed (× 10 ⁻⁴ mol g ⁻¹)	Amount of oxygen desorbed (× 10 ¹⁹ atom g ⁻¹)
Bulk VPO_s	923	971	162.3846	1.1246	6.7726
Silica	-	-	-	-	-
T400VPO_s/Si	839	937	156.6986	0.2932	1.7657
T460VPO_s/Si	848	966	152.2072	0.1549	0.9325
T520VPO_s/Si	798	946	160.2106	0.1186	0.7140

By applying the Redhead (1962) equation (Equation 4.2) to T_{max}, an increase in the desorption energy was also obtained, i.e. from 156.70 to 160.21 kJ mol⁻¹. However, they were lower as compared to that of the bulk VPO_s, i.e. 162.38 kJ mol⁻¹. The amounts of oxygen desorbed thermally also decreased with the calcination temperatures at 1.7657×10^{19} atom g⁻¹, 0.9325×10^{19} atom g⁻¹, and 0.7140×10^{19} atom g⁻¹ for T400VPO_s/Si, T460VPO_s/Si, and T520VPO_s/Si, respectively. This indicated that the lattice oxygen from silica supported VPO_s catalysts were more labile as compared to that of the bulk VPO_s catalyst. However, the mobility of lattice oxygen decreased as the calcination temperatures increased.

5.3.5 Temperature-programmed Reduction (TPR) in H₂ Analyses

Fresh samples were prepared and analysed by TPR (5.55 % H₂/N₂, 1 bar, 25 cm³ min⁻¹). As the temperature was increased from ambient temperature to 1100 K, two reduction peaks appeared in the profiles. The results of TPR analysis were shown in Figure 5.10 and tabulated in Table 5.9. The reduction activation energies were obtained by applying the Redhead (1962) equation (Equation 4.2) onto the T_{max}.

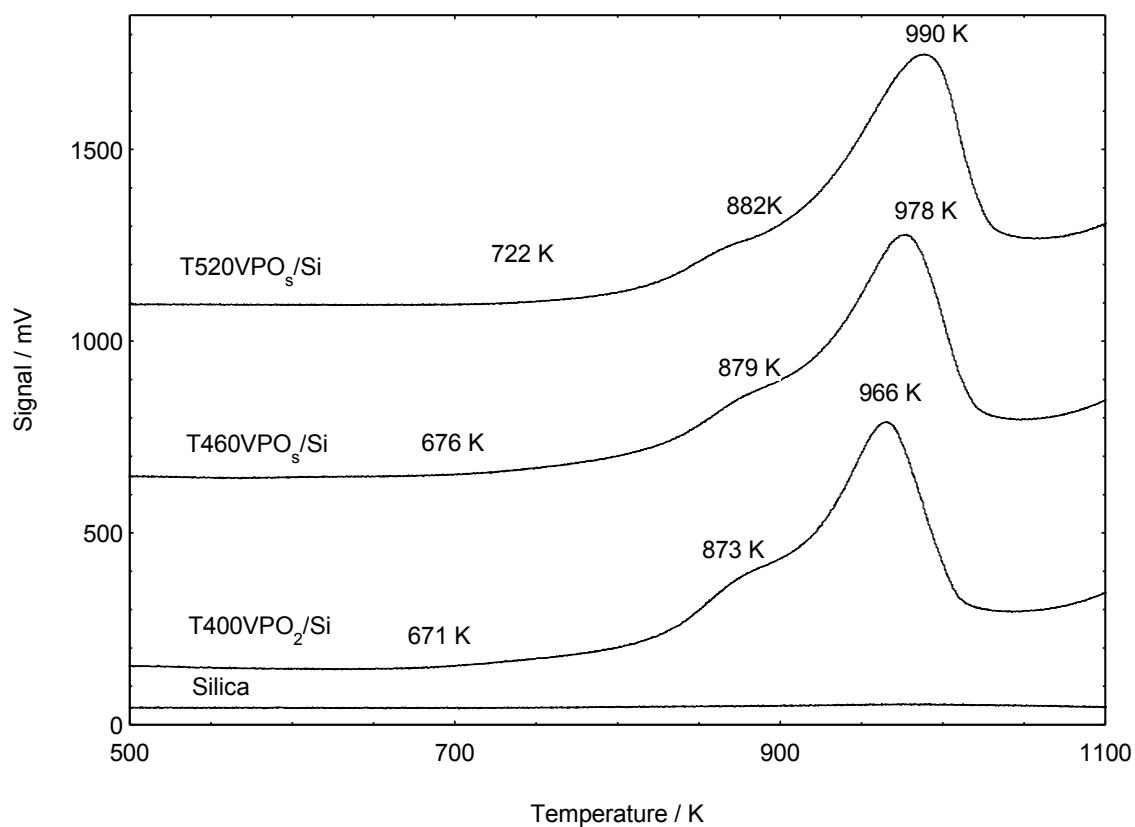


Figure 5.10: TPR in H₂ profiles of silica and silica supported VPO_s catalysts

Table 5.9: Amounts of oxygen atoms removed and values of reduction activation energy obtained by TPR analyses for bulk VPO_s and silica supported VPO_s catalysts

Catalyst	T _{onset} (K)	T _{max} (K)	Reduction activation energy, E _r (kJ mol ⁻¹)	Oxygen Atom Removed (× 10 ⁻⁴ mol/g)	Oxygen Atom removed (atom/g × 10 ¹⁹)
Bulk VPO_s	620	754	126.0947	0.9326	56.1588
		975	163.0535	1.8404	110.8313
Total oxygen atoms removed				2.7544	166.9901
Silica	-	-	-	-	-
Si-T400VPO_s	671	876	146.4973	1.5243	9.1794
		966	161.5484	3.1159	18.7641
Total oxygen atoms removed				4.6402	27.9436
Si-T460VPO_s	659	872	145.8284	1.0615	6.3924
		978	163.5553	2.9716	17.8950
Total oxygen atoms removed				4.0331	24.2873
Si-T520VPO_s	722	869	145.3267	0.5393	3.2476
		990	165.5621	2.9312	17.6517
Total oxygen atoms removed				3.4705	20.8993

Bare silica cannot be reduced at these temperatures as no reduction peak was observed. Thus, the reducibility obtained must be totally attributed to the supported VPO_s phase (Overbeek *et al.*, 1996a). The assignation of both reduction peaks to V⁵⁺-O²⁻ and V⁴⁺-O⁻ species and the role of these two oxygen species have explained in Section 4.2.5 and 5.2.5.

By referring to the data of TPR, both of the amounts of V⁵⁺-O²⁻ and V⁴⁺-O⁻ removed from silica supported VPO_s were observed to decrease with the calcination temperatures, i.e. 9.1794×10^{19} , 6.3924×10^{19} , and 3.2476×10^{19} atom g⁻¹ of V⁵⁺-O²⁻; 18.7641×10^{19} , 17.8950×10^{19} and 17.6571×10^{19} atom g⁻¹ of

$V^{4+}-O^-$ for T400VPO_s/Si, T460VPO_s/Si, and T520VPO_s/Si, respectively. Additionally, two peaks for each silica supported VPO_s catalyst were shifted to the right as the calcination temperature was increased, and the reduction energies needed were generally increased from T400VPO_s/Si to T520VPO_s/Si (Table 5.9). Therefore, a decrease for both activity and selectivity to maleic anhydride (MA) was expected in the catalytic reaction. However, practically T460VPO_s/Si was found to have the best catalytic performance among the three silica supported VPO_s catalysts. This would be discussed later in Section 5.3.6.

Even though the amount of oxygen atoms removed from the silica supported VPO_s catalysts was lower than that of the bulk VPO_s catalyst, but a higher reactivity was still anticipated. As explained in Section 5.2.5, Li *et al.* (2006b) had reported that the increase of *n*-butane conversion was due to steric effect and proposed a molecular structure of silica supported (VO)₂P₂O₇ (Figure 5.6). Hence, the immobilised VPO_s phase on silica support could increase the number of active sites exposed to the reacting molecules and facilitate the partial oxidation of *n*-butane.

5.3.6 Catalytic Oxidation of *n*-Butane to Maleic Anhydride

The influence of various calcination temperatures on the activity and selectivity to MA of silica supported VPO_s was investigated in a fixed bed microreactor at 673 K, a typical reaction temperature for VPO catalysts (Leong *et al.*, 2011). Catalytic performances of the catalysts were presented in terms of percentage in Table 5.10.

Overall, silica supported VPO_s have a significant increase of catalytic activity. As explained in Section 5.2.5, this phenomenon strongly supports that the terminal oxygen has a direct relationship with the *n*-butane conversion (Chen and Munson, 2002; Li *et al.*, 2006b).

T460VPO_s/Si had achieved both the highest catalytic activity and selectivity to MA as compared to T400VPO_s/Si and T520VPO_s/Si, *i.e.* 33 % and 93 %, respectively. The inconsistency with the data from TPR analyses could be attributed to the different transition states which were involved in the reduction process when different reducing agents were used, *i.e.* H₂ in TPR analyses and *n*-butane in catalytic tests. However, results from catalytic tests would be more reliable as compared to that from TPR analyses.

Table 5.10: Catalytic performances of bulk VPO_s and silica supported VPO_s catalysts

Catalyst	<i>n</i> -butane conversion (%)	Product selectivity (%)		
		MA	CO ₂	CO
Bulk VPO_s	21	73	15	11
T400VPO_s/Si	25	83	11	6
T460VPO_s/Si	33	93	3	5
T520VPO_s/Si	19	81	11	8

5.4 Conclusions

There were two series of silica supported VPO_s catalysts successfully synthesised via wetness impregnation of VOHPO₄·1.5H₂O precursors. In the first series of silica supported VPO_s catalysts, a range of 5–30 wt% of VPO_s loadings were supported on bare silica support. Then the precursor for 30%VPO_s/Si in the first series was calcined at another two different temperatures to give second series of silica supported VPO_s catalysts. The influences of various VPO_s loadings and different activation temperatures onto the physico-chemical properties and catalytic performance were studied. The silica supported VPO_s phases were found to be in the amorphous form at 5 wt% loading. Above 5 wt% loading, the VPO_s phase gradually became more crystalline as the VPO_s loadings increased, as obtained from XRD and SEM results. At low loading (5%VPO_s/Si), the strong SiO₂-VPO_s interaction effect on the upper layers of VPO_s components has increased the average oxidation state of V to 4.25. Then it decreased gradually with an increasing of P/V atomic ratio. TPD analyses have revealed that higher mobility of lattice oxygen existed for high VPO_s loadings of catalysts. The

reducibility of silica supported VPO_s catalysts was found to be increased with the amounts of VPO_s loading via TPR analyses. The *n*-butane conversion was increased as the VPO_s loadings increased, i.e. from 6 % to 33 %. The better catalytic activity of 20% VPO_s/Si , 15% VPO_s/Si and 30% VPO_s/Si , as compared to that for bulk VPO_s , i.e. 21 % strongly supports that the terminal oxygen in $(\text{VO})_x$ has a direct relationship with the activity and it occurred through a single site mechanism on VPO catalysts. The selectivity of silica supported VPO_s catalysts was increased, i.e. from 52 % to 93 %. The optimised silica supported VPO_s catalysts is 30% VPO_s/Si because it gives highest MA selectivity and catalytic activity. On the other hand, the active phase that supported on silica in second series has been confirmed by XRD analyses also. When the precursor for 30% VPO_s/Si calcined at high temperature, i.e. 793 K, the rosette-plates were flattened together and blocky type crystallite was found. This suggests a sintering effect happened at high activation temperature, i.e. 793 K. The P/V atomic ratio and the average oxidation number of V for 30% VPO_s/Si did not affected significantly by various activation temperatures. The calcination temperature at 733 K was found to be the optimum activation temperature for silica supported VPO_s catalyst since T460 VPO_s/Si gave the best catalytic performance among the samples.

REFERENCES

- Abdelouahab, F. B., Olier, R., Ziyad, M. and Volta, J. C. (1995). The role of Fe and Co dopants during the activation of the $\text{VO}(\text{HPO}_4) \cdot 0.5\text{H}_2\text{O}$ precursor of the vanadium phosphorus catalyst as studied by *in Situ* Laser Raman Spectroscopy. *Journal of Catalysis*, 157 (2), 687–697.
- Abon, M. and Volta, J. C. (1997). Vanadium phosphorus oxides for *n*-butane oxidation to maleic anhydride. *Applied Catalysis A: General*, 157 (1–2), 173–192.
- Abon, M., Herrmann, J. M. and Volta, J. C. (2001). Correlation with the redox $\text{V}^{5+}/\text{V}^{4+}$ ratio in vanadium phosphorus oxide catalysts for mild oxidation of *n*-butane to maleic anhydride. *Catalysis Today*, 71 (1–2), 121–128.
- Agaskar, P. A., DeCaul, L., and Grasselli, R. K. (1993). A molecular level mechanism of *n*-butane oxidation to maleic anhydride over vanadyl Pyrophosphate. *Catalysis Letters*, 23 (3–4), 339–351.
- Ait-Lachgar, K., Tuel, A., Brun, M., Herrmann, J. M., Kraft, J. M., Martin, J. R., Volta J. C. and Abon, M. (1998). Selective oxidation of *n*-butane to maleic anhydride on vanadyl pyrophosphate: II. Characterization of the oxygen-treated catalyst by electrical conductivity, Raman, XPS, and NMR spectroscopic techniques. *Journal of Catalysis*, 177 (2), 224–230.
- Alonso, M., Lorences, M. J., Pina, M. P., Patience, G. S. (2001). Butane partial oxidation in an externally fluidized bed-membrane reactor. *Catalysis Today*, 67 (1–3), 151–157.
- Anastas, P. T. and Warner, J. C. (1998). What is green chemistry? In: *Green Chemistry: Theory and practice*. (pp. 1–135). New York: Oxford University Press.
- Ballarini, N., Cavani, F., Cortelli, C., Gasparini, F., Mignani, A., Pierelli, F., Trifiro, F., Fumagalli, C. and Mazzoni, G. (2005). The contribution of homogeneous and non-oxidative side reactions in the performance of vanadyl pyrophosphate, catalyst for the oxidation of *n*-butane to maleic anhydride, under hydrocarbon-rich conditions. *Catalysis Today*, 99 (1–2), 115–122.
- Ballarini, N., Cavani, F., Cortelli, C., Ligi, S., Pierelli, F., Trifiro, F., Fumagalli, C., Mazzoni, G. and Monti, T. (2006). VPO catalyst for *n*-butane oxidation to maleic anhydride: A goal achieved, or a still open challenge? *Topics in Catalysis*, 38 (1–3), 147–156.

- Bartholomew, C. H. and Farrauto, R. J. (2006). Catalysts or industrial application. In: *Fundamentals of industrial catalytic processes*. (pp. 1–49). New Jersey: John Wiley & Sons, Inc.
- Bartley, J. K., Kiely, C. J., Wells, R. P. K. and Hutchings, G. J. (2001). Vanadium(V) phosphate prepared using solvent-free method. *Catalysis Letters*, 72 (1–2), 99–105.
- Bartley, J. K., Wells, R. P. K. and Hutchings, G. J. (2000). The unexpected role of aldehydes and ketones in the standard preparation method for vanadium phosphate catalysts. *Journal of Catalysis*, 195 (2), 423–427.
- Batis, N. H., Batis, H., Ghorbel, A., Vedrine, J. C. and Volta, J. C. (1991). Synthesis and characterization of new VPO catalysts for partial *n*-butane oxidation to maleic anhydride. *Journal of Catalysis*, 128 (1), 248–263.
- Bej, S. K. and Rao, M. S. (1991). Selective oxidation of *n*-butane to maleic anhydride. 3. Modeling studies. *Industrial and Engineering Chemistry Research*, 30 (8), 1829–1832.
- Bej, S.K. and Rao, M. S. (1992a). Selective oxidation of *n*-butane to maleic anhydride. 4. Recycle reactor studies. *Industrial and Engineering Chemistry Research*, 31 (9), 2075–2079.
- Bej, S. K. and Rao, M. S. (1992b). Selectivity oxidation of *n*-butane to maleic anhydride, a comparative study between promoted and unpromoted VPO catalysts. *Applied Catalysis A: General*, 83 (2), 149–163.
- Bergeret, G., David, M., Broyer, J. P., Volta, J. C. and Hecquer, G. (1987). A contribution to the knowledge of the active sites of VPO catalysts for butane oxidation to maleic anhydride. *Catalysis Today*, 1 (1–2), 37–47.
- Borders, E. (1987). Crystallochemistry of V–P–O phases and application to catalysis. *Catalysis Today*, 1 (5), 499–526.
- Bordes, E. (1993). Nature of the active and selective sites in vanadyl pyrophosphate, catalyst of oxidation of *n*-butane, butene and pentane to maleic anhydride. *Catalysis Today*, 16 (1), 27–38.
- Bordes, E., Courtine, P. and Johnson, J. W. (1984). On the topotactic dehydration of $\text{VOHPO}_4 \cdot 0.5\text{H}_2\text{O}$ into vanadyl pyrophosphate. *Journal of Solid State Chemistry*, 55 (3), 270–279.
- Bragg, W. L. (1913). The diffraction of short electromagnetic waves by a crystal. *Proceedings of the Cambridge Philosophical Society*, 17, 43–57.

- Brunauer, S., Emmett, P. H. and Teller, E. (1938). Adsorption of gases in multimolecular layers. *Journal of the American Chemical Society*, 60 (2), 309–319.
- Brutovsky, M., Kladekova, D., Reiffova, K. and Kosturiak, A. (1997). Vanadium-phosphorus catalysts modified with magnesium, calcium and barium. *Collection of Czechoslovak Chemical Communications*, 62 (3), 392–396.
- Bueno, J. M. C., Bethke, G. K., Kung, M. C. and Kung, H. H. (1998). Supported VPO catalysts for selective oxidation of butane III: Effect of preparation procedure and SiO₂ support. *Catalysis Today*, 43 (1–2), 101–110.
- Busca, G., Cavani, F., Centi, G. and Trifiro, F. (1986a). Nature and mechanism of formation of vanadyl pyrophosphate: active phase in *n*-butane selective oxidation. *Journal of Catalysis*, 99 (2), 400–414.
- Busca, G., Centi, G. and Trifiro, F. (1986b). *n*-Butane selective oxidation on vanadium-based oxides: Dependence on catalyst microstructure. *Applied Catalysis*, 25 (1–2), 265–272.
- Carreon, M. A., Gulians, V. V., Pierelli, F. and Cavani, F. (2004). Ordered mesostructured mixed metal oxides: Microporous VPO phases for *n*-butane oxidation to maleic anhydride. *Catalysis Letters*, 92 (1–2), 11–16.
- Cavani, F. and Trifiro, F. (1994). Catalysing butane oxidation to make maleic anhydride. *Chemtech*, 25 (34), 18–25.
- Cavani, F. and Trifiro, F. (2004). Oxidation of *n*-butane to maleic anhydride. In: Baerns, M. (Ed.), *Basic principles in applied catalysis*. (pp. 19–84). New York: Springer.
- Centi, G. (1993). Vanadyl Pyrophosphate—A Critical Overview. *Catalysis Today*, 24 (16), 5–26.
- Centi, G. and Perathoner, S. (2003). Reaction mechanism and control of selectivity in catalysis by oxides: Some challenges and open questions. *International Journal of Molecular Sciences*, 2 (5), 183–196.
- Centi, G., Cavini, F., and Trifiro, F. (2001). New reactor technology options. In: *Selective oxidation by heterogeneous catalysis*. (pp. 37–53). New York: Kluwer Academic/Plenum Publishers.
- Centi, G., Fornasari, G. and Trifiro, F. (1984). On the mechanism of *n*-butane oxidation to maleic anhydride: Oxidation in oxygen-stoichiometry-controlled conditions. *Journal of Catalysis*, 89 (1), 44–51.

- Centi, G., Golinelli, G. and Trifiro, F. (1989a). Nature of the active sites of $(VO)_2P_2O_7$ in the selective oxidation of *n*-butane: Evidence from doping experiments. *Applied Catalysis*, 48 (1), 13–24.
- Centi, G., Trifiro, F., Busca, G., Ebner, J. and Gleaves, J. (1989b). Nature of active species of $(VO)_2P_2O_7$ for selective oxidation of *n*-butane to maleic anhydride. *Faraday Discussion of Chemistry Society*, 87 (0), 215–225.
- Centi, G., Nieto, J. L., Ungarelli, F. and Trifiro, F. (1990). On the polyfunctional nature of $(VO)_2P_2O_7$. *Catalysis Letters*, 4 (2), 309–318.
- Centi, G., Trifiro, F., Ebner, J. R. and Franchetti, V. M. (1988). Mechanistic aspects of maleic anhydride synthesis from C4 hydrocarbons over phosphorus vanadium oxide. *Chemical Reviews*, 88 (1), 55–80.
- Chattaraj, P. K. (2001). Chemical reactivity and selectivity: Local HSAB principle versus frontier orbital theory. *Journal of Physical Chemistry A*, 105 (2), 511–513.
- Che, M. and Tench, A. J. (1982). Characterisation and reactivity of mononuclear oxygen species on oxide surface. *Advance Catalysis*, 31, 77–133.
- Chen, B. and Munson, E. J. (2002). Investigation of the mechanism of *n*-butane oxidation on vanadium phosphorus oxide catalysts: evidence from isotopic labeling studies. *Journal of the American Chemical Society*, 124 (8), 1638–1652.
- Cheng, W. and Wang, W. (1997). Effect of calcination environment on the selective oxidation of *n*-butane to maleic anhydride over promoted and unpromoted VPO catalyst. *Applied Catalysis A: General*, 156 (1), 57–69.
- Chorkendorff, I. and Niemantsverdriet, J. W. (2007). Introduction to catalysis. In: *Concepts of modern catalysis and kinetics*. 2nd Edition. (pp. 2–167). Germany: WILEY-VCH Verlag GmbH & Co. KGaA.
- Contractor, R. M., Bergna, H. E., Horowitz, H. S., Blackstone C. M., Malone, B., Torardi, C. C., Griffiths, B., Chodhry, U. and Sleight, A. W. (1987). Butane oxidation to maleic anhydride over vanadium phosphate catalysts. *Catalysis today*, 1 (1–2), 49–58.
- Cornaglia, L. M. and Lombardo, E. A. (1993). Acidity and catalytic behavior of vanadium-phosphorus-oxygen catalysts. *Applied Catalysis A: General*, 100 (1), 37–50.

- Cornaglia, L. M., Carrare, C., Petunchi, J. O. and Lombardo, E. A. (1999). The role of cobalt as promoter of equilibrated vanadium-phosphorus-oxygen catalysts. *Applied catalysis A: General*, 183 (1), 177–187.
- Cornaglia, L., Irusta, S., Lombardo, E. A., Durupty, M. C. and Volta, J. C. (2003). The beneficial effect of cobalt on VPO catalysts. *Catalysis Today*, 78 (1–4), 291–301.
- Coulston, G. W., Bare, S. R., Kung, H., Birkeland, K., Bethke, G. K., Harlow, R., Herron, N. and Lee, P. L. (1997). The kinetic significance of V^{5+} in *n*-butane oxidation catalysed by vanadium phosphates. *Science*, 275 (5297), 191–193.
- Ebner, J. and Gleaves, J. (1988). The vanadium phosphorus oxide catalyst. In: Martel, A. E. and Sawyer, D. T. (Eds.), *Oxygen complexes and oxygen activation by transition metals*. (pp. 273–284). New York and London: Plenum Press.
- Ebner, J. and Thompson, M. (1991). Key structure-activity relationships in the vanadium phosphorus oxide catalyst system. In: Grasselli, R. and Sleight, A. (Eds.), *Studies in surface science and catalysis*. (pp. 31–42). London and New York: Elsevier Science.
- Ellison, I. J., Hutchings, G. J., Sananes, M. T. and Volta, J. C. (1994). Control of the composition and morphology of vanadium phosphate catalyst precursors from alcohol treatment of $VOPO_4 \cdot 2H_2O$. *Journal of the Chemical Society, Chemical Communications*, 8 (9), 1093–1094.
- Fadoni, M. and Lucarelli, L. (1999). Temperature programmed desorption, reduction, oxidation and flow chemisorption for the characterisation of heterogeneous catalysts—Theoretical aspects, instrumentation and applications. *Studies in Surface Science and Catalysis*, 120 (A), 177 – 225.
- Faith, M., Kubias, B., Eberle, H. -J., Estenfelder, M., Steinike, U. and Schneider, M. (2000). Tribomechanical pretreatment of vanadium phosphates: structural and catalytic effect. *Catalysis Letters*, 68 (1–2), 13–18.
- Felthouse, T. R., Burnett, J. C., Horrell, B., Mummey, M. J. and Kuo, Y. (2000). Maleic anhydride, maleic acid, and fumaric acid. In: Kirk-Othmer (Ed.). *Kirk-Othmer encyclopedia of chemical technology*. (pp. 893–928). New York: John Wiley & Sons, Inc.
- Feng, R., Yang, X., Ji, W., Chen, Y. and Au, C. (2007). VPO catalysts supported on H_3PO_4 -treated ZrO_2 highly active for *n*-butane oxidation. *Journal of Catalysis*, 246 (1), 166–176.

- Funada, C. and Greiner, E. (2009). *Maleic Anhydride*. URL: <http://www.sriconsulting.com/CEH/Public/Reports/672.5000/>. Accessed on 19th June 2011.
- Garbassi, F., Bart, J. C. J., Tassinari, R., Vlaic, G. and Lagarde, P. (1986). Catalytic *n*-butane oxidation activity and physicochemical characterisation of vanadium-phosphorus oxides with variable P/V ratio. *Journal of Catalysis*, 98 (2), 317–325.
- Geem, P. C. and Nobel, A. P. P. (1987). Influence of the P/V ratio on the oxidation of *n*-butane and trans-2-butene to maleic anhydride over phosphorus vanadium oxide catalysts. *Catalysis Today*, 1 (1–2), 5–16.
- Gleaves, J. T., Yablonsky, G., Zheng, X., Fushimi, R. and Mills, P. L. (2010). Temporal analysis of products (TAP) Recent advances in technology for kinetic analysis of multi-component catalysts. *Journal of Molecular Catalysis A: Chemical*, 315 (2), 108–134.
- Goh, C. K., Taufiq-Yap, Y. H., Hutchings, G. J., Dummer, N. and Bartley, J. (2008). Influence of Bi-Fe additive on properties of vanadium phosphate catalysts for *n*-butane oxidation to maleic anhydride. *Catalysis Today*, 131 (1), 408–412.
- Gopal, R. and Calvo, C. (1972). Crystal structure of β VPO₅. *Journal of Solid State Chemistry*, 5 (3), 432–435.
- Granados, M. L., Conesa, J. C. and Fernandezgarcia, M. (1993). Physicochemical study of structural disorder in vanadyl pyrophosphate. *Journal of Catalysis*, 24 (36), 671–687.
- Grasselli, R. (1983). Selective oxidation and ammoxidation catalysis: History of catalyst design. In: Nonnelle, J., Delmon, B. and Derouane, E. (Eds.), *Surface properties and catalysis by nonmetals*. (pp. 273–288). London: Springer.
- Grzybowska-Swierkosz, B. (2000). 8 Catalysis. *Annual Reports on the Progress of Chemistry Section C*, 96, 297–334.
- Gulianti, V. V., Benziger, J. B., Sundaresan, S., Wachs, I. E., Jehng, J. -M. and Roberts, J. E. (1996). The effect of the phase composition of model V–P–O catalysts for partial oxidation of *n*-butane. *Catalysis Today*, 28 (4), 275–295.
- Gulianti, V. V., Benziger, J. B., Sundaresan, S., Wachs, I. E. and Yao, N. (1995). Evolution of the active surface of the vanadyl pyrophosphate catalysts. *Catalysis Letters*, 32 (3–4), 379–386.

- Hagen, J. (2006). Individual steps in heterogeneous catalysis. In: *Industrial catalysis: A practical approach*. 2nd Edition. (pp. 5–6). Germany: WILEY-VCH Verlag GmbH & Co. KGaA.
- Hannour, F. K., Martin, A., Kubias, B., Lucke, B., Bordes, E. and Courtine, P. (1998). Vanadium phosphorus oxides with P/V = 2 used as oxidation and ammoxidation catalysts. *Catalysis Today*, 40 (2–3), 263–272.
- Harding, W. D., Birkeland, K. E. and Kung, H. H. (1994). Selective oxidation of butane on phosphorus-modified silica supported vanadia catalysts. *Catalysis Letters*, 28 (1), 1–7.
- Hartley, F. R. (1985). Catalysis. In: *Supported metal complexes: Catalysis by metal complexes*. (pp. 1–3). Holland: D. Reidel Publishing Company.
- Herrmann, J. M., Vernoux, P., Bere, K. E. and Abon, M. (1997). *In situ* study of redox and of p-type semiconducting properties of vanadyl pyrophosphate and of V–P–O catalysts during the partial oxidation of *n*-butane to maleic anhydride. *Journal of Catalysis*, 167 (1), 106–117.
- Hiyoshi, N., Yamamoto, N., Ryumon, N., Kamiya, Y. and Okuhara, T. (2004). Selective oxidation of *n*-butane in the presence of vanadyl pyrophosphate synthesized by intercalation-exfoliation-reduction of layered VOPO₄·2H₂O in 2-butanol. *Journal of Catalysis*, 221 (1), 225–233.
- Hodges, P. (2010). *Maleic anhydride (MA) uses and market data*. URL: <http://www.icis.com/v2/chemicals/9076023/maleic-anhydride.html>. Accessed on 19th June 2011.
- Hodnett, B. K. and Delmon, B. (1985). Factors influencing the activity and selectivity of vanadium-phosphorus oxide catalysts for *n*-butane oxidation to maleic anhydride. *Applied Catalysis*, 15(1), 141–150.
- Hodnett, B. K. and Delmon, B. (1984). Influence of calcination conditions on the phase composition of vanadium-phosphorus oxide catalysts. *Applied Catalysis*, 9 (2), 203–211.
- Hodnett, B. K., Permann, Ph. and Delmon, B. (1983). Influence of P/V ratio on the phase composition and catalytic activity of vanadium phosphate based catalysts. *Applied Catalysis*, 6 (2), 231–244.
- Hutchings, G. J. (1991). Effect of promoters and reactant concentration on the selective oxidation of *n*-butane to maleic anhydride using vanadium phosphorus oxide catalysts. *Applied Catalysis*, 72 (1), 1–32.

- Hutchings, G. J. (1993). Vanadium phosphorus oxide catalysts for the selective oxidation of *n*-butane to maleic anhydride. *Catalysis Today*, 16 (1), 139–146.
- Hutchings, G. J. (2004). Vanadium phosphate: A new look at the active components of catalysts for the oxidation of butane to maleic anhydride. *Journal of Materials Chemistry*, 14 (23), 3385–3395.
- Hutchings, G. J. and Higgins, R. (1996). Effect of promoters on the selective oxidation of *n*-butane with Vanadium-Phosphorus Oxide Catalysts. *Journal of Catalysis*, 162 (2), 153–168.
- Hutchings, G. J. and Higgins, R. (1997). Selective oxidation of *n*-butane to maleic anhydride with vanadium phosphorus catalysts prepared by comminution in the presence of dispersants. *Applied Catalysis A: General*, 154 (1–2), 103–115.
- Hutchings, G. J., Sananes, M. T., Sajip, S., Kiely, C. J., Burrows, A., Ellison, I. J. and Volta, J. C. (1997). Improved method of preparation of vanadium phosphate catalysts. *Catalysis Today*, 33 (1–3), 16–171.
- Imai, H., Kamiya, Y. and Okuhara, T. (2007). Selective oxidation of *n*-butane over nanosized crystallites of $(VO)_2P_2O_7$ synthesised by an exfoliation-reduction process of $VOPO_4 \cdot 2H_2O$ in a mixture of 2-butanol and ethanol. *Journal of Catalysis*, 251 (1), 195–203.
- Ishimura, I., Sugiyama, S. and Hayashi, H. (2000). Vanadyl hydrogenphosphate sesquihydrate as a precursor for preparation of $(VO)_2P_2O_7$ and cobalt incorporated catalysts. *Journal of Molecular Catalysis*, 158 (2), 559–565.
- Jackson, S. (2009). Promoted catalyst. In: *Metal Oxide Catalysis*. (pp. 519–527). Weinheim: Wiley-VCH.
- Ji, W., Xu, L., Wang, X., Hu, Z., Yan, Q. and Chen, Y. (2002). Effects of ball milling on the doped vanadium phosphorus oxide catalysts. *Catalysis Today*, 74 (1–2), 101–110.
- Johnson, J. W., Johnston, D. C., Jacobson, A. J. and Brody, J. F. (1984). Preparation and characterization of vanadyl hydrogen phosphate hemihydrate and its topotactic transformation to vanadyl pyrophosphate. *Journal of the American Chemical Society*, 106 (26), 8123–8128.
- Johnsson, J. E., Grace, J. R., and Graham, J. J. (1987). Fluidized-Bed reactor model verification on a reactor of industrial scale. *AIChE Journal*, 33 (4), 619–627.

- Kamiya, Y., Nishikawa, E., Okuhara, T. and Hattori, T. (2001). Catalytic property of vanadyl pyrophosphates for selective oxidation of *n*-butane at high *n*-butane concentrations. *Applied catalysis A: General*, 206 (1), 103–112.
- Kamiya, Y., Nishikawa, E., Satsuma, A. and Okuhara, T. (2003). Preparation and characterization of lamellar vanadyl alkylphosphates as catalyst precursors for the selective oxidation of butane. *Bulletin of the Chemical Society of Japan*, 76 (4), 837–846.
- Kesteman, E., Merzouki, M., Taouk, B., Bordes, E., and Contractor, R. (1995). Systematic control of crystal morphology during preparation of selective vanadyl pyrophosphate. In: Poncelet, G., Marten, J., Delmon B., Jacobs, P. A., Grange, P. (Eds), *Studies in surface science and catalysis* (pp. 707–716). Amsterdam: Elsevier Science.
- Kiely, C. J., Burrow, A., Sajip, S., Hutchings, G. J., Senanes, M. T., Tuel, A., and Volta, J. C. (1996). Characterisation of variations in vanadium phosphate catalyst microstructure with preparation route. *Journal of Catalysis*, 162 (1), 31–47.
- Kiely, C. J., Sajip, S., Ellison, I. J., Sananes, M. T., Hutchings, G. J. and Volta, J. C. (1995). Electron microscopy studies of vanadium phosphorus oxide catalysts derived from $\text{VOPO}_4 \cdot 2\text{H}_2\text{O}$. *Catalysis Letters*, 33 (3–4), 357–368.
- Klug, P. H. and Alexander, L. E. (1974). X-ray diffraction procedures for polycrystalline and amorphous materials. In: *X-ray diffraction procedures*. 2nd Edition. (pp. 177–424). New York: John Wiley & Sons.
- Kung, H.H. (1986). Desirable catalyst properties in selective oxidation reactions. *Industrial and Engineering Chemistry Product Research and Development*, 25 (2), 171–178.
- Ladwig, G. (1965). On the Constitution of the $\text{VPO}_5(\text{nH}_2\text{O})$. *Journal of Inorganic and General Chemistry*, 338, 266–278.
- Ledoux, M. J., Crouzer, C., Pham-Huu, C., Turines, V., Kourtakis, K., Mills, P. L. and Lerou, J. J. (2001). High-yield butane to maleic anhydride direct oxidation on vanadyl pyrophosphate supported on heat-conductive materials: β -SiC, Si_3N_4 , and BN. *Journal of Catalysis*, 203 (2), 495–508.
- Leong, L. K., Chin, K. S. and Taufiq-Yap, Y. H. (2011). The effect of Bi promoter on vanadium phosphate catalysts synthesized via sesquihydrate route. *Catalysis Today*, 164 (1), 341–346.

- Leonowicz, M. E., Johnson, J. W., Brody, J. F., Shannon, H. F., Newsam, J. M. (2003). Vanadyl hydrogenphosphate: $\text{VO}(\text{HPO}_4) \cdot 4\text{H}_2\text{O}$ and $\text{VO}(\text{HPO}_4)0.5\text{H}_2\text{O}$. *Journal of Solid State Chemistry*, 56 (3), 370–378.
- Lerou, J. J. and Mills, P. L. (1993). Du Pont butane oxidation process. In: Weijnen, M. P. C. and Drinkenburg, A. A. H. (Eds.), *Precision process technology*. (pp. 175–195). Dordrecht: Kluwer Academic.
- Li, X., Ji, W., Zhao, J., Zhang, Z. and Au, C. (2006a). *n*-butane oxidation over VPO catalysts supported on SBA-15. *Journal of Catalysis*, 238 (1), 232–241.
- Li, X., Ji, W., Zhao, J., Zhang, Z. and Au, C. (2006b). A comparison study on the partial oxidation of *n*-butane and propane over VPO catalysts supported on SBA-15, MCM-41, and fumed SiO_2 . *Applied Catalysis A: General*, 306, 8–16.
- Mallada, R., Sajip, S., Kiely, C. J., Menendez, M. and Santamaria, J. (2000). Influence of the reaction atmosphere on the characteristics and performance of VPO catalysts. *Journal of Catalysis*, 196 (1), 1–7.
- Mars, P. and van Krevelen, D. W. (1954). Oxidations carried out by means of vanadium oxide catalysts. *Special Supplement to Chemical Engineering Science*, 3 (1), 41–59.
- Martinez-Lara, M., Moreno-Real, L., Pozaz-Tormo, R., Jimenez-Lopez, A., Bruque, S. and Poncelet, P. R. G. (1992). Catalytic activity of vanadyl phosphate supported on TiO_2 (anatase) and SiO_2 . *Canadian Journal of Chemistry*, 70 (1), 5–13.
- Matsuura, I., Ishimura, T. and Kimura, N. (1995). Preparation and characterization of vanadyl hydrogen phosphate hydrates; $\text{VO}(\text{HPO}_4) \cdot 1.5\text{H}_2\text{O}$ and $\text{VO}(\text{HPO}_4) \cdot 0.5\text{H}_2\text{O}$. *Chemistry Letters*, (9), 769–770.
- Matsuura, I. and Yamazaki, M. (1990). Reactivity and structure of vanadyl pyrophosphate as a butane oxidation catalyst. In: Centi, G. and Trifiro, F. (Eds.), *Studies in surface science and catalysis* (pp. 563–572). Amsterdam: Elsevier Science.
- McCormick, R. (1997). Methane Partial Oxidation over Vanadyl Pyrophosphate and the Effect of Fe and Cr Promoters on Selectivity. *Journal of Catalysis*, 172 (1), 160–169.
- Misono, M. (2002). Selective oxidation of butanes toward green/sustainable chemistry. *Topics in Catalysis*, 21 (1–3), 89–96.

- Morishige, H., Tamaki, J., Miura, N. and Yamazoe, N. (1990). Amorphous V–P mixed oxide with P/V = 2.0 as active phase for butane oxidation. *Chemistry letters*, (9), 1513–1516.
- Moser, T. P. and Schrader, G. L. (1985). Selective oxidation of *n*-butane to maleic anhydride by model V–P–O Catalyst. *Journal of Catalysis*, 92 (2), 216–231.
- Mota, S., Abon, M., Volta, J. C., and Dalmon, J. A. (2000). Selective oxidation of *n*-butane on a VPO catalyst: Study under fuel-rich conditions. *Journal of Catalysis*, 193 (2), 308–318.
- Nakamura, M., Kawai, K. and Fujiwara, Y. (1974). The structure and the activity of vanadyl phosphate catalysts. *Journal of Catalysis*, 34 (3), 345–355.
- Nie, W., Wang, X., Ji, W., Yan, Q., Chen, Y., and Au, C. T. (2001). A study on VPO specimen supported on aluminium-containing MCM-41 for partial oxidation of *n*-butane to MA. *Catalysis Letters*, 76 (3–4), 201–206.
- Nie, W., Wang, Z., Ji, W., Chen, Y., and Au, C. T. (2003). Comparative studies on the VPO specimen supported on mesoporous Al-containing MCM-41 and large pore silica. *Applied Catalysis A: General*, 244 (2), 265–272.
- Niemantsverdriet, J. W. (2007). Temperature Programmed Techniques. In: *Spectroscopy in catalysis*. 3rd Edition. (pp. 11–35). USA: Wiley-VCH.
- Niwa, M. and Murakami, Y. (1982). Reaction mechanism of ammoxidation of toluene IV. Oxidation state of vanadium oxide and its reactivity for toluene oxidation. *Journal of Catalysis*, 76 (1), 9–16.
- Okuhara, T., Ryumon, N., Yamamoto, N. and Hiyoshi, N. (2002). 55 A highly selective vanadyl pyrophosphate synthesised by exfoliation-reduction in mixed alcohols for *n*-butane oxidation. *Studies in Surface Science and Catalysis*, 145, 271–274.
- Overbeek, R. A., Pekelharing, A. R. C. J., Dillen, A. J. and Geus, J. W. (1996a). Preparation, characterization and testing of newly developed silica-supported V–P–O catalysts. *Applied Catalysis A: General*, 135 (2), 231–248.
- Overbeek, R. A., Warringa, P. A., Crombag, M. J. D., Visser, L. M., Dillen, A. J. and Geus, J. W. (1996b). Preparation, characterization and testing of newly developed titania-supported V–P–O catalysts. *Applied Catalysis A: General*, 135 (2), 209–230.

- Pepera, M. C., Callahan, J. L., Desmond, M. J., Milberger, E. C., Blum, P. R. and Bremer, N. J. (1985). Fundamental study of the oxidation of butane over vanadyl pyrophosphate. *Journal of the American Chemical Society*, 107 (17), 4883–4892.
- Pierini, B. T. and Lombardo, E. A. (2005). Structure and properties of Cr promoted VPO catalyst. *Materials Chemistry and Physics*, 92 (1), 197–204.
- Pillai, U. R., Sahle-Demessie, E. and Varma, R. S. (2003). Alternative routes for catalyst preparation: Use of ultrasound and microwave irradiation for preparation of vanadium phosphorus oxide catalyst and their activity for hydrocarbon oxidation. *Applied Catalysis A: General*, 252 (1), 1–8.
- Ramis, G., Cristiani, C., Forzatti, P. and Busca, G. (1990). On the consistency of data obtained from different techniques concerning the surface of vanadia-titania catalysts: Reply to the comment of Israel E. Wachs. *Journal of Catalysis*, 124 (2), 574–576.
- Redhead, P.A. (1962). Thermal desorption of gases. *Vacuum*, 12 (4), 203–211.
- Rothenberg, G. (2008). Catalyst/substrate interactions and Sabatier's principle. In: *Catalysis: Concepts and green applications*. (pp. 11–66). Netherlands: WILEY-VCH Verlag GmbH & Co. KGaA.
- Roussy, G., Thiebaut, J. M., Souiri, M., Marchal, E., Kiennemann, A. and Maire, G. (1994). Controlled oxidation of methane doped catalysts irradiated by microwaves. *Catalysis Today*, 21 (2–3), 349–355.
- Sananes, M. T., Hutchings, G. J. and Volta, J. C. (1995). On the role of the $\text{VO}(\text{H}_2\text{PO}_4)_2$ precursor for *n*-Butane Oxidation into Maleic Anhydride. *Journal of Catalysis*, 154 (2), 253–260.
- Sartoni, L., Bartley, J. K., Wells, R. P. K., Kiely, C. J., Volta, J. C. and Hutchings, G. J. (2004). Promotion of vanadium phosphate catalysts using gallium compounds: Effect of low Ga/V molar ratios. *Journal of Molecular Catalysis A: Chemical*, 220 (1), 85–92.
- Sheldon, R. (2000). Atom utilisation, E factors and the catalytic solution. *Comptes Rendus de l'Académie des Science-Series IIC-Chemistry*, 3 (7), 541–551.
- Sheldon, R. A. and Kochi, J. K. (1981). Introduction to metal-catalysed oxidations. In: *Metal-catalysed oxidations of organic compounds*. (pp. 1–2). New York: Academic Press.

- Sheldon, R. A., Arends, I. and Hanefeld, U. (2007). Catalytic oxidation. In: *Green chemistry and catalysis*. (pp. 133–221). Germany: WILEY-VCH Verlag GmbH & Co. KGaA.
- Sookraj, S. H. and Engelbrecht, D. (1999). Selective oxidation of light hydrocarbons over promoted vanadyl pyrophosphate. *Catalysis Today*, 49 (1–3), 161–169.
- Takenaka, S., Tanaka, T., Yamazaki, T., Funabiki, T. and Yoshida, S. (1997). Structure of active species in alkali-ion-modified silica-supported vanadium oxide. *Journal of Physical Chemistry B*, 101 (44), 9035–9040.
- Taufiq-Yap, Y. H., Looi, M. H., Waugh, K. C., Hussein, M. Z., Zainal, Z. and Samsuddin, R. (2001). The effect of the duration of *n*-butane/air pretreatment on the morphology and reactivity of $(VO)_2P_2O_7$ catalysts. *Catalysis Letters*, 74 (1), 99–104.
- Thompson, D. J., Fanning, M. O. and Hodnett, B. K. (2003). Modeling the active sites in vanadyl pyrophosphate. *Journal of Molecular Catalysis A: Chemical*, 198 (1–2), 125–137.
- Taufiq-Yap, Y. H., Leong, L. K., Hussein, M. Z., Irmawati, R. and Abd Hamid, S. B. (2004). Synthesis and characterization of vanadyl pyrophosphate catalysts via vanadyl hydrogen phosphate sesquihydrate precursor. *Catalysis Today*, 93–95, 715–722.
- Taufiq-Yap, Y. H. (2006). Effect of Cr and Co promoters addition on vanadium phosphate catalysts for mild oxidation of *n*-butane. *Journal of Natural Gas Chemistry*, 15 (2), 144–148.
- Taufiq-Yap, Y. H., Goh, C. K., Hutching, G. J., Dummer, N. and Bartley, J. K. (2006a). Effects of mechanochemical treatment to the vanadium phosphate catalysts derived from $VOPO_4 \cdot 2H_2O$. *Journal of Molecular Catalysis A: Chemical*, 260 (1–2), 24–31.
- Taufiq-Yap, Y. H., Kamiya, Y. and Tan, K. P. (2006b). Promotional effect of bismuth as dopant in Bi-doped vanadyl pyrophosphate catalysts for selective oxidation of *n*-butane to maleic anhydride. *Journal of Natural Gas Chemistry*, 15 (4), 297–302.
- Taufiq-Yap, Y. H., Hasbi, A. R. M., Hussein, M. Z., Hutchings, G. J., Bartley, J. and Dummer, N. (2006c). Synthesis of vanadium phosphate catalysts by hydrothermal method for selective oxidation of *n*-butane to maleic anhydride. *Catalysis Letters*, 106 (3–4), 177–181.

- Taufiq-Yap, Y. H., Leong, L. K. and Irmawati, R. (2007a). *n*-Butane oxidation over γ -Al₂O₃ supported vanadium phosphate catalysts. *Journal of Natural Gas Chemistry*, 16 (3), 1–7.
- Taufiq-Yap, Y. H., Rownaghi, A. A., Hussein, M. Z. and Irmawati, R. (2007b). Preparation of vanadium phosphate catalysts from VOPO₄·2H₂O: Effect of microwave irradiation on morphology and catalytic property, *Catalysis Letters*, 119 (1–2), 64–71.
- Taufiq-Yap, Y. H. and Saw, C. S. (2008). Effect of different calcinations environments on the vanadium phosphate catalysts for selective oxidation of propane and *n*-butane. *Catalysis Today*, 131 (1–4), 285–291.
- Taufiq-Yap, Y. H., Wong, Y. C., Zainal, Z. and Hussein, M. Z. (2009). Synthesis of self-assembled nanorod vanadium oxide bundles by sonochemical treatment. *Journal of Natural Gas Chemistry*, 18 (3), 312–318.
- Taufiq-Yap, Y. H., Goh, C. K., Hutchings, C. K., Dummer, N., and Bartley, J. K. (2011a). Influence of milling media on the physicochemicals and catalytic properties of mechanochemical treated vanadium phosphate catalysts. *Catalysis Letters*, 141 (3), 400–407.
- Taufiq-Yap, Y. H., Nurul Suziana, N. M. and Hussein, M. Z. (2011b). Influences of the various metal dopants for the nanosized vanadium phosphate catalysts. *Catalysis Letters*, 141 (1), 136–148.
- Thompson, M. and Ebner, J. (1992). Site isolation in vanadium phosphorus oxide alkane oxidation. In: Ruiz, P. and Delmon, B. (Eds.), *New developments in selective oxidation by heterogeneous catalysis-72*. (pp. 353–362). London and New York: Elsevier Science.
- Torardi, C. C. and Calabrese, J. C. (1984). Ambient- and low-temperature crystal structure of vanadyl pyrophosphate (VO)₂H₄P₂O₉. *Inorganic Chemistry*, 23 (10), 1308–1310.
- Varma, R. L., and Saraf, D. N. (1979). Selective oxidation of C₄ hydrocarbons to maleic anhydride. *Industrial and Engineering Chemistry Product Research and Development*, 18 (1), 7–13.
- Volta, J. C. (2000). Vanadium phosphorus oxides, a reference catalyst for mild oxidation of light alkanes: A review. *Chemistry*, 3 (9), 717–723.
- Wachs, I. E., Jehng, J., Deo, G., Weckhuysen, B. M., Gulians, V. V., Benziger, J. B. and Sundaresan, S. (1997). Fundamental studies of butane oxidation over model-supported vanadium oxide catalysts: molecular structure-reactivity relationships. *Journal of catalysis*, 170 (1), 75–88.

- Wachs, I. E., Weckhusyen, B. M., Andreini, A., Vuurman, M. A., Boer, M., Amiridis, M. D. (1996). Selective catalytic reduction of NO with NH₃ over supported vanadia catalysts. *Journal of Catalysis*, 161 (1), 211–221.
- Wang, D., Kung, M. C. and Kung, H. H. (2000). Oxidation of butane over vanadium-phosphorus oxides of P/V ≥ 2 . *Catalysis Letters*, 65 (1–3), 9–17.
- Wenig, R. W. and Schrader, G. L. (1986). Vanadium-phosphorus-oxygen industrial catalysts for *n*-butane oxidation: characterization and kinetic measurements. *Industrial and Engineering Chemistry Fundamental*, 25 (4), 612–620.
- Xiao, C. Y., Chen, X., Wang, Z. Y., Ji, W. J., Chen, Y. and Au, C. T. (2004). The novel and highly selective fumed silica-supported VPO for partial oxidation of *n*-butane to maleic anhydride. *Catalysis Today*, 93–95 (0), 223–228.
- Xu, L., Chen, X., Ji, W., Yan, Q. and Chen, Y. (2002). Influence of the way of preparing vanadium phosphorus oxide (VPO) precursor and introducing multi-additives on the reaction performance. *Reaction Kinetics and Catalysis Letters*, 76 (2), 335–341.
- Xue, E. and Ross, J. (2000). The use of membrane reactors for catalytic *n*-butane oxidation to maleic anhydride with a butane-rich feed. *Catalysis Today*, 61 (1–4), 3–8.
- Xue, E., Ross, J. R. H., Mallada, R., Mellada, R., Menendez, M., Santamaria, J., Perregard, J. and Nielsen, P. E. H. (2001). Catalytic oxidation of butane to maleic anhydride enhanced yields in the presence of CO₂ in the reactor feed. *Applied Catalysis A: General*, 210 (1–2), 271–274.
- Yamamoto, N., Hiyoshi, N. and Okuhara, T. (2002). Thin-layered sheets of VOHPO₄·0.5H₂O prepared from VOPO₄·2H₂O by intercalation *n*-exfoliation-reduction in alcohol. *Chemistry of Materials*, 14 (9), 3882–3888.
- Ye, Y., Rihko-Struckmann, L., Munder, B., Rau, H. and Sundmacher, K. (2004). Feasibility of an electrochemical membrane reactor for the partial oxidation of *n*-butane to maleic anhydride. *Industrial and Engineering Chemistry Research and Development*, 43 (16), 4551–4558.
- Zazhigalov, V. A., Haber, J., Stoch, J., Bacherikova, I. V., Kamashko, G. A. and Pyatnitskaya, A. I. (1996). *n*-Butane Oxidation on VPO catalysts. influence of alkali and alkaline-earth metal ions as additions. *Applied Catalysis A: General*, 134 (2), 225–137.

- Zazhigalov, V. A., Haber, J., Stoch, J., Kharlamov, A. I., Bogutskaya, L. V., Bacherikova, I. V. and Kowal, A. (1997). Influence of the mechanochemical treatment on the reactivity of V-containing oxide system. *Solid States Inoics*, 101–103 (2), 1257–1262.
- Zazhigalov, V. A., Haber, J., Stoch, J., Kharlamov, A. I., Bacherikova, I. V. and Bogutskaya, L. V. (1998). Mechanochemistry in preparation of VPO chemistry catalysts for paraffins oxidation. *Studies in Surface Science and Catalysis*, 118, 385–394.
- Zazhigalov, V. A., Zaitsev, Y. P., Belousov, V. M. and Parltitz, B. (1986). Studies of immobilized V–P/SiO₂ catalysts. *Reaction Kinetics and Catalysis Letters*, 32 (1), 209–214.
- Zhanglin, Y., Forissier, M., Sneed, R. P., Vedrine, J. C. and Volta, J. C. (1994). On the mechanism of *n*-butane oxidation to maleic anhydride on VPO catalysts: I. A kinetics study on a VPO catalyst as compared to VPO references phases. *Journal of catalysis*, 145 (2), 256–266.
- Zhou, Z. Q., Xu, H. Y., Ji, W. J. and Chen, Y. (2004) Preparation of novel composite VPO/fumed silica catalyst for partial oxidation of *n*-butane. *Catalysis Letters*, 96 (3–4), 221–226.

APPENDIX A

Calculation for the Chromium Dopant Used

Molecular weight of $\text{VOPO}_4 \cdot 2\text{H}_2\text{O}$ = $197.9426 \text{ g mol}^{-1}$

$$\begin{aligned} 10 \text{ g of } \text{VOPO}_4 \cdot 2\text{H}_2\text{O} &= \frac{10 \text{ g}}{197.9426 \text{ g mol}^{-1}} \\ &= 0.0505 \text{ mol} \end{aligned}$$

$$\begin{aligned} \text{Molecular weight of } \text{Cr}(\text{NO}_3)_3 \cdot 9\text{H}_2\text{O} &= 51.9961 \text{ g mol}^{-1} + 3 \times (14.0070 \text{ g mol}^{-1} + 3 \times 15.9994 \text{ g mol}^{-1}) + \\ &\quad 9 \times (2 \times 1.0079 \text{ g mol}^{-1} + 15.9994 \text{ g mol}^{-1}) \\ &= 400.1485 \text{ g mol}^{-1} \end{aligned}$$

Example of calculation:

For VPO_5 -Cr1%

Since $\text{Cr} / \text{V} = 0.01$; $\text{V} = 0.0505 \text{ mol}$

Thus $\text{Ca} = 0.000505 \text{ mol}$

Total Mass of Ca needed

$$\begin{aligned} &= \text{Number of mole of calcium needed} \times \text{Molecular weight of Calcium nitrate} \\ &\quad \text{Tetrahydrate} \\ &= 0.000505 \text{ mol} \times 51.9961 \text{ g mol}^{-1} \\ &= 0.0263 \text{ g} \end{aligned}$$

Thus, 0.0263 g of $\text{Cr}(\text{NO}_3)_3 \cdot 9\text{H}_2\text{O}$ was added into 150 cm^3 1-butanol with 10 g $\text{VOPO}_4 \cdot 2\text{H}_2\text{O}$ of volumetric flask and top up with 0.1 M H_2SO_4 .

APPENDIX B

Calculation for the Silica Support Used

$$V/Si = \frac{\text{Weight of } VOPO_4 \cdot 2H_2O}{\text{Weight of } VOPO_4 \cdot 2H_2O + \text{Weight of Si support}}$$

Example of calculation:

For 5% VPO_s/Si

$$V/Si = 0.05$$

$$0.05 = \frac{5 \text{ g}}{5 \text{ g} + \text{Weight of Si support}}$$

$$0.25 \text{ g} - 0.05 \times \text{Weight of Si support} = 5 \text{ g}$$

$$\begin{aligned} \text{Weight of Si support} &= \frac{5 \text{ g} - 0.25 \text{ g}}{0.05} \\ &= 95 \text{ g} \end{aligned}$$

Thus, 95 g of silica support was added during wetness impregnation to produce 5 wt% of silica supported VPOs catalysts, Si-5.

APPENDIX C

Calculation of Crystallite Size by Using Powder XRD Technique

$$FWHM \text{ (rad)} = FWHM \text{ (}^\circ\text{)} \times \left(\frac{\pi}{180^\circ} \right)$$

According to Scherrer's formula,

$$\text{Crystallite size, } T \text{ (}\text{\AA}\text{)} = \frac{0.89 \lambda}{FWHM \times \cos \theta}$$

Given $\lambda_{\text{Cu K}\alpha} = 1.54 \text{ \AA}$

Example of calculation:

For VPO_s-Cr1%

Peak appears at $2\theta = 22.8704$ correspond to (020) plane.

$$\begin{aligned} FWHM \text{ (rad)} &= 1.2100^\circ \times \left(\frac{\pi}{180^\circ} \right) \\ &= 0.0211^\circ \end{aligned}$$

$$\begin{aligned} T \text{ (}\text{\AA}\text{)} &= \frac{0.89 \times 1.54 \text{ \AA}}{0.0211^\circ \times \cos 11.4352^\circ} \\ &= 66.2101 \text{ \AA} \end{aligned}$$

For Bulk VPO_s

	2 θ (°)	θ (°)	FWHM (°)	FWHM (rad)	T (Å)
(020) plane	22.8645	11.4323	1.3783	0.0241	58.0226
(204) plane	28.4923	14.2462	0.8222	0.0144	98.2005
(221) plane	29.9200	14.9600	0.7696	0.0134	105.8720

For VPO_s-Cr1%

	2 θ (°)	θ (°)	FWHM (°)	FWHM (rad)	T (Å)
(020) plane	22.7851	11.3926	1.3611	0.0238	58.7457
(204) plane	28.3742	14.1871	0.8085	0.0141	100.2637
(221) plane	29.8400	14.9200	0.7876	0.0137	103.5342

For VPO_s-Cr3%

	2 θ (°)	θ (°)	FWHM (°)	FWHM (rad)	T (Å)
(020) plane	22.7593	11.3797	1.3500	0.0236	59.2409
(204) plane	28.3633	14.1417	0.8030	0.0140	100.9596
(221) plane	29.7909	14.8955	0.7462	0.0130	109.0968

For VPO_s-Cr5%

	2 θ (°)	θ (°)	FWHM (°)	FWHM (rad)	T (Å)
(020) plane	22.7729	11.3865	1.3008	0.0227	61.5911
(204) plane	28.3550	14.1775	0.7300	0.0127	111.3116
(221) plane	29.8071	14.9036	0.7423	0.0130	109.1009

For 15%VPO_s/Si

	2 θ (°)	θ (°)	FWHM (°)	FWHM (rad)	T (Å)
(204) plane	28.2950	14.1475	0.6900	0.0120	117.3700
(221) plane	29.8050	14.9025	0.7100	0.0124	114.4548

For 20%VPO_s/Si

	2 θ (°)	θ (°)	FWHM (°)	FWHM (rad)	T (Å)
(204) plane	28.4300	14.2150	0.6600	0.0115	122.7420
(221) plane	29.9483	14.9742	0.5967	0.0104	136.2326

For VPO_s25%/Si

	2 θ (°)	θ (°)	FWHM (°)	FWHM (rad)	T (Å)
(204) plane	28.4533	14.2267	0.6267	0.0109	129.2711
(221) plane	29.9000	14.9500	0.6000	0.0105	135.4681

For 15%VPO_s/Si / T460VPO_s/Si

	2 θ (°)	θ (°)	FWHM (°)	FWHM (rad)	T (Å)
(204) plane	28.5233	14.2617	0.5933	0.0104	136.5696
(221) plane	30.0166	15.0053	0.5533	0.0097	146.9419

For T400VPO_s/Si

	2 θ (°)	θ (°)	FWHM (°)	FWHM (rad)	T (Å)
(204) plane	28.3700	14.1850	0.7400	0.0129	109.4199
(221) plane	29.8550	14.9275	0.7300	0.0127	111.3399

For T520VPO_s/Si

	2 θ (°)	θ (°)	FWHM (°)	FWHM (rad)	T (Å)
(204) plane	28.3600	14.1800	0.6266	0.0109	129.6948
(221) plane	29.8700	14.9350	0.5800	0.0101	140.4475

APPENDIX D

Preparations of Reagents for Redox Titration

I. Preparation of Diphenylamine, Ph₂NH indicator

1 g of diphenylamine was weighted and dissolved in the few mL of concentrated sulphuric acid, H₂SO₄ in a 100 mL volumetric flask then continued top up to 100 mL.

II. Preparation of 2 M and 0.1 M Sulphuric Acid, H₂SO₄ Solution

Concentrated H₂SO₄ (95-98%)

$$\begin{aligned} 1 \text{ L} &= 1.84 \text{ kg} \\ &= \frac{1840 \text{ g}}{1000 \text{ cm}^3} \\ &= 1.84 \text{ g cm}^{-3} \end{aligned}$$

$$\begin{aligned} \text{Molecular Weight of H}_2\text{SO}_4 &= 2(1.00 \text{ g mol}^{-1}) + 32.07 \text{ g mol}^{-1} \\ &\quad + 4(16.00 \text{ g mol}^{-1}) \\ &= 98.07 \text{ g mol}^{-1} \end{aligned}$$

$$\begin{aligned} \text{Concentration of 95-98\% of H}_2\text{SO}_4 &= \frac{1.84 \text{ g cm}^{-3}}{98.07 \text{ g mol}^{-1}} \times \frac{95}{100} \times 1000 \\ &= 17.82 \text{ mol L}^{-1} \\ &= 17.82 \text{ M} \end{aligned}$$

$$M_1 V_1 = M_2 V_2$$

where M₁ is concentration of 95-98% of H₂SO₄

M₂ is concentration of diluted H₂SO₄

V₁ is volume of 95-98% of H₂SO₄

V₂ is volume of diluted H₂SO₄

$$\begin{aligned} (17.82 \text{ M})(V_1) &= (2 \text{ M})(1000 \text{ mL}) \\ V_1 &= 112.23 \text{ mL} \end{aligned}$$

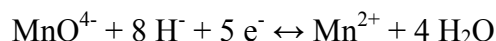
Thus, 112.23 mL of 95-98% of H₂SO₄ was diluted to 1000 mL to prepare 2 M H₂SO₄.

$$\begin{aligned} (17.82 \text{ M})(V_1) &= (0.1 \text{ M})(1000 \text{ cm}^3) \\ V_1 &= 5.61 \text{ cm}^3 \end{aligned}$$

Thus, 5.61 mL of 95-98% of H₂SO₄ was diluted to 1000 mL to prepare 0.1 M H₂SO₄.

III. Preparation of 0.01 N Potassium Permanganate, KMnO_4

$$\text{Normality, } N (\text{eq L}^{-1}) = M (\text{mol L}^{-1}) \times n (\text{eq mol}^{-1})$$



$$\begin{aligned}\text{Molarity, } M (\text{mol/L}) &= \frac{N (\text{eq L}^{-1})}{n (\text{eq mol}^{-1})} \\ &= \frac{0.01 \text{ eq L}^{-1}}{5 \text{ eq mol}^{-1}} \\ &= 0.002 \text{ M} \\ &= 0.002 \text{ mol L}^{-1}\end{aligned}$$

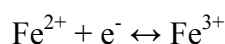
$$\begin{aligned}\text{Molecular Weight for } \text{KMnO}_4 &= 39.10 \text{ g mol}^{-1} + 54.94 \text{ g mol}^{-1} + 4(16.00 \text{ g mol}^{-1}) \\ &= 158.04 \text{ g mol}^{-1}\end{aligned}$$

$$\begin{aligned}\text{Weight for } \text{KMnO}_4 \text{ in } 1000 \text{ cm}^3 \text{ diluted (0.1 M) } \text{H}_2\text{SO}_4 &= 0.002 \text{ mol L}^{-1} \times 158.04 \text{ g mol}^{-1} \\ &= 0.3161 \text{ g L}^{-1}\end{aligned}$$

Thus, 0.3161 g of KMnO_4 was transferred into 1000 mL volumetric flask and top up with 0.1 M H_2SO_4 .

IV. Preparation of 0.01 N Ammonium Iron (II) Sulphate, $(\text{NH}_4)_2\text{Fe}(\text{SO}_4)_2 \cdot 6\text{H}_2\text{O}$ (Redox Titration)

$$\text{Normality, } N (\text{eq/L}) = M (\text{mol/L}) \times n (\text{eq/mol})$$



$$\begin{aligned}\text{Molarity, } M (\text{mol/L}) &= \frac{N (\text{eq/L})}{n (\text{eq/mol})} \\ &= \frac{0.01 \text{ eq/L}}{1 \text{ eq/mol}} \\ &= 0.01 \text{ M} \\ &= 0.01 \text{ mol L}^{-1}\end{aligned}$$

$$\begin{aligned}\text{Molecular weight for } (\text{NH}_4)_2\text{Fe}(\text{SO}_4)_2 \cdot 6\text{H}_2\text{O} &= 2(14.00 \text{ g mol}^{-1}) + 20(1.00 \text{ g mol}^{-1}) + 55.85 \text{ g mol}^{-1} + 2(32.07 \text{ g mol}^{-1}) + 14 \\ &\quad (16.00 \text{ g mol}^{-1}) \\ &= 391.99 \text{ g mol}^{-1}\end{aligned}$$

$$\begin{aligned}\text{Weight for } (\text{NH}_4)_2\text{Fe}(\text{SO}_4)_2 \cdot 6\text{H}_2\text{O} \text{ in } 1000 \text{ cm}^3 \text{ diluted (0.1 M) } \text{H}_2\text{SO}_4 &= 0.01 \text{ mol L}^{-1} \times 391.99 \text{ g/mol} \\ &= 3.9199 \text{ g L}^{-1}\end{aligned}$$

Thus, 3.9199 g of $(\text{NH}_4)_2\text{Fe}(\text{SO}_4)_2 \cdot 6\text{H}_2\text{O}$ was transferred into 1000 cm^3 volumetric flask and top up with 0.1 M H_2SO_4 .

APPENDIX E

Calculation of Oxidation State of Vanadium by Using Redox Titration

According to Niwa and Murakami,

$$T_1 = \text{V}^{4+} + 2\text{V}^{3+} = 20 [\text{MnO}_4^-] V_1 \quad (1)$$

$$T_2 = \text{V}^{5+} + \text{V}^{4+} + \text{V}^{3+} = 20 [\text{Fe}^{2+}] V_2 \quad (2)$$

$$T_3 = \text{V}^{5+} = 20 [\text{Fe}^{2+}] V_3 \quad (3)$$

$$(2) - (3): \quad \text{V}^{4+} + \text{V}^{3+} = 20 [\text{Fe}^{2+}] V_2 - 20 [\text{Fe}^{2+}] V_3 \quad (4)$$

$$(1) - (4): \quad \text{V}^{3+} = 20 [\text{MnO}_4^-] V_1 - 20 [\text{Fe}^{2+}] V_2 + 20 [\text{Fe}^{2+}] V_3 \quad (5)$$

Substitute (5) into (1):

$$\begin{aligned} \text{V}^{4+} + 2(20 [\text{MnO}_4^-] V_1 - 20 [\text{Fe}^{2+}] V_2 + 20 [\text{Fe}^{2+}] V_3) &= 20 [\text{MnO}_4^-] V_1 \\ \text{V}^{4+} &= 20 [\text{MnO}_4^-] V_1 - 40 [\text{MnO}_4^-] V_1 + 40 [\text{Fe}^{2+}] V_2 - 40 [\text{Fe}^{2+}] V_3 \\ &= 40 [\text{Fe}^{2+}] V_2 - 40 [\text{Fe}^{2+}] V_3 - 20 [\text{MnO}_4^-] V_1 \end{aligned} \quad (6)$$

Substitute (5) and (6) into (2):

$$\begin{aligned} 20 [\text{Fe}^{2+}] V_2 &= \text{V}^{5+} + (40 [\text{Fe}^{2+}] V_2 - 40 [\text{Fe}^{2+}] V_3 - 20 [\text{MnO}_4^-] V_1) + \\ &\quad (20 [\text{MnO}_4^-] V_1 - 20 [\text{Fe}^{2+}] V_2 + 20 [\text{Fe}^{2+}] V_3) \\ \text{V}^{5+} &= 20 [\text{Fe}^{2+}] V_3 \end{aligned} \quad (7)$$

From (5):

$$\begin{aligned} \text{V}^{3+} &= 20 (0.01) V_1 - 20 (0.01) V_2 + 20 (0.01) V_3 \\ &= 0.2 V_1 - 0.2 V_2 + 0.2 V_3 \end{aligned} \quad (8)$$

From (6):

$$\begin{aligned} \text{V}^{4+} &= 40 (0.01) V_2 - 40 (0.01) V_3 - 20 (0.01) V_1 \\ &= 0.4 V_2 - 0.4 V_3 - 0.2 V_1 \end{aligned} \quad (9)$$

From (7):

$$\begin{aligned} \text{V}^{5+} &= 20 (0.01) V_3 \\ &= 0.2 V_3 \end{aligned} \quad (10)$$

The average oxidation state of vanadium is calculated as

$$V_{AV} = \frac{3V^{3+} + 4V^{4+} + 5V^{5+}}{V^{3+} + V^{4+} + V^{5+}}$$

Example of calculation:

For Bulk VPO_s

From (5):

$$\begin{aligned} V^{3+} &= 20 (0.01) V_1 - 20 (0.01) V_2 + 20 (0.01) V_3 \\ &= 0.2 V_1 - 0.2 V_2 + 0.2 V_3 \\ &= 0.2(8.50 \text{ cm}^3) - 0.2 (15.35 \text{ cm}^3) + 0.2 (3.05 \text{ cm}^3) \\ &= -0.76 \text{ cm}^3 \end{aligned}$$

From (6):

$$\begin{aligned} V^{4+} &= 40 (0.01) V_2 - 40 (0.01) V_3 - 20 (0.01) V_1 \\ &= 0.4 V_2 - 0.4 V_3 - 0.2 V_1 \\ &= 0.4(15.35 \text{ cm}^3) - 0.4 (3.05 \text{ cm}^3) + 0.2 (8.50 \text{ cm}^3) \\ &= 3.22 \text{ cm}^3 \end{aligned}$$

From (7):

$$\begin{aligned} V^{5+} &= 20 (0.01) V_3 \\ &= 0.2 V_3 \\ &= 0.2 (3.05 \text{ cm}^3) \\ &= 0.61 \text{ cm}^3 \end{aligned}$$

The average oxidation state of vanadium is calculated as

$$V_{AV} = \frac{3V^{3+} + 4V^{4+} + 5V^{5+}}{V^{3+} + V^{4+} + V^{5+}}$$

Since the value for V^{3+} was negative, it was neglectable,

$$\begin{aligned} V_{AV} &= \frac{4 (3.22 \text{ cm}^3) + 5(0.61 \text{ cm}^3)}{(3.22 \text{ cm}^3) + (0.61 \text{ cm}^3)} \\ &= 4.1593 \end{aligned}$$

$$\begin{aligned} \text{Since } V_{AV} \text{ of VPOs} &= 4.1593 \\ \text{Thus } V^{5+} (\%) &= 15.93 \% \\ V^{4+} (\%) &= (100-15.93) \% \\ &= 84.07 \% \end{aligned}$$

For Bulk VPO _s						
	KMnO ₄ [V ₁]		(NH ₄) ₂ Fe(SO ₄) ₂ [V ₂]		(NH ₄) ₂ Fe(SO ₄) ₂ [V ₃]	
	1	2	1	2	1	2
Initial (cm ³)	0.00	8.50	0.00	18.45	15.35	33.80
Final (cm ³)	8.50	17.00	15.35	33.80	18.45	36.80
Volume Used (cm ³)	8.50	8.50	15.35	15.35	3.10	3.0
Average of volume used (cm ³)	8.50		15.35		3.05	
For VPO _s -Cr1%						
	KMnO ₄ [V ₁]		(NH ₄) ₂ Fe(SO ₄) ₂ [V ₂]		(NH ₄) ₂ Fe(SO ₄) ₂ [V ₃]	
	1	2	1	2	1	2
Initial (cm ³)	17.00	24.30	0.00	10.00	23.00	33.00
Final (cm ³)	24.30	31.70	23.00	33.00	27.50	37.30
Volume Used (cm ³)	7.30	7.40	23.00	23.00	4.50	4.30
Average of volume used (cm ³)	7.35		23.00		4.40	
					</	

For VPO₅-Cr3%

	KMnO ₄ [V ₁]		(NH ₄) ₂ Fe(SO ₄) ₂ [V ₂]		(NH ₄) ₂ Fe(SO ₄) ₂ [V ₃]		
	1	2	1	2	1	2	
Initial (cm ³)	0.00	9.65	0.00	14.70	12.40	27.00	V ⁵⁺ (%) = 17.84 %
Final (cm ³)	9.65	19.35	12.40	27.00	14.70	29.25	V ⁴⁺ (%) = 82.16 %
Volume Used (cm ³)	9.65	9.70	12.40	12.30	2.30	2.25	
Average of volume used (cm ³)	9.68		12.35		2.28		

For VPO₅-Cr5%

	KMnO ₄ [V ₁]		(NH ₄) ₂ Fe(SO ₄) ₂ [V ₂]		(NH ₄) ₂ Fe(SO ₄) ₂ [V ₃]		
	1	2	1	2	1	2	
Initial (cm ³)	19.35	27.35	29.95	2.0	0.00	12.10	V ⁵⁺ (%) = 20.39 %
Final (cm ³)	27.35	35.15	39.85	12.10	2.00	14.20	V ⁴⁺ (%) = 79.61 %
Volume Used (cm ³)	8.00	7.80	9.90	10.10	2.00	2.10	
Average of volume used (cm ³)	7.90		10.10		2.05		

	KMnO ₄ [V ₁]		(NH ₄) ₂ Fe(SO ₄) ₂ [V ₂]		(NH ₄) ₂ Fe(SO ₄) ₂ [V ₃]		
	1	2	1	2	1	2	
Initial (cm ³)	38.50	10.00	30.00	0.50	10.60	16.10	V ⁵⁺ (%) = 25.29 %
Final (cm ³)	48.30	20.20	40.20	10.60	16.10	21.60	V ⁴⁺ (%) = 74.71 %
Volume Used (cm ³)	10.10	10.20	10.20	10.10	5.50	5.50	
Average of volume used (cm ³)		10.15		10.15		5.50	

	KMnO ₄ [V ₁]		(NH ₄) ₂ Fe(SO ₄) ₂ [V ₂]		(NH ₄) ₂ Fe(SO ₄) ₂ [V ₃]		
	1	2	1	2	1	2	
Initial (cm ³)	20.00	28.90	30.00	1.00	18.50	23.30	V ⁵⁺ (%) = 21.50 %
Final (cm ³)	28.90	38.00	47.50	18.50	23.30	27.70	V ⁴⁺ (%) = 78.50 %
Volume Used (cm ³)	8.90	9.10	17.50	17.50	4.80	4.40	
Average of volume used (cm ³)	9.00		17.50		4.60		

For 15%VPO ₃ /Si						
	KMnO ₄ [V ₁]		(NH ₄) ₂ Fe(SO ₄) ₂ [V ₂]		(NH ₄) ₂ Fe(SO ₄) ₂ [V ₃]	
	1	2	1	2	1	2
Initial (cm ³)	0.30	9.70	27.20	0.80	19.50	23.70
Final (cm ³)	9.70	19.30	45.80	19.30	23.70	27.80
Volume Used (cm ³)	9.40	9.60	18.60	18.50	4.20	4.10
Average of volume used (cm ³)	9.50		18.55		4.15	

V⁵⁺ (%) = 17.70 %
V⁴⁺ (%) = 82.30 %

V⁵⁺ (%) = 15.60 %
V⁴⁺ (%) = 84.40 %

	KMnO ₄ [V ₁]		(NH ₄) ₂ Fe(SO ₄) ₂ [V ₂]		(NH ₄) ₂ Fe(SO ₄) ₂ [V ₃]	
	1	2	1	2	1	2
Initial (cm ³)	8.90	20.00	25.00	0.50	20.00	21.70
Final (cm ³)	18.80	30.00	43.80	19.40	21.70	23.30
Volume Used (cm ³)	9.90	10.00	18.80	18.90	1.70	1.60
Average of volume used (cm ³)	9.95		10.10		1.65	
					V⁵⁺ (%) = 6.32 %	
					V⁴⁺ (%) = 93.68 %	

	KMnO ₄ [V ₁]		(NH ₄) ₂ Fe(SO ₄) ₂ [V ₂]		(NH ₄) ₂ Fe(SO ₄) ₂ [V ₃]		
	1	2	1	2	1	2	
Initial (cm ³)	0.00	8.50	0.50	9.50	0.00	0.05	V⁵⁺ (%) = 0.53 %
Final (cm ³)	8.50	17.10	9.50	18.50	0.05	0.10	
Volume Used (cm ³)	8.50	8.60	9.00	9.00	0.05	0.05	V⁴⁺ (%) = 99.47 %
Average of volume used (cm ³)	8.55		9.00		0.05		

	KMnO ₄ [V ₁]		(NH ₄) ₂ Fe(SO ₄) ₂ [V ₂]		(NH ₄) ₂ Fe(SO ₄) ₂ [V ₃]	
	1	2	1	2	1	2
Initial (cm ³)	30.00	10.00	20.00	0.50	19.10	25.00
Final (cm ³)	42.10	22.20	38.30	19.10	19.20	15.20
Volume Used (cm ³)	12.10	12.20	18.80	18.60	1.00	2.00
Average of volume used (cm ³)	12.15		18.70		0.50	
					V⁵⁺ (%) = 2.02 %	
					V⁴⁺ (%) = 97.98 %	

	KMnO ₄ [V ₁]		(NH ₄) ₂ Fe(SO ₄) ₂ [V ₂]		(NH ₄) ₂ Fe(SO ₄) ₂ [V ₃]		
	1	2	1	2	1	2	
Initial (cm ³)	15.00	31.50	22.00	0.00	22.00	25.00	V ⁵⁺ (%) = 10.38%
Final (cm ³)	31.30	47.90	44.00	22.00	24.70	27.50	V ⁴⁺ (%) = 89.62%
Volume Used (cm ³)	16.30	16.40	22.00	22.00	2.70	2.50	
Average of volume used (cm ³)	16.35		22.00		2.60		

APPENDIX F

I. Preparation of 8 M HNO₃

$$\begin{aligned}\text{Molarity for 65\% of HNO}_3 &= \frac{\text{Density of HNO}_3}{\text{Molecular Weight of HNO}_3} \times \frac{65}{100} \times 1000 \\ &= \frac{1.4090 \text{ g cm}^{-3}}{63.0130 \text{ g mol}^{-1}} \times \frac{65}{100} \times 1000 \\ &= 14.5343 \text{ mol L}^{-1} \\ &= 14.5343 \text{ M}\end{aligned}$$

$$M_1 V_1 = M_2 V_2$$

Where

M_1 = concentration of 65% of HNO₃ (14.5343 M)

V_1 = volume of 65% of HNO₃

M_2 = concentration of 8M HNO₃

V_2 = volume of 8M HNO₃

$$M_1 V_1 = M_2 V_2$$

$$(14.5343 \text{ M}) V_1 = (8 \text{ M}) (250 \text{ mL})$$

$$\begin{aligned}V_1 &= \frac{(8 \text{ M}) (250 \text{ mL})}{14.5343 \text{ M}} \\ &= 137.65 \text{ mL}\end{aligned}$$

Thus 137.65 mL of 65% of HNO₃ was diluted to 250 mL with deionised water.

II. Preparation of Stock Solution of Phosphorus, P (ICP-OES)

Molecular weight of NH₄H₂PO₄

$$\begin{aligned}&= (14.0067 + 10079 \times 4 + 30.9738 + 15.9994 \times 4) \text{ g mol}^{-1} \\ &= 115.0255 \text{ g mol}^{-1}\end{aligned}$$

$$\text{Atomic weight of P} = 30.9738 \text{ g mol}^{-1}$$

$$\begin{aligned}50 \text{ ppm of stock solution for P} &= 50 \text{ mg L}^{-1} \\ &= 0.05 \text{ g L}^{-1}\end{aligned}$$

$$\begin{aligned}\text{Number of mole of P} &= \frac{0.05 \text{ g L}^{-1}}{30.9738 \text{ g mol}^{-1}} \\ &= 1.6145 \times 10^{-3} \text{ mol L}^{-1}\end{aligned}$$

$$\begin{aligned}\text{Mass of NH}_4\text{H}_2\text{PO}_4 &= 1.6145 \times 10^{-3} \text{ mol L}^{-1} \times 115.0255 \text{ g mol}^{-1} \\ &= 0.1857 \text{ g L}^{-1}\end{aligned}$$

Thus, 0.1857 g of $\text{NH}_4\text{H}_2\text{PO}_4$ was transferred into 1000 mL volumetric flask and top up with deionised water.

Preparation of standard solution of phosphorus, P

$$M_1 V_1 = M_2 V_2$$

Where

M_1 = concentration of stock solution (50 ppm)

V_1 = volume of stock solution

M_2 = concentration of standard solution

V_2 = volume of standard solution (250 mL)

Example of calculation for standard solution of 20 ppm

$$\begin{aligned}M_1 V_1 &= M_2 V_2 \\ (50 \text{ ppm}) V_1 &= (20 \text{ ppm}) (250 \text{ mL}) \\ V_1 &= \frac{(20 \text{ ppm}) (250 \text{ mL})}{50 \text{ ppm}} \\ &= 100 \text{ mL}\end{aligned}$$

Thus, 100 mL of stock solution for phosphorus was dissolved in 8 M HNO_3 then diluted to 250 mL with deionised water to produce 20 ppm standard solution of phosphorus.

III. Preparation of Stock Solution of Vanadium, V

Preparations of Reagents for ICP-OES

$$\begin{aligned}\text{Molecular weight of NH}_4\text{VO}_3 &= (14.0067 + 10079 \times 4 + 50.9415 + 15.9994 \times 3) \text{ g mol}^{-1} \\ &= 116.9780 \text{ g mol}^{-1}\end{aligned}$$

$$\text{Atomic weight of V} = 50.9415 \text{ g mol}^{-1}$$

$$\begin{aligned}50 \text{ ppm of stock solution for V} &= 50 \text{ mg L}^{-1} \\ &= 0.05 \text{ g L}^{-1}\end{aligned}$$

$$\begin{aligned}\text{Number of mole of V} &= \frac{0.05 \text{ g L}^{-1}}{50.9415 \text{ g mol}^{-1}} \\ &= 9.8155 \times 10^{-4} \text{ mol L}^{-1} \\ \text{Mass of NH}_4\text{VO}_3 &= 9.8155 \times 10^{-4} \text{ mol} \times 116.9780 \text{ g mol}^{-1} \\ &= 0.1148 \text{ g L}^{-1}\end{aligned}$$

Thus, 0.1148 g of NH_4VO_3 was transferred into 1000 mL volumetric flask and top up with deionised water.

Preparation of standard solution of vanadium, V

$$M_1 V_1 = M_2 V_2$$

Where

M_1 = concentration of stock solution (50 ppm)

V_1 = volume of stock solution

M_2 = concentration of standard solution

V_2 = volume of standard solution (250 mL)

Example of calculation for standard solution of 10 ppm

$$M_1 V_1 = M_2 V_2$$

$$(50 \text{ ppm}) V_1 = (10 \text{ ppm}) (250 \text{ mL})$$

$$\begin{aligned}V_1 &= \frac{(10 \text{ ppm}) (250 \text{ mL})}{50 \text{ ppm}} \\ &= 50 \text{ mL}\end{aligned}$$

Thus, 50 mL of stock solution for vanadium was dissolved in 8 M HNO_3 then diluted to 250 mL with deionised water to produce 10 ppm standard solution of vanadium.

IV. Preparation of Stock Solution of Chromium, Cr

Molecular weight of $\text{Cr}(\text{NO}_3)_3 \cdot 9\text{H}_2\text{O}$

$$\begin{aligned}&= 51.9961 \text{ g mol}^{-1} + 3 \times (14.0070 \text{ g mol}^{-1} + 3 \times 15.9994 \text{ g mol}^{-1}) + \\ &\quad 9 \times (2 \times 1.0079 \text{ g mol}^{-1} + 15.9994 \text{ g mol}^{-1}) \\ &= 400.1485 \text{ g/mol}\end{aligned}$$

$$\text{Atomic weight of Cr} = 51.9961 \text{ g mol}^{-1}$$

50 ppm of stock solution for $V = 50 \text{ mg / L}$
 $= 0.05 \text{ g / L}$

$$\begin{aligned}\text{Number of mole of Cr} &= \frac{0.05 \text{ g L}^{-1}}{51.9961 \text{ g mol}^{-1}} \\ &= 9.6161 \times 10^{-4} \text{ mol L}^{-1}\end{aligned}$$

$$\begin{aligned}\text{Mass of Cr(NO}_3)_3 \cdot 9\text{H}_2\text{O} &= 9.6161 \times 10^{-4} \text{ mol} \times 400.1485 \text{ g mol}^{-1} \\ &= 0.3849 \text{ g L}^{-1}\end{aligned}$$

Thus, 0.3849 g of $\text{Cr(NO}_3)_3 \cdot 9\text{H}_2\text{O}$ was transferred into 1000 mL volumetric flask and top up with deionised water.

Preparation of standard solution of chromium, Cr

$$M_1 V_1 = M_2 V_2$$

Where

M_1 = concentration of stock solution (50 ppm)

V_1 = volume of stock solution

M_2 = concentration of standard solution

V_2 = volume of standard solution (250 mL)

Example of calculation for standard solution of 5 ppm

$$M_1 V_1 = M_2 V_2$$

$$(50 \text{ ppm}) V_1 = (5 \text{ ppm}) (250 \text{ mL})$$

$$\begin{aligned}V_1 &= \frac{(5 \text{ ppm}) (250 \text{ mL})}{50 \text{ ppm}} \\ &= 25 \text{ mL}\end{aligned}$$

Thus, 25 mL of stock solution for chromium was dissolved in 8 M HNO_3 then diluted to 250 mL with deionised water to produce 10 ppm standard solution of vanadium.

V. Preparation of 100 ppm sample solution

$$\begin{aligned} 0.025 \text{ g sample in 250 mL} &= \frac{0.025 \text{ g}}{250 \text{ mL of HNO}_3} \\ &= \frac{0.1 \text{ g}}{1000 \text{ mL of HNO}_3} \\ &= 0.1 \times 10^3 \text{ mg L}^{-1} \\ &= 100 \text{ ppm} \end{aligned}$$

Thus, 0.0250 g of sample was transferred into 250 mL volumetric flask and dissolved by 10 mL of 8 M HNO₃. Then, top up to 250 mL with deionised water to produce 100 ppm sample solution.

APPENDIX G

Calculation of P/V and Cr/V mole ratio by using ICP-OES analysis

$$\frac{P}{V} = \frac{\text{Concentration of P / Atomic Weight of P}}{\text{Concentration of V / Atomic Weight of V}}$$

$$\frac{Cr}{V} = \frac{\text{Concentration of Cr / Atomic Weight of Cr}}{\text{Concentration of V / Atomic Weight of V}}$$

Example of calculation:

For VPO₅-Cr1%

$$\begin{aligned} \frac{P}{V} &= \frac{24.38 \text{ mg L}^{-1} / 30.9738 \text{ g mol}^{-1}}{25.77 \text{ mg L}^{-1} / 50.9415 \text{ g mol}^{-1}} \\ &= 1.5560 \end{aligned}$$

$$\begin{aligned} \frac{Cr}{V} &= \frac{0.034 \text{ mg L}^{-1} / 51.9961 \text{ g mol}^{-1}}{25.77 \text{ mg L}^{-1} / 50.9415 \text{ g mol}^{-1}} \\ &= 0.0129 \end{aligned}$$

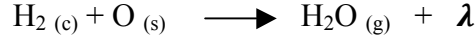
Data for ICP-OES analyses

Catalysts	Concentration of P (mg L⁻¹)	Concentration of V (mg L⁻¹)	Concentration of Cr (mg L⁻¹)	P/N mole ratio	Cr/V mole ratio
Bulk VPO_s	22.83	35.76	-	1.05	-
VPO_s-Cr1%	24.38	25.77	0.34	1.56	0.013
VPO_s-Cr3%	23.65	25.29	0.89	1.54	0.034
VPO_s-Cr5%	22.49	24.80	1.34	1.49	0.053
5%VPO_s/Si	21.37	31.95	-	1.10	-
10%VPO_s/Si	42.20	57.84	-	1.20	-
15%VPO_s/Si	43.31	57.91	-	1.23	-
20%VPO_s/Si	74.19	100.01	-	1.22	-
25%VPO_s/Si	82.43	101.17	-	1.34	-
30%VPO_s/Si or T460VPO_s/Si	103.30	124.02	-	1.37	-
T400VPO_s/Si	109.70	128.87	-	1.40	-
T520PO_s/Si	109.00	128.97	-	1.39	-

Appendix H

Calculation of Desorption Activation Energy (E_d) or Reduction Activation Energy (E_r) for TPD of O_2 and TPR in H_2 Analysis respectively

The values of the activation energies for the reaction :



where c = chemisorbed species,
s = surface/lattice oxygen species,
g = gaseous species,
 λ = oxygen vacancy site

$$\begin{aligned} \text{Rate} &= k [H_2]_m [O_s] \\ -\frac{d[H_2]}{dt} &= A \exp\left(\frac{-E_r}{RT}\right) [H_2]_m [O_s] \end{aligned} \quad (i)$$

Solution of equation (i) at T_m gives :

$$\frac{E_r}{RT_m^2} = [H_2]_m \left(\frac{A}{\beta}\right) \exp\left(\frac{-E_r}{RT_m}\right) \quad (ii)$$

From the Redhead equation :

$$k_1 = A \exp\left(\frac{-E_r}{RT_m}\right) \quad (iii)$$

Therefore from the equation (ii),

$$k_2 = A [H_2]_m \exp\left(\frac{-E_r}{RT_m}\right)$$

Since k_1 and k_2 are the same at T_m and let $k = \chi$ at T_m

$$\begin{aligned} \left(\frac{\chi}{A[H_2]_m}\right) &= \exp\left(\frac{-E_r}{RT_m}\right) \text{ or } \left(\frac{A[H_2]_m}{\chi}\right) = \exp\left(\frac{E_r}{RT_m}\right) \\ \left(\frac{E_r}{RT_m}\right) &= \ln\left(\frac{A[H_2]_m}{\chi}\right) \end{aligned}$$

$$E_r = R T_m \ln \left(\frac{A[H_2]_m}{\chi} \right)$$

Example of calculation:

For Bulk VPO_s in TPD of O₂ analysis

Temperature of the peak maximum, $T_{\max} = 971 \text{ K}$

Crude approximation of the reduction activation energy;

$$\begin{aligned} E &= T_m \times 0.066 \\ &= 971 \times 0.066 \\ &= 64.086 \text{ k cal mol}^{-1} \end{aligned}$$

$$\begin{aligned} \chi &= A \exp \left(\frac{-E_r}{RT_m} \right) \\ &= 10^{13} \text{ s}^{-1} \exp \left(\frac{-57.29 \text{ kcal mol}^{-1}}{0.001987 \text{ kcal K}^{-1} \text{ mol}^{-1} (868 \text{ K})} \right) \\ &= 0.0375 \text{ s}^{-1} \end{aligned}$$

$$\begin{aligned} [H_2] &= \frac{n}{v} = \frac{0.05}{RT} \\ &= \frac{0.05 \text{ atm}}{(82.056 \text{ atm K}^{-1} \text{ mol}^{-1} \text{ cm}^3)(298 \text{ K})} \\ &= 2.0 \times 10^{-6} \text{ mol cm}^{-3} \end{aligned}$$

$$\begin{aligned} E_d &= R T_m \ln \left(\frac{A[H_2]_m}{\chi} \right) \\ &= 0.001987 \text{ kcal}^{-1} \text{ mol}^{-1} (868 \text{ K}) \ln \left(\frac{10^{13} \text{ cm}^3 \text{ mol}^{-1} \text{ s}^{-1} (2.0 \times 10^{-6} \text{ mol cm}^{-3})}{0.0375 \text{ s}^{-1}} \right) \\ &= 38.8109 \text{ kcal mol}^{-1} \quad (1 \text{ cal} = 4.184 \text{ J}) \\ &= 162.38 \text{ kJ mol}^{-1} \end{aligned}$$

APPENDIX I

Calculation of Amount of Oxygen species Desorbed or Removed from Catalysts through TPD of O₂ and TPR in H₂ Analysis respectively

$$\begin{aligned} &\text{Total oxygen removed or desorbed (atom g}^{-1}\text{)} \\ &= \text{Amount of oxygen removed (}\mu\text{ mol g}^{-1}\text{)} \times 6.022 \times 10^{23} \text{ atom mol}^{-1} \\ &= \text{Amount of oxygen removed (atom g}^{-1}\text{)} \end{aligned}$$

Example of calculation:

For Bulk VPO_s via TPR in H₂ Analysis

$$\begin{aligned} \text{Total oxygen atom removed} &= 2754.6229 \mu\text{mol g}^{-1} \times 6.022 \times 10^{23} \text{ atom mol}^{-1} \\ &= 2.75462 \times 10^{-3} \text{ atom g}^{-1} \end{aligned}$$

BIODATA OF THE AUTHOR

Ms. Loh Pei Xuan was born on 28th March 1986 in Mersing. She completed her primary and secondary studies in SJK(C) Chiao Ching, Endau and S.M.K. Ungku Husin, Endau, respectively. She moved on to study her Lower and Upper Six in Kolej Tunku Abdul Rahman (KTAR), Setapak. Subsequently, she obtained her degree in Bachelor of Science (Hons.) Chemistry from Universiti Tunku Abdul Rahman (UTAR), Setapak in 2009. He further enrolled in Master of Science in the field of Selective Oxidation Catalysis in the university immediately after her graduation. During her postgraduate study, she was employed as teaching assistant to conduct laboratory practical sessions in the Faculty of Engineering and Science, UTAR, Setapak, Kuala Lumpur.

List of Seminars/Conferences Participated:

- (i) 1st seminar on Catalysis Science and Technology, Universiti Putra Malaysia, Serdang, Malaysia, December 3, 2008 (Poster Presenter).
- (ii) 10th Asian Conference on Analytical Sciences (ASIANALYSIS X) and Simposium Kimia Analysis Malaysia Ke-22 (SKAM-22), Putra World Trade Centre, Kuala Lumpur, Malaysia, August 11–13, 2009 (Oral Presenter).
- (iii) 6th Singapore International Chemical Conference (SICC-6), Singapore International Convention & Exhibition Centre, Suntec City, Singapore, December 15–18, 2009.
- (iv) 6th Tokyo Conference on Advanced Catalytic Science and Technology (TOCAT6) and 5th Asia Pacific Congress on Catalysis (APCAT5), Sapporo Convention Centre, Sapporo, Japan, July 18–23, 2010 (Poster Presenter).